UNIVERSIDADE DE SÃO PAULO
FFCLRP – DEPARTAMENTO DE FÍSICA
PROGRAMA DE PÓS GRADUAÇÃO EM FÍSICA APLICADA EM MEDICINA E BIOLOGIA

Estudo da conectividade estrutural cerebral humana no envelhecimento sadio baseado em tratos

Maíra Siqueira Pinto

Dissertação apresentada à Faculdade de Filosofia, Ciências e Letras de Ribeirão Preto da USP, como parte das exigências para a obtenção do título de Mestre em Ciências, Área: Física Aplicada à Medicina e Biologia.

RIBEIRÃO PRETO - SP
2018

MAÍRA SIQUEIRA PINTO

Estudo da conectividade estrutural cerebral humana no envelhecimento sadio baseado em tratos

Versão Corrigida
(Versão original encontra-se na unidade que aloja o Programa de Pós-graduação)

Dissertação apresentada à Faculdade de Filosofia, Ciências e Letras de Ribeirão Preto da Universidade de São Paulo como parte das exigências para a obtenção do título de Mestre em Ciências.

Área de concentração:
Física Aplicada à Medicina e Biologia

Orientador:
Prof. Dr. Carlos Ernesto Garrido Salmon

Ribeirão Preto – SP
2018

FICHA CATALOGRÁFICA

Pinto, Maíra Siqueira

Estudo da conectividade estrutural cerebral humana no envelhecimento sadio baseado em tratos / Maíra Siqueira Pinto; Carlos Ernesto Garrido Salmon. Ribeirão Preto – SP, 2018.

123p.

Dissertação (Mestrado – Programa de Pós-Graduação em Física Aplicada a Medicina e Biologia) – Faculdade de Filosofia, Ciências e Letras de Ribeirão Preto da Universidade de São Paulo, 2018.

1. Conectividade estrutural. 2. Tractografia. 3. Envelhecimento sadio. 4. Diffusion MRI. 5. Espessura cortical

DEDICATÓRIA

Aos leitores.

AGRADECIMENTOS

À minha família que me apoiou em todos os momentos, desde o início da graduação, até o exato momento em que finalizo mais uma etapa. Agradeço por toda a paciência, incentivo e palavra de carinho. Agradeço aos meus irmãos, Gustavo e Marina, meu pai, Roberto, meus avós, tios e primos. Principalmente à minha mãe, Helimara, que possibilitou que meu sonho se tornasse realidade, meu maior e mais sincero, obrigada!

Ao meu orientador, Garrido, que por seis anos me ensina, guia e apoia. Incentivando-me e abrindo caminhos para que eu pudesse chegar nesse momento. Professor, o senhor foi uma pessoal essencial na minha trajetória até aqui, obrigada por me fazer enxergar minha própria capacidade de ir tão longe, obrigada!

Aos colegas do laboratório InBrain, que desde a iniciação científica estão lá em todos os momentos, com conselhos, palpites, indicações, conversas instigantes, parceria nos congressos e momentos de descontração. Obrigada, André, Gustavo, Ícaro, João, Pedro, Mileni, Hohana, Fábio, Danilo, Felipe, Jeam e Luciana. Agradeço também à Prof. Renata, pelo apoio desde a iniciação científica. Gostaria de deixar um agradecimento em especial para meu colega e amigo, Bruno, que foi fundamental durante meu mestrado, obrigada Bruninho!

Aos professores e funcionários do Departamento de Física e aos membros da secretária, Nilza, Ricardo e Raquel, que ajudaram em tudo que foi possível. Ao Prof. Antonio Carlos dos Santos, que nos cedeu as imagens utilizadas na pesquisa, e aos técnicos da ressonância do HCRP que ajudaram na obtenção dessas imagens.

Aos amigos de Ribeirão e Taubaté, que ajudaram, incentivaram e compartilharam as felicidades e os momentos de frustração, Stephanie, Felipe (Leite), Maria Luiza (Cobrinha), Vivian, Matheus, Letícia, Aline, Camila, meninas do time Aliança Rubgy Ribeirão, amizades e colegas de congressos e todas as pessoas que viveram um pouco desses 2 anos comigo.

A realização deste projeto foi possível através do financiamento de processo nº 2015/26227-7, Fundação de Amparo à Pesquisa do Estado de São Paulo (FAPESP).

EPÍGRAFE

“Quando estiver do outro lado,
Lembre-se
De onde veio.
Lá, grandes aventuras podem surgir.
Mas aqui,
Há pessoas que te fazem sorrir.”

(Vivian Monezi Tetzner)

RESUMO

PINTO, M. S. **Estudo da conectividade estrutural cerebral humana no envelhecimento sadio baseado em tratos.** 2018. 123p. Dissertação (Mestrado – Programa de Pós-Graduação em Física Aplicada em Medicina e Biologia) – Faculdade de Filosofia, Ciências e Letras de Ribeirão Preto, Universidade de São Paulo, Ribeirão Preto – SP, 2018.

O cérebro humano muda de forma complexa e heterogênea ao longo da vida, o processo de envelhecimento normal tem associado significativas alterações nas conexões axonais. Neste estudo, avaliamos as mudanças relacionadas à idade em parâmetros físicos associados à integridade das substâncias branca e cinzenta cerebral em sujeitos saudáveis, assim como a possivel correlação entre eles em tratos específicos. Imagens estruturais (1 mm isotrópica) e imagens ponderadas em difusão (2 mm isotrópica e b=1000 s/mm^2) de 158 indivíduos saudáveis entre 18 a 83 anos foram coletadas retrospectivamente no Hospital das Clinícas de Ribeirão Preto, após sua aquisição em aparelho de ressonância magnética de 3 Teslas. A partir das imagens estruturais, a espessura cortical foi estimada e o efeito de idade nela foi avaliado em diversas regiões tomando com base o atlas de Destrieux. As imagens ponderadas em difusão foram processadas para caracterizar a difusão intravoxel utilizando dois modelos: tensor de difusão (DT) e deconvolução esférica restrita (CSD). Mapas de anisotropia fracionada (FA) e densidade aparente da fibra (AFD) foram estimados e usados em analise estatistica de três grupos separados por faixa etária. Os tratos cerebrais mais relevantes foram segmentados por tres procedimentos: manualmente, automaticamente com uma ferramenta especifica e com base em regiões corticais automaticante segmentadas. Parâmetros físicos de difusão (anisotropia e difusibilide) foram avaliados nos tratos segmentados para determinar as alterações relacionadas à idade. A análise de conectoma baseada em dois parcelamentos corticais foi realizada para avaliar também o efeito da idade em parâmetros caracteristicos da rede estrutural cerebral. A relação trato-cortical foi avaliada considerando a anisotropia de cada trato e as espessuras das áreas corticais nas extremidades do trato correspondente. Uma análise adicional foi realizada para avaliar uma possivel associação de

conetividades estrutural e funcional no corpo caloso (CC). Houve afinamento cortical significativo em 88,5% das regiões durante a vida (p <0,05, corrigido); a região frontal foi a mais afetada no envelhecimento inicial (após 40 anos), e as regiões occipital e temporal nos idosos (após 60 anos). Similarmente, a análise de grupo demonstrou um padrão global de redução de FA e AFD na substância branca, com uma maior taxa de degradação de integridade a partir da sexta década de vida. A seleção manual de tratos baseada no modelo de DT mostrou-se a metodologia mais confiavél na precisa definição dos tratos nos nossos dados. Seguindo essa metodologia, a análise dos parâmetros de anistropia e difusão também indicou degeneração de substância branca no envelhecimento normal em todos os tratos cerebrais estudados e corroborou o gradiente ântero-posterior de degeneração no CC. O fornix foi o trato mais afetado bilatreamente com redução de 3.5% e aumento de 4% por década nesses parâmetros, respectivamente; seguido do CC. Na avaliação do efeito da idade nas estimativas do conectoma, independentemente do modelo de difusão e do atlas cortical usado, houve uma diminuição da eficiência global com o envelhececimento, do número de conexões e da eficiência local, principalmente nas regiões pré-frontal, temporal e parietal e suas conexões. Nas análises trato-corticais, as regiões corticais conectadas por tratos mostraram padrões de afinamento similares para a maioria dos tratos, e uma correlação significativa entre a taxa média de afinamento cortical e as taxas de alteração de FA e difusibilidade média (MD) foram encontradas. Em todos os tratos avaliados, a idade foi o principal efeito controlando das alterações dos parâmetros de difusão; não houve correlações diretas com espessura cortical para a maioria dos tratos. Somente para o fornix, os valores de FA e MD mostraram correlação com a espessura cortical do giro subcalosal (parcelamento de Destrieux) em ambos os hemisférios durante o envelhecimento (p <0,05 corrigido). Para os outros tratos, CC, fascículo longitudinal inferior, fascículo uncinado, fascículo occipitofrontal inferior, trato cortico-espinal, parte cingulada do cíngulo e fascículo arqueado, a idade foi o principal efeito no controle das alterações dos parâmetros, mas não houve correlações diretas entre FA e MD e espessura cortical durante o processo de envelhecimento.

Palavras-chave: 1. Conectividade estrutural. 2. Tractografia. 3. Envelhecimento sadio. 4. dMRI. 5. Espessura cortical

ABSTRACT

PINTO, M. S. **Study of human structural brain connectivity in healthy aging based on tracts.** 2018. 123p. Dissertation (MSc. – Postgraduate Program in Physics Applied to Medicine and Biology) – College of Philosophy, Sciences and Literature of Ribeirão Preto, University of São Paulo, Ribeirão Preto – SP, 2018.

The human brain changes in a complex and heterogeneous way throughout life, the normal aging process is associated to significant alterations in the axonal connections. In this study, we evaluated the age-related changes in physical parameters associated with the brain white and gray matter integrity in healthy subjects, as well as the possible correlation between them in specific tracts. Structural images (1 mm isotropic) and diffusion weighted images (2 mm isotropic, b = 1000 s /mm^2) of 158 healthy individuals aged between 18 and 83 years were retrospectively collected at the Clinics Hospital of Ribeirao Preto, after their acquisition in a 3T MR scanner. From the structural images, the cortical thickness was estimated and the age effect was evaluated in several regions based on the Atlas of Destrieux. The diffusion-weighted images were processed to characterize the intravoxel diffusion using two models: diffusion tensor (DT) and constrained spherical deconvolution (CSD). Fractional anisotropy (FA) and apparent density of fiber (AFD) maps were estimated and used in statistical group analysis between the three groups separated by age. The most relevant brain tracts were segmented by three procedures: manually, automatically with a specific tool and based on automatic segmented cortical regions. Physical parameters of diffusion (anisotropy and diffusivities) were evaluated in the segmented tracts to determine the age-related changes. The connectome analysis based on two cortical parcellations was performed to evaluate the age effect on characteristic structural brain network parameters. The tract-cortical relationship was evaluated considering the anisotropy of each tract and the thickness of the cortical areas at the end of the corresponding tract. Further analysis was performed to evaluate a possible association of structural and functional connectivity in the corpus callosum (CC). There was significant cortical thinning in 88.5% of the regions during life ($p < 0.05$, corrected for multiple

comparisons); the frontal region was the most affected in the initial aging (after 40 years), and the occipital and temporal regions in the elderly (after 60 years). Similarly, the group analysis demonstrated a global pattern of reduction of FA and AFD in the white matter, with a higher rate of degradation of integrity from the sixth decade of life. The manual selection of tracts from the DT model proved to be the most reliable methodology in the precise definition of the tracts for our data. Following this methodology, analysis of anisotropy and diffusion parameters also indicated degeneration of white matter in normal aging in all studied brain tracts and corroborated to the antero-posterior gradient of degeneration in the CC. Fornix was the most affected tract bilaterally, with a 3.5% reduction and an increase of 4% per decade in these parameters, respectively; followed by CC. In the evaluation of the age effect on the connectome estimates, regardless of diffusion model and cortical atlas, there was a decrease in global efficiency, number of connections and local efficiency with aging, mainly in the prefrontal, temporal and parietal and its connections. In the tract-cortical analysis, cortical regions connected by tracts demonstrated similar thinning patterns for the majority of tracts, and a significant relation between mean cortical thinning rate and FA/MD alteration rates were found. In all evaluated tracts, age was the main effect controlling diffusion parameters alterations; there were no direct correlations with cortical thickness for the majority of tracts. Only for the fornix, the values of FA and MD showed significant correlation with the cortical thickness of the subcallosal gyrus in both hemispheres during aging ($p < 0.05$ corrected). For the other tracts, CC, Inferior Longitudinal Fasciculus, Uncinated Fasciculus, Inferior Fronto-occipital Fasciculus, Corticospinal Tract, Cingulum and Arcuate Fasciculus, age was the main effect controlling alterations in the parameters, but there were no direct correlations between FA and MD and cortical thickness during the aging process.

Key words: 1. Structural connectivity. 2. Tractography. 3. Healthy aging. 4. dMRI. 5. Cortical thinning.

LIST OF FIGURES

LIST OF TABLES

LIST OF ABBREVIATIONS

3D-T1	Three Dimensional T1 image
AD	Axial Diffusivity
AF	Arcuate Fasciculus
AFD	Apparent Fiber Density
BET	Brain Extraction Tool
CC	Corpus Callosum
CGC	Cingulate part of Cingulum
CGH	Hippocampal part of Cingulum
COG	Center of Gravity
CSD	Constrained Spherical Deconvolution
CSF	Cerebrospinal Fluid
CST	Corticospinal Tract
Dex	Destrieux atlas
DK	Desikan-Killiany atlas
dMRI	Diffusion Magnetic Resonance Imaging
DT	Diffusion Tensor
DTI	Diffusion Tensor Image
DWI	Diffusion Weighted Images
EPI	Echo Planar Imaging
FA	Fractional Anisotropy
FACT	Fiber Assignment by Continuous Tracking
FC	Functional Connectivity
FD	Fiber Density
FDT	FMRIB's Diffusion Toolbox
FX	Fornix
fMRI	Functional Magnetic Resonance Imaging
FOD	Fiber Orientation Distribution
FOV	Field of View
GE	Gradient Echo
GM	Gray Matter
IFOF	Inferior Fronto-Occipital Fasciculus
ILF	Inferior Lateral Fasciculus

MD	Mean Diffusivity
MRI	Magnetic Resonance Imaging
NKI	Nathan Kline Institute
PGSE	Pulsed Gradient Spin Echo
RD	Radial Diffusivity
ROI	Region of Interest
SE	Spin Echo
SIFT	Spherical-deconvolution Informed Filtering of Tractograms
SLF	Superior Lateral Fasciculus
SNR	Signal-to-Noise Ratio
TE	Echo Time
TR	Repetition Time
UF	Uncinate Fasciculus
VOI	Volume of Interest
WM	White Matter

Summary

1. Introduction

In this first chapter we will introduce the main composition of the human brain, describe some neuroimaging findings about the aging process of the cerebrum, and discuss how our research can provide additional information about the brain structural connectivity changes in the lifespan.

1.1. The human encephalon

The encephalon is an organ of the central nervous system of the human body, and it is composed by three main parts: the brainstem, the cerebellum and the cerebrum. Brainstem connects the brain to the spinal cord, and it is responsible for several basic functions, for example, breathing and sleeping. The cerebellum in the basis of the encephalic control of coordination and balance of the body. The cerebrum is the biggest part, divided in two hemispheres, each one divided

Figure 1 Subdivisions of the human brain and a diagram of the cerebral lobes

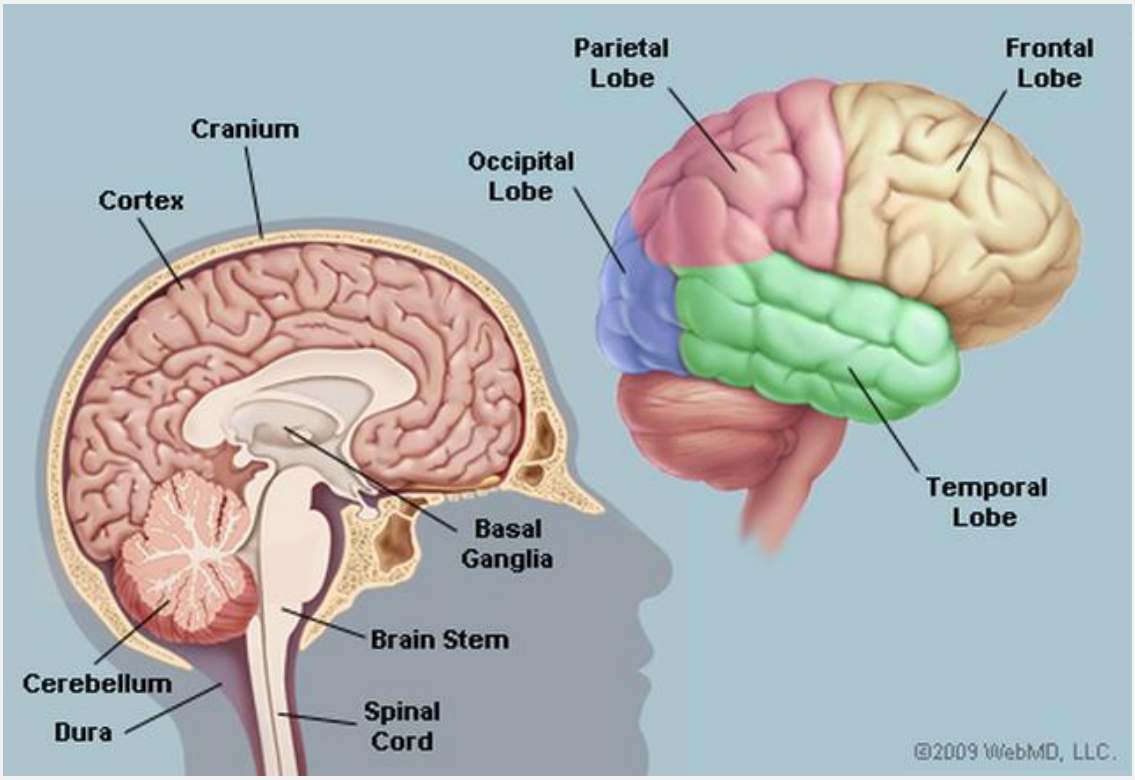

Source: 2009 WebMD, LLC. All rights reserved.

into four lobes: frontal, parietal, temporal and occipital. There are some structures in the center of the brain, called basal nuclei, that coordinates the information between many brain regions, Figure 1.

In general, this complex organ controls all body functions, interprets, processes and stores all the received information from the rest of the body. Each part of the healthy brain has some specific functions, as the frontal lobes are responsible for personality, intelligence, speech, judgment, motor function and problem solving, the parietal lobes manage body position, perception, interpretation and sensations, temporal lobes control memory, hearing and organization, and occipital lobes are responsible for vision interpretations. The brain is surrounded by a fluid for protection, called cerebrospinal fluid (CSF), it is also present in the brain cavities, the ventricles.

There are two types of cells that compose the brain, the nerve cells, aka neurons, and glia cells, Figure 2. The neurons consist of a cell body, dendrites and an axon, it transports information through electrical and chemical signals, communicating with other neurons via synapses. Glia cells perform many functions as metabolic and structural support, protection and nourishment, depending of which cell it is. Astrocytes transport nutrients, hold neurons in place and regulate the blood brain barrier, oligodendrocytes create the myelin sheaths in the neurons that provide support and insulation, ependymocytes line the

Figure 2 Representation of the neuron architecture and the glia cells

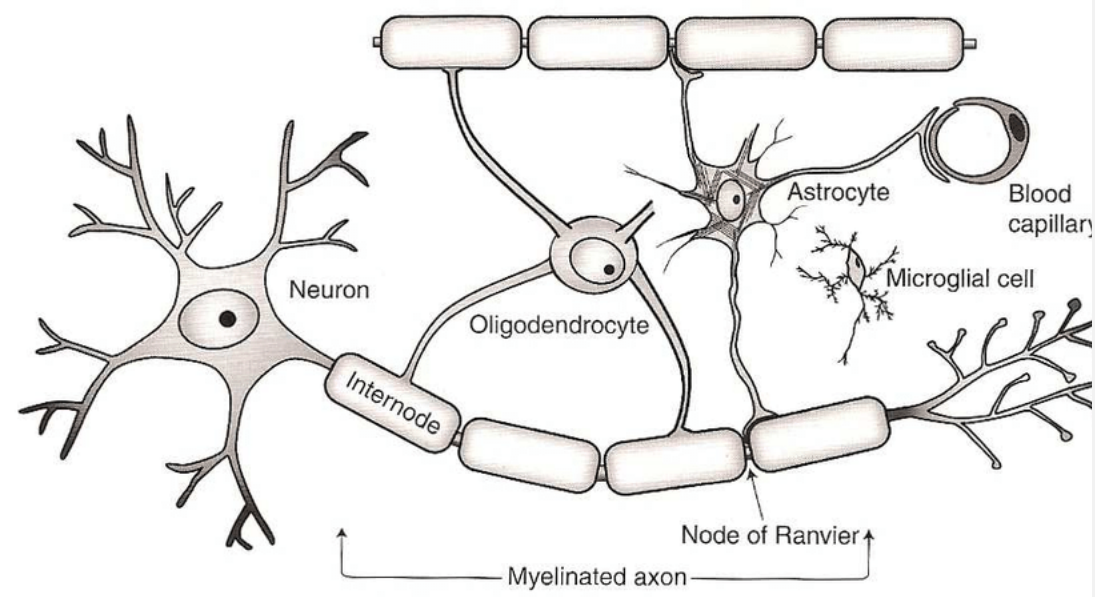

Source: Johansen-Berg, H. and Behrens, T. (2014). *Diffusion MRI*. Amsterdam:

ventricles and secrete CSF, and microglia act as immune defense of the central nervous system, clearing dead neurons. There are usually more glia cells than neurons, 10-50 to 1 proportion.

The brain has two main types of tissue: gray and white matter, Figure 3. Gray matter (GM), consists of neuron cell bodies, dendrites, myelinated and unmyelinated axons, glia cells and capillaries, and white matter (WM) consists of myelinated and unmyelinated axons (connecting different parts of the GM), cell bodies, dendrites and glia cells. The distinction between them is that GM contains many more cell bodies relatively to myelinated axons, while WM contains few cell bodies and is composed mainly by long myelinated axons.

Figure 3 Schematic illustration of the human brain

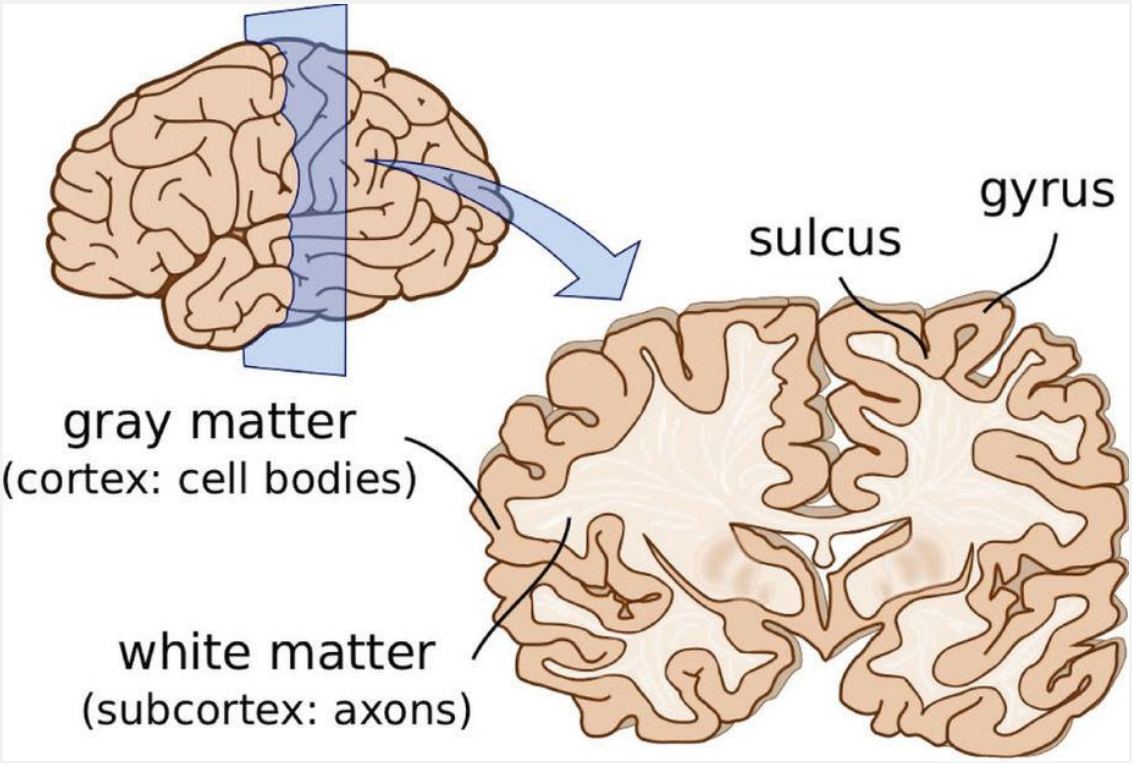

Source: BUDDAY, S.; RAYBAUD, C.; KUHL, E. A mechanical model predicts morphological abnormalities in the developing human brain. Scientific Reports, v. 4, n. 1, 10 jul. 2014.

The cortex is the outer surface of the brain, composed by over 10 billion nerve cells of gray matter that control brain functioning. The thickness of the human cortex correlates with the neuronal organization, it varies regionally between 1 and 4.5 mm, with an average of 2.5 mm. It can be divided into up to six layers, with characteristic cell distributions and cortical (and subcortical) connections:

molecular (I), external granular (II), pyramidal (III), inner granular (IV), ganglionic (V) and multiform (VI). These connections transport information through encoded electrical impulses, from the cell body, through the myelinated axon transferring to the dendrite of another neuron, along the WM pathways, from one part of the cortex (or subcortical region) to another (gyri, sulci or deep structures).

White matter is composed of bundles of myelin coated axons, often called tracts that conduct neural information between gray matter regions. Terms other than ‘‘tract’’ are used to describe white matter pathways include bundle, capsule, fasciculus, funiculus, lemniscus, and peduncle. The three major groups of white matter pathways include association, commissural and projection fibers (WAKANA et al., 2004), Figure 4 illustrates these fiber groups. Association fibers connect cortical areas within the same cerebral hemisphere and can be short (U-shaped) or long (uncinate fasciculus, cingulum, superior longitudinal fasciculus, inferior longitudinal fasciculus, vertical occipital fasciculus, occipitofrontal fasciculus, fornix and arcuate fasciculus) fibers. Commissural or transverse fibers connect the two hemispheres of the brain, as corpus callosum, anterior commissure, posterior commissure and hippocampal commissure. Projection fibers connect the cortex with the lower parts of the brain and spinal cord, can be efferent (internal capsule, corticospinal, corticonuclear and corticothalamic) and afferent (geniculocalcarine radiation, auditory radiation and thalamic radiation) fibers.

Figure 4 Illustration of the projection, commissural and association brain fibers

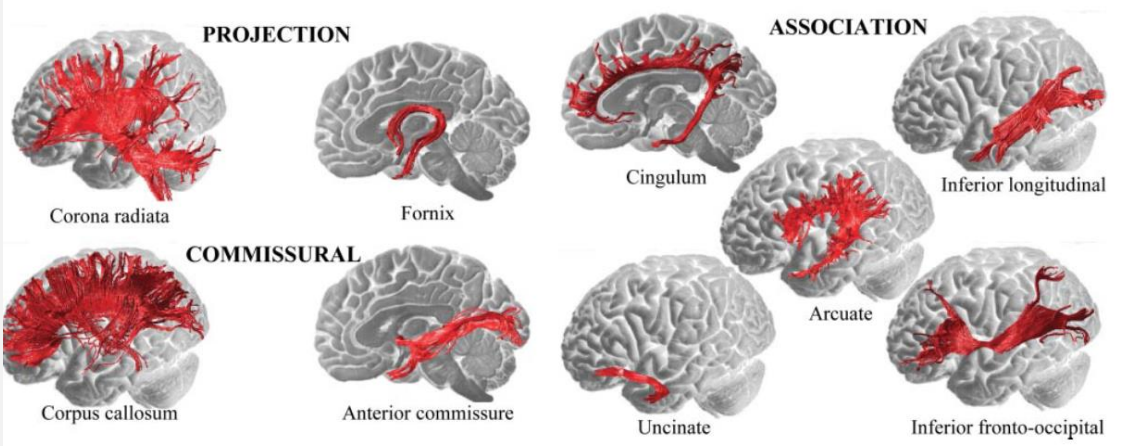

Source: CATANI, M.; FFYTCHE, D. H. The rises and falls of disconnection syndromes. Brain, v. 128, n. 10, p. 2224–2239, 1 set. 2005 (adapted)

The brain microstructure is changing in the life span, first in a developmental process and after reaching a peak of development, the natural aging process starts. The aging process is associated to many chemical, neurocognitive, functional and structural alterations in the brain, some of these normal structural changes will be described next.

1.2. Morphometric changes associated to brain aging: neuroimaging findings

The human brain structure undergoes continuous and non-linear changes over the lifespan. Normal aging is accompanied by complex neurobiological changes that affect the brain's functional and structural organization and the individual's cognitive abilities. The underlying mechanism of these alterations is still unresolved. Detailed knowledge about aging of the human brain would be helpful to understand the aging process. Many studies have attempted to elucidate the aging of the human brain, demonstrating that the brain undergoes structural and functional changes, and those are influenced by many factors such as genetic and the environment, among these changes it was demonstrated brain tissue shrinkage and cognitive decline (ESIRI, 2007; SULLIVAN; PFEFFERBAUM, 2007). Post-mortem studies in human brain confirm these findings demonstrating that between the ages of 20 and 60 years old the adult brain loses about 0.1% of its weight per year, the loss rate is higher from 70 years old (DEKABAN; SADOWSKY, 1978).

The brain volume can be estimated using magnetic resonance imaging techniques, in the literature a reduction in brain volume during lifespan is demonstrated (JERNIGAN; PRESS; HESSELINK, 1990; PFEFFERBAUM et al., 1994). Cross-sectional and longitudinal studies suggest that in healthy adults, age-related volume reduction is small, diffuse and uniform in white matter and more pronounced in gray matter, especially frontal and parietal cortices, compared to temporal and occipital cortices (SCAHILL et al., 2003; TROLLOR; VALENZUELA, 2001). Due to reduced brain volume, the ventricular system expands to fill the vacant space. In the elderly, accelerated regional volume

shrinkage in white and grey matter, may reflect heterogeneity arising from common occult conditions, such as preclinical or undetected dementia, hypertension, metabolic disorders or alcoholism (GUTTMANN, 1998; RAZ et al., 2005).

Studies on the relationship of cortical thickness in the aging process are important because they provide a local measure of alterations in grey matter morphology across the cortical surface. The patterns of regional change place important constraints on how atrophy may relate to the complex cognitive changes associated with aging. Cortical thinning presents itself since middle age, beginning in the third decade of life, in a widespread way, with significant age-related thinning in primary sensory, primary somatosensory and motor and association cortices, at mean rates of 0.01 mm/decade and greater rate (0.07mm/decade) in the primary motor cortex (SALAT et al., 2004). According to the literature, the frontal and temporal lobes are the most affected cortical regions, with shrinkage range of -0.8%/year in the frontal cortex and -0.67%/year in the temporal cortex (FREEMAN et al., 2008).

Although the evidence of differential age-associated regional brain shrinkage and cortical thinning is consistent across multiple studies (RAZ et al., 2010; RAZ; RODRIGUE, 2006; SALAT et al., 2004), less is known about age-related changes in microstructural properties of cerebral white matter, even though white matter changes in normal aging are very likely to play an important role in contributing to age-related cognitive decline. The absence of neuronal loss for whole-brain cell counting with increasing age, can be due to changes in the cortical structure, associated with WM structural changes, like changes in neuronal size, dendritic and axonal simplifications or glia cells alterations, rather than neuronal loss, implicating in age-related cognitive changes (FREEMAN et al., 2008; PAKKENBERG; GUNDERSEN, 1997).

1.3. WM integrity during the aging process: neuroimaging process

Numerous alterations in the brain structure and function with age affect total brain volume and WM integrity, that predicts cognitive decline. Studies demonstrated that cognitive decline related to the aging process are expressed after a threshold of structural deterioration (RAZ, 2000).

Diffusion imaging is the only imaging technique that enables investigations of WM microstructure and organization through fitting brain water diffusion data to a model and quantifying diffusion properties. Using a model called Diffusion Tensor, that will be further explained in the next section, it is possible to compute the eigenvalues and eigenvectors that describe the tensor in each voxel, to extract diffusion parameters: fractional anisotropy - FA (directionality of the diffusion of water), mean diffusivity - MD (the ability of water to diffuse, averaged over all directions), axial diffusivity - AD (diffusion of water in the main tensor direction) and radial diffusivity - RD (diffusion of water in the radial directions) (TOFTS, 2003). These parameters underlie on the WM microstructure, as axonal properties (constituents, diameters and packing density), myelin sheaths (constituents and role) and glia cells, and changes in these parameters can be interpreted as changes in the integrity of WM tissues. Several studies reported age-related differences in microstructural integrity of cerebral white matter, showing widespread declines in FA and increasing MD (SALAT et al., 2005; SULLIVAN; PFEFFERBAUM, 2006; SULLIVAN et al., 2001). MD regards the diffusion degree and FA measures the degree of diffusion directionality in the tissue, thus, increased MD and reduced FA associated with normal aging may be related to a number of age-related changes in white matter, as reduction in axon density (SULLIVAN; PFEFFERBAUM, 2006), decline in number and length of myelinated fibers (MARNER et al., 2003) and breakdown in the myelin sheaths (SULLIVAN; PFEFFERBAUM, 2006), among others.

From the modeling of diffusion within each voxel, it is possible to trace the possible fiber tracts in WM using tractography to visualize these brain connections. Tractography can be used to quantify diffusion metrics for the selected streamlines and provide quantitative measures from the brain tracts that

may reflect structural integrity of white matter fiber tracts. Several studies have related FA decrease and MD increase with age, suggesting these as sensitive markers of aging, that may precede atrophy in several brain regions (GIORGIO et al., 2010; HUGENSCHMIDT et al., 2008; MICHIELSE et al., 2010; TEIPEL et al., 2014; VOINESKOS et al., 2012). An anteroposterior gradient of age-related decline in FA is presented (SULLIVAN; ADALSTEINSSON; PFEFFERBAUM, 2006), and hypothesized as underlying cognitive decline of frontally-based functions (KOCHUNOV et al., 2007; SALAT et al., 2005). These alterations in the diffusion parameters in brain tracts during life span have been observed for several connections: corpus callosum (LEBEL; CAVERHILL-GODKEWITSCH; BEAULIEU, 2010; MICHIELSE et al., 2010; TEIPEL et al., 2014; VOINESKOS et al., 2012), uncinate fasciculus (HASAN et al., 2009; MALYKHIN et al., 2008; METZLER-BADDELEY et al., 2011), internal capsule (NUSBAUM et al., 2001), corticospinal tract (JANG; SEO, 2015; TANG et al., 2010) , fornix (JANG; CHO; CHANG, 2011; LEBEL et al., 2012), cingulum bundle (METZLER-BADDELEY et al., 2011; MICHIELSE et al., 2010), inferior longitudinal fasciculus (BENDER; VOLKLE; RAZ, 2016; VOINESKOS et al., 2012; WANG et al., 2016) and inferior occipitofrontal fasciculus (BENDER; VOLKLE; RAZ, 2016; WANG et al., 2016).

One more integrity parameter that can be analyzed from the diffusion data is the fiber density, which is a difficult parameter to be assessed, and can be defined in different ways. Fiber density (FD) can be defined as the density of WM fibers of a bundle passing through a voxel (ROBERTS et al., 2005), that demonstrated a strong correlation with the aging process, in different parts of the brain, as prefrontal, precentral, parahippocampal and cingulate gyrus, genu of the corpus callosum and temporal lobes (STADLBAUER et al., 2012). There is also a new definition for fiber density, known as Apparent Fiber Density (AFD), which measures the proportion space occupied by fibers within the voxel (RAFFELT et al., 2012). According to the best of our knowledge, there are no studies evaluating this parameter in the aging process yet. Both of these definitions agree in the matter that fiber density studies provide complementary information for assessing WM properties, and can be valuable to evaluate age-related changes.

The connectome is a way of describing the structural network connections between brain regions and how they are connected. Many authors describe that the brain structural networks in the human cerebral cortex, obtained from diffusion

data, are reproducible, complex and densely connected, and could be employed to track diseases (BASSETT et al., 2011; HAGMANN et al., 2008; OWEN et al., 2013; SPORNS; TONONI; KÖTTER, 2005). The structural connectivity network alterations in the brain during the aging process have been proven by several studies in the last decade. GONG et al. 2010 demonstrated age- and sex-related effects in the cortical organization and anatomical connectivity in the cerebral cortex . MONTEMBEAULT et al. 2012 provided evidence that reduced structural association characterizes the aging brain. WU et al. 2012 indicated that the organization of structural brain networks are affected by normal aging. ZHU et al. 2012 suggested that age changes structural network properties, reducing global efficiency and increasing local clustering. Mapping the connections and its alterations in pathologies, development and aging is a useful way to assess the structural changes that occur in the brain. Our research aims to evaluate the alterations in the WM structure and how it can be correlated with the GM structural alterations that can be detected through the cortical thinning of the regions that connects the endings of the tracts.

1.4. WM integrity and cortical thickness association in the lifespan

From previous findings, in the lifespan there are generalized and heterogeneous cortical thinning across the cortex, and a wide distribution of white matter degeneration, with a specific pattern. The changes in the cortical structure can be associated with WM structural changes, in a bidirectional way, ie, GM damage, related to neuronal functioning, is expected to lead to WM degeneration, and vice versa (DE STEFANO et al., 2003; WALLER, 1850). The literature relating both of these integrity parameters of the human brain is very scarce and it is of great interest to find an association between regional cortical thickness and diffusion integrity parameters of the connecting brain tracts. Since GM integrity would be responsible for the information processing and WM integrity responsible for the structural connections between the brain regions, instinctively one might presume that there should be some kind of association between them, however, as mentioned before the causality between them is still undefined.

Whole-brain analyses of the relationship between age-related alterations of FA and cortical GM thickness described a linear and positive relationship across the lifespan, considering that the age-related change in cortical density is a potential cause of the linear relationship between the FA and GM thickness in the aging process, presumed to relate with cerebral myelination alterations (KOCHUNOV et al., 2011). Another study examined the heterogeneous patterns of age-related GM and WM changes in the limbic system, proving diffusion measures of the limbic tracts were consistent with the GM degeneration patterns identified, supporting that structural integrity may provide important information about the cognitive alterations during aging (GRIEVE et al., 2011). Longitudinal studies allow the study of the unique aging process of each subject, a recent longitudinal study, with a 3.6 years follow-up on this relationship in specific brain tracts, demonstrated that changes in WM microstructure and cortical thickness are correlated in healthy adults in multiple cortical areas, some in the tract endings areas, and others that are not, leading to a understanding that WM and GM relations in healthy aging are global and tract specific (STORSVE et al., 2016).
With that in mind, the main goal of this project is to evaluate the relationship, if any, between white matter and gray matter cortical integrity in specific brain tracts and its cortical endings, that according to our knowledge, have not been evaluated yet. Cortical thickness measurements and diffusion parameters will be taken as biomarkers for the aging process, the diffusion parameters are depending on the intravoxel characterization and tractography algorithm chosen, that will also be evaluated in this study. Our hypothesis is that exist tract-cortical relations in the normal aging process for specific brain connections.

1.5. Objectives

The main goal of this project is to study the alterations in the structural connectivities of the brain throughout healthy aging, evaluating age-related regional cortical thinning and diffusion parameter changes. Voxel-based morphometry and tractography analysis will be applied for fiber integrity quantification, evidencing if there is a correlation between these two structural integrity parameters in the aging process.

The specific goals are to answer the following questions:

- Do the diffusion parameters follow a similar spatial alteration pattern in the brain aging?
- Are white matter alterations tract specific in the aging process?
- How the brain structural connectome is affected in healthy aging?
- Can the diffusion model affect the inferences about white matter integrity in the aging process using our MRI data?
- Are cortical thickness and tract integrity related for specific fiber tracts?

2. Theory

The data used to evaluate the aging alterations in the GM and WM integrity were magnetic resonance images obtained with two different techniques. In this chapter we will present the basic concepts of the image acquisitions and the integrity parameters that can be obtained from them.

2.1. Introduction to Magnetic Resonance Imaging

Magnetic Resonance Imaging (MRI) is a powerful imaging technique for visualization and analysis of a broad range of properties of soft tissues of the body. There are many books that can be consulted about this topic. Here our aim is to establish the bases of this phenomenon and its feasibility of creating medical images. Magnetic Resonance phenomenon is based on the ability to manipulate and detect the magnetic interactions of the protons in hydrogen atoms (H) in water, fat and other molecules, between them and with external magnetic fields. The proton in the hydrogen nuclei is positively charged and has a magnetic dipole moment. When an external static field (B_0) is applied, this proton starts precessing around this field, with an angular frequency referred as Larmor frequency (equation 1), that depends on the strength of the static field and the gyromagnetic ration of the nucleus, in water the hydrogen proton has a γ value of 2.68×10^8 rad/s/tesla.

$$\omega_0 = \gamma \cdot B_0 \qquad \text{(Eq. 1)}$$

When several protons are considered, a liquid magnetization ($\vec{M}$) is generated from the sum of the individual magnetic moments. Basically, the proton spins are aligned parallel and antiparallel to the magnetic field, and the sum of those results in the net magnetization, that contributes to the signal to be detected in MRI. The magnetization vector can be described by two components, longitudinal and transverse, referred to $\overrightarrow{B_0}$ direction. The longitudinal magnetization, aligned along the external field direction, can be hit by pulsing radiofrequency waves ($\overrightarrow{B_1}$) that remove the magnetization from equilibrium state, making the protons spin at a particular resonance frequency in its direction. Once the RF pulse stops, the

magnetization goes back to the equilibrium, aligned to the static field, this movement involves relaxations processes. The temporal variation of the transverse component of the magnetization in the relaxation process is detected by the receiver coil and generates the MR signal, detecting the NMR phenomenon.

Moreover, the transverse magnetization can be explored to provide spatial information, space coding is done by the application of external magnetic fields, called gradients, that have a linear spatial pattern to codify the magnetization frequency according to the spatial position. The gradients are applied in the physical directions (x, y and z) in different moments of the sequence. The slice selective gradient ($\overrightarrow{G_S}$) is applied simultaneously to the RF pulse, selects the slice position and its thickness. The phase or preparation gradient ($\overrightarrow{G_P}$) is applied without any RF pulse and before the reading process, it is used to create planes in the sample containing transverse magnetization with equal phases, due to spatial frequency variation. The readout or frequency gradient ($\overrightarrow{G_F}$) is applied without any RF pulse and during the reading process, creating a frequency-encoded signal to be detected. The intensity of the image signal is mainly due to the proton density within the voxel, aka, water concentration in that location. There are other effects that influence the signal intensity, as the relaxation times T1 and T2 (longitudinal and transverse relaxation times).

There are different sequences with combinations of RF and gradient pulses that make possible a range of image contrasts, due to the physical properties of the tissues in the body, as different proton densities and relaxations times. Two pulse sequence parameters that are very important for contrast in the images are the repetition time (TR) and echo time (TE). TR is the time interval between consecutive excitation RF pulses and TE is the time interval between the RF pulse and the echo. In the brain, some imaging characteristics can be quantified and used to analyze different aspects of its composition and evaluate its integrity.

2.2. Anatomical Image – T1-weighted

A common imaging sequence to evaluate the anatomical structure of the brain is a high spatial resolution T1-weighted image, in which the contrast and brightness are predominately determined by T1 properties of the tissues. T1 is the longitudinal relaxation time, that means the inverse of the rate at which the excite protons return to the longitudinal equilibrium. This parameter is quite different for each soft tissue in the brain, making it possible to delineate them in the image. T1-weighted images are produced using short TE and TR in a Magnetization Prepared Rapid Acquisition Gradient Echo (MP-RAGE) sequence, Figure 5. An initial 180 degree inversion pulse is applied, followed by a GE imaging sequence. The magnetization aligned with the external field (M_0) in the longitudinal plane is inverted in the preparation pulse, to provide the desired contrast, then, with a 90 degree pulse, the magnetization is excited to the transverse plane using frequency-encoded gradient fields. The frequency gradient is used twice in succession in opposite polarities, the first is negative to dephase the spinning

Figure 5 3D MP-RAGE pulse sequence.

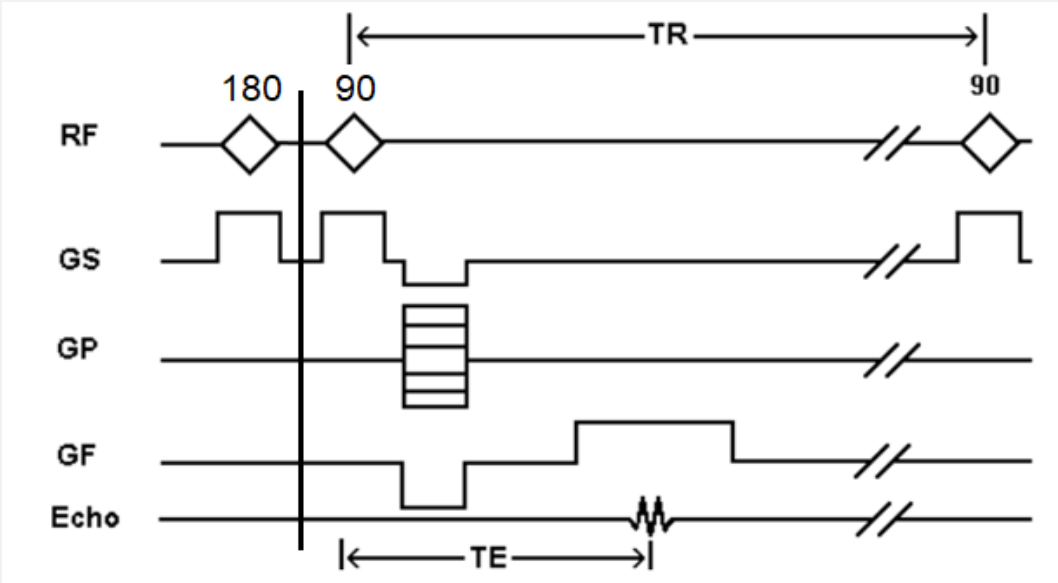

RF - radiofrequency pulses separated by a Time of Repetition (TR); GS – gradient slice selection channel; GP – gradient phase encoding channel; GF – gradient frequency channel and Echo row (indicating acquisition channel), where the echo occurs after a Time of Echo after the RF pulse (TE).

Source: Prof. Frank Gaillard on March 1, 2013. Available at: https://radiopaedia.org/images/2987629.

protons and right after a positive one to rephase the protons is. Due to the different T1 characteristic of the tissues, this sequence allows a good contrast in the brain, creating anatomical images to be studied, Figure 6.

Figure 6 Structural 3D-T1 images used to measure cortical thickness of gray matter.

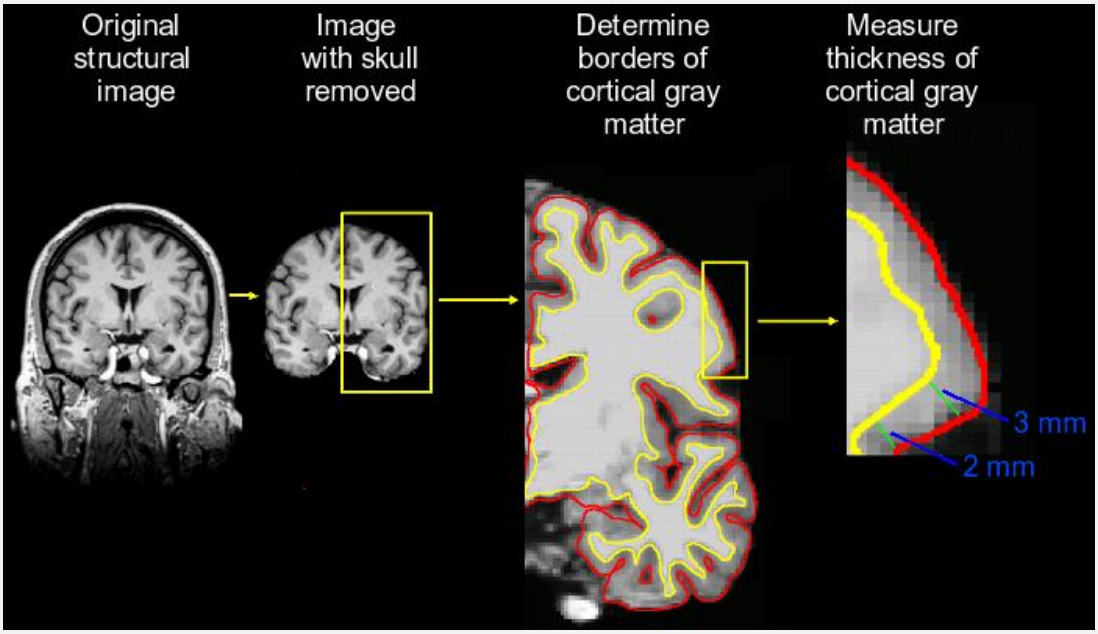

Source: Available at: http://www.martinos.org/neurorecovery/technology.htm

Figure 6 demonstrates the idea of how the anatomical 3D-T1 images can be used to extract structural information, as the thickness of cortical gray matter. This measure is automated using FreeSurfer software (FISCHL; DALE, 2000) that uses the image GM/WM contrast to determine the borders of the cortical gray matter and uses the distance between the borders to obtain its thickness in each part of the brain.

2.3. Diffusion Imaging

Diffusion is a mass transport process that describes the molecular and particular movement in a fluid, by the thermal random movement. This motion is best described in statistical terms by a displacement distribution. The displacement distribution describes the proportion of molecules that undergo displacement in a specific direction and to a specific distance. In a fluid with no restrictions to the movement, the one-dimensional displacement of an individual free molecule can be described by a Gaussian distribution. For this specific case of isotropic

diffusion, we have the same displacement distribution (same function and parameters to describe it) for each direction in the 3D-space, for example the molecular water in the cerebrospinal fluid (CSF), Figure 7a. In an environment with restrictions to the movement, the molecular diffusion becomes preferential in a specific direction, Figure 7b, called anisotropic diffusion.

Figure 7 Isotropic and anisotropic diffusion.

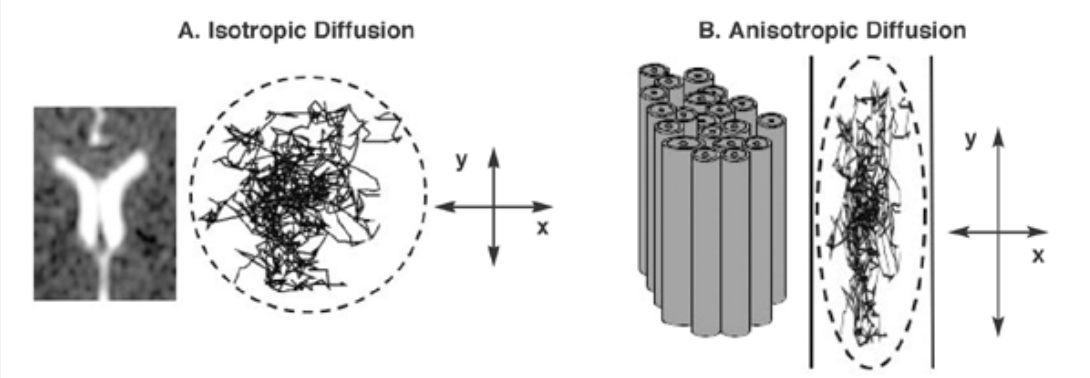

(A) Isotropic diffusion: Water molecules diffusion in an unconstrained environment, as in the cerebrospinal fluid, motion occurs equally and randomly in all directions. (B) Anisotropic diffusion: In white matter tracts the motion is oriented more in one direction than another due to the WM architecture.

Source: Rosenbloom M, Sullivan EV, Pfefferbaum A. Using magnetic resonance imaging and diffusion tensor imaging to assess brain damage in alcoholics. Alcohol Res Health. 2003;27(2):146-52.

The limitations to the movement can be in two ways, restricted or hindered. In the first case, the displacement of the water molecules is restricted in one direction and there is no movement across the other directions, due to a confinement of the molecules by barriers in the environment. The second one limits the diffusion of the molecules in the adjacent directions due to a restriction in the environment that does not confine the molecules completely.

We are interested in the diffusion of water in brain tissues, due to the architecture of white matter fibers, the movement of water in it is more hindered in one direction, depending on the position of the brain that is being analyzed and its composition. In this circumstances, the random movement of water molecules depends of many factors, as restrictions due to cell membranes, macromolecules and cytoskeleton (BASSER; MATTIELLO; LEBIHAN, 1994; MOSELEY et al., 1990; TANNER; STEJSKAL, 1968). The parallel orientation of the nerve fiber

tracts make the diffusion of water molecules in white matter hindered and anisotropic in the extracellular space, Figure 7b.
Using the correct pulse sequence in the MR scanner it is possible to evaluate the diffusion of water in the tissues and estimate the characteristics of the white matter fibers bundles.

2.3.1. Image Acquisition

Diffusion weighted imaging (DWI) sensitizes and detects the signal reduction due to the random movements of water protons in the tissues, enhancing diffusive attenuation with the application of pulsed magnetic field gradients. The magnetic field gradients introduce a linear magnetic field inhomogeneity in a specific direction, dependent of the combination of the physical gradients in the MR scanner.
This kind of acquisition became possible in 1965, when Stejskal and Tanner introduced the pulsed gradient spin echo (PGSE) sequence (STEJSKAL; TANNER, 1965). In the most simple example of this diffusion weighted sequence, short gradient pulses (with duration of δ, G amplitude and separated by a diffusion time Δ), called as diffusion gradients, are applied before and after the refocusing RF pulse in a spin echo sequence, Figure 8.
Even with no diffusion gradients the water molecules are spreading around in diffusion movements, thus, each molecule accumulates a phase according to the path it went. The transverse magnetization is the result of phase coherence of many molecules, in the diffusion process there is a loss of phase coherence and, therefore, a loss of transverse magnetization.
The application of the gradient pulses helps to emphasize the loss of phase coherence in the preferential diffusion directions. These gradient pulses dephase and rephase the water protons, sensitizing the signal to molecular motions (diffusion weighted). Due to the motion of the water molecules, the perfect refocusing occurs when the water protons have not changed position between the application of the two dephase-rephase gradient. So, if there is water movement in the direction of the applied gradient, the signal is attenuated, due to imperfect rephasing of these molecules. This is measured by the diffusion

coefficient (*D*), that is the magnitude of diffusion within the tissue, in the gradient direction used for the acquisition.

Figure 8 MRI pulse sequence for diffusion weighted imaging.

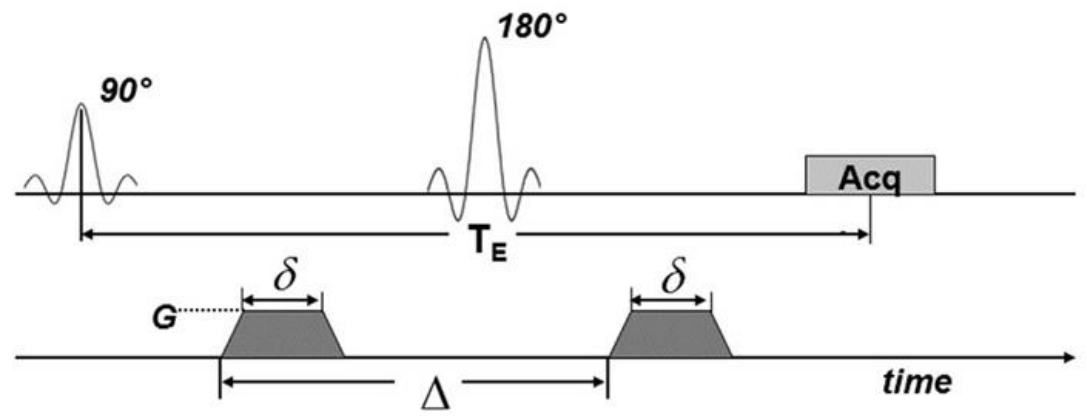

Diffusion gradients (dark shading) were applied on both sides of the 180° pulse. TE is the echo time; Acq indicates the signal acquisition block. G is the amplitude of the diffusion gradients, δ is their duration and Δ is the delay time between them.

Source: VAGHEFI, E. An exploration into diffusion tensor imaging in the bovine ocular lens. Frontiers in Physiology, v. 4, 2013

The brain fibers architecture make the diffusion of water in the white matter tissues anisotropic and hindered, in this manner, depending on the gradient direction, signal loss can be identified in regions of known fiber bundles, fasciculi and tracts. In Figure 9, the isotropic region selected in red is the cerebrospinal fluid, and the ones in yellow (top-down) are corpus callosum (latero-lateral connection), corticospinal tract (cranio-caudal connection) and inferior fronto-occipital fasciculus (antero-posterior connection).

The signal of the DW images can be modeled as shown in equation 2, in which the exponential attenuation is produced by the product of factor *b* and the diffusion coefficient *D*.

$$S = S_0 \cdot e^{-bD} \qquad \text{(Eq. 2)}$$

Where *S* is the DW signal and S_0 is non-DW signal (SE acquisition without the gradients). Factor *b* is a function of the diffusion weighted gradients, this factor reflects the strength and timing of the gradients, equation 3.

$$b = (\delta G \Delta)^2 \left(\Delta - \frac{\delta}{3}\right) \qquad \text{(Eq. 3)}$$

Figure 9 Diffusion weighted images.

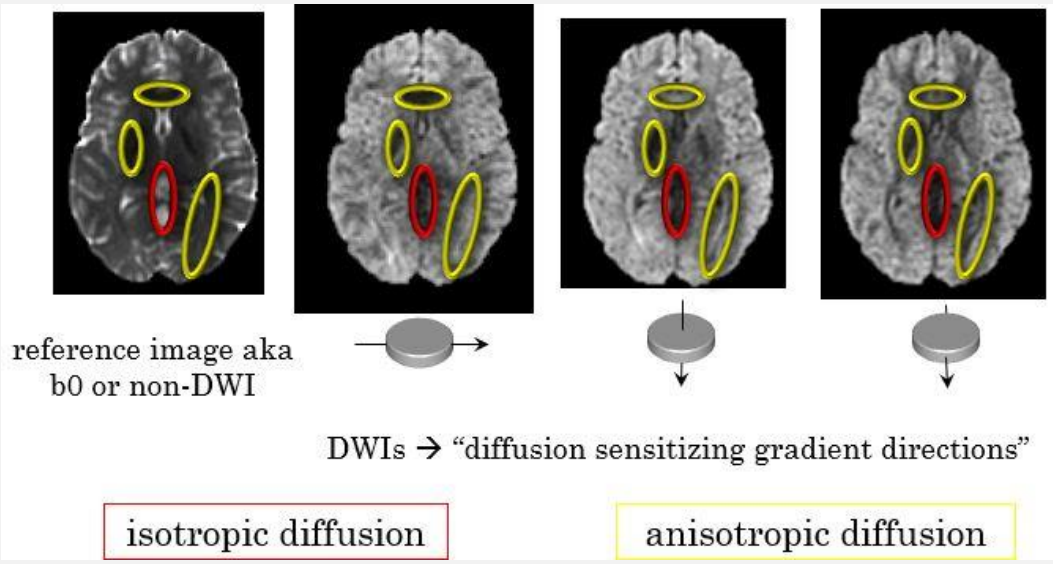

Highlighted regions of isotropic (red) and anisotropic diffusion (yellow), in three orthogonal directions of the applied diffusion gradients.

Source: Prof. Dr. Alexander Leemans lecture

The diffusion coefficient for one specific direction can be estimated by collecting two images: S_0 with no diffusion gradients applied (aka, non-DW or *b0* image) and *S* with diffusion gradients applied in a desired direction with non-zero *b* factor. Both images are weighted by the same magnetization M_0, and recovery times *T1* and *T2*, the only difference is the diffusion effect in the second one. Thus, the diffusion coefficient for that direction can be calculated as:

$$D = \frac{\log[S_0/S]}{b} \qquad \text{(Eq. 4)}$$

As mentioned, the *D* value is for one specific direction, in which the image was acquired, therefore, instead of acquiring one DW image in only one direction, it is better to acquire DW images in several directions, so the signal loss in each one is due to the displacement of water molecules in the directions of the applied gradients. Increasing the number of DW images acquired with diffusion gradients in different directions, considering the head as a sphere that we want to cover more completely as we can we can obtain more information about the intravoxel diffusion in each part of the brain.

This kind of acquisition of diffusion weighted images in different directions, all with one value of *b* factor (usually in the clinic 1000s/mm^2), is called single shell

acquisition, in which there is a Gaussian distribution of diffusion. For b-values higher than 1000s/mm^2 the diffusion pattern is non-Gaussian, enabling different signal visualizations describing the displacement patterns of the water molecules in the brain in these different environments.

Describing the diffusion pattern using MRI images have the potential of providing useful information about the cellular physiology, structure and its connections within the brain (TOFTS, 2005). For that it is necessary to use an adequate model according to the acquired images, to extract the information that will be able to relate the diffusion parameters extracted from the image processing with biological tissue properties.

2.3.2. Modeling

There are many different models to describe the intravoxel diffusion in living tissues. In the context of the present work, two of them will be discussed: Diffusion Tensor (DT) model and Constrained Spherical Deconvolution (CSD) model. These were chosen according to the data we have, the first model is the standard model to describe diffusion with one main diffusion direction per voxel, the second one is a more refined one that allows more than one diffusion direction per voxel.

DT model characterizes the Gaussian diffusion pattern using a tensor to describe the displacement of water molecules in three main axis. The MR signal from the DW acquisitions (in different directions using only one b-value) can be described as equation 5.

$$S_k = S_0 e^{-b\, g_k^t \cdot \vec{\vec{D}} \cdot g_k} \qquad \text{(Eq. 5)}$$

Where, S_k is the DW signal along diffusion gradient g_k, S_0 is the non-DW signal (*b0*), *b* is the diffusion weighting factor and $\vec{\vec{D}}$ is the apparent diffusion tensor. The diffusion tensor, $\vec{\vec{D}}$, is a 3x3 matrix of diffusivities characterizing the displacements in three axis, equation 6.

$$\vec{\vec{D}} = \begin{bmatrix} D_{xx} & D_{xy} & D_{xz} \\ D_{yx} & D_{yy} & D_{yz} \\ D_{zx} & D_{zy} & D_{zz} \end{bmatrix} \qquad \text{(Eq. 6)}$$

The tensor is a 3D covariate matrix of displacements, in which the diagonal elements are the diffusivities in the orthogonal axes and the other elements are the correlations between the diffusivities in these axes. For this model, it is necessary at least six DW images acquisitions to determine the tensor parameters.

From the tensor diagonalization three eigenvalues ($\lambda_1, \lambda_2\ and\ \lambda_3$) and eigenvectors ($\overrightarrow{v_1}, \overrightarrow{v_2}\ and\ \overrightarrow{v_3}$) can be extracted ($\lambda_1>\lambda_2>\lambda_3$). From these new parameters, DT model can be interpreted as an ellipsoid that represents the shape of diffusion within each voxel, Figure 10.

Figure 10 Ellipsoid representing the diffusion tensor.

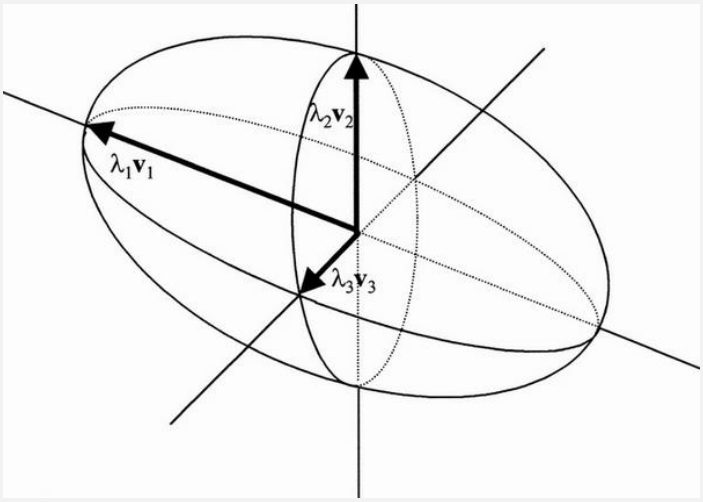

Eigenvalues and eigenvectors in each ellipsoid axis.

Source: Wiegell MR, Larsson HB, Wedeen VJ. Fiber crossing in human brain depicted with diffusion tensor MR imaging. Radiology. 2000;217(3):897-903

The main ellipsoid axis and its shape represent the main diffusion direction and how anisotropic is the water diffusion within each voxel of an image. Combining color encoded anisotropy information with the ellipsoid representation it is a very nice way of visualizing the diffusion tensors within the brain, Figure 11. The colors represent the main direction of the diffusion, according to the first eigenvector of the tensor (v_1). In a general convention, green, blue and red colors indicate the antero-posterior, cranio-caudal and latero-lateral directions, respectively. The eccentricity of the ellipse is related to how anisotropic it is the diffusion.

Figure 11 Ellipsoids representing the diffusion tensor in each voxel in a mid-sagittal view of the brain.

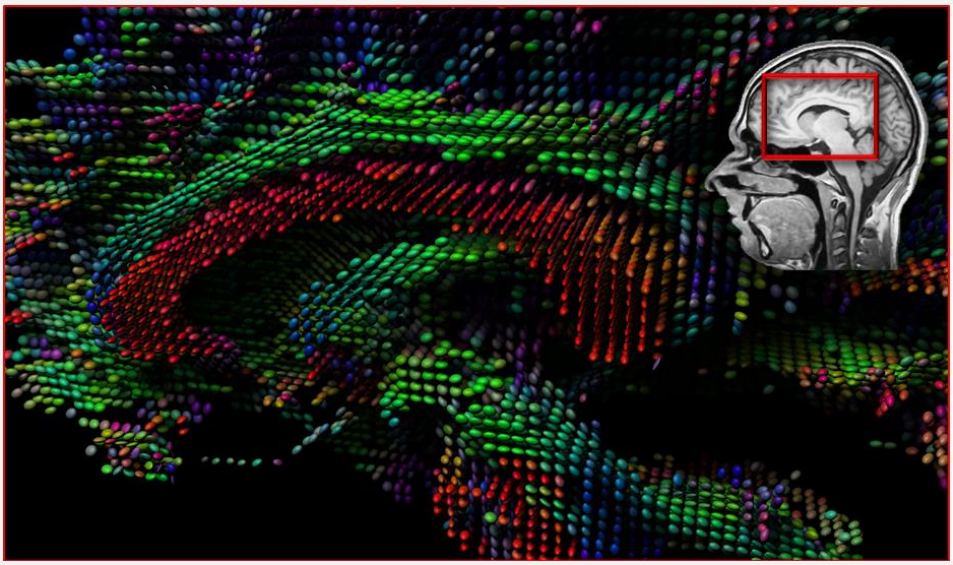

Eigenvalues and eigenvectors in each ellipsoid axis.

Source: Prof. Dr. Alexander Leemans lecture

The DT model has been widely used and provides many useful information, however, there are some limitations and weaknesses, as the modeling in voxels containing more than one fiber bundle (ALEXANDER; BARKER; ARRIDGE, 2002; BEHRENS et al., 2007), being unable to distinct many fiber orientations within the voxel (ASSAF et al., 2004), resulting in a poor fit of the diffusion data in many brain regions. Around one third of the WM voxels present voxels with crossing fibers (BEHRENS et al., 2007).

The spherical deconvolution method estimates the fiber orientation distribution (FOD) within the voxel from the DW data without prior knowledge about the number of fiber bundles crossing in the same place (TOURNIER et al., 2004). For optimal use of this model, it is indicated high-angular resolution DW data, with *b* values in a range of 2000-3000mm/s^2 and more than 40 diffusion gradient directions.

This method expresses the DW signal, $S(\theta, \phi)$, from high angular diffusion data, as a convolution, over spherical coordinates, between the response function and the *FOD*, equation 7, illustrated in Figure 12.

$$S(\theta, \phi) = F\ (\theta, \phi) \otimes R(\theta) \qquad \text{(Eq. 7)}$$

Figure 12 2D illustration of the DW signal S within a voxel containing two fiber bundles with different orientations

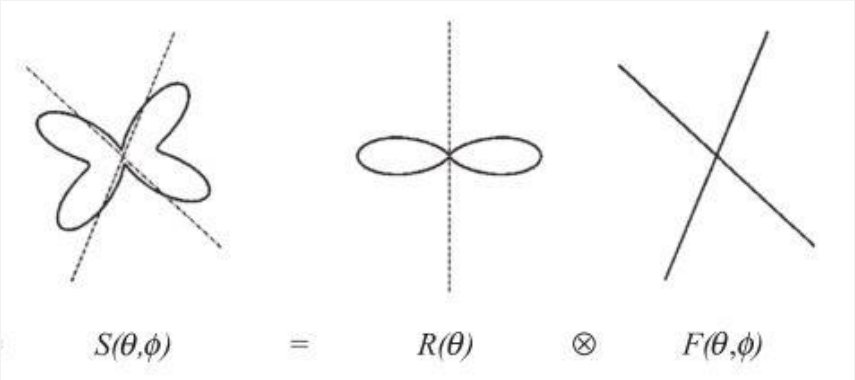

The convolution over spherical coordinated between the response function R and the fiber orientation distribution F.

Source: TOURNIER, J.-D. et al. Direct estimation of the fiber orientation density function from diffusion-weighted MRI data using spherical deconvolution. NeuroImage, v. 23, n. 3, p. 1176–1185, nov. 2004. (adapted)

The axially symmetric response function, *R(θ)*, describes the attenuation of the signal for a single fiber bundle align in the z-axis, and the FOD, *F(θ, ϕ),* describe the fiber orientations within the voxel. The response function *R* is estimated from de DW data, using the voxels with higher values of fractional anisotropy, assumed to contain only one fiber bundle. The *FOD* can be estimated by performing the reverse function of the spherical deconvolution, equation 8:

$$F\ (\theta, \phi) = \ S(\theta, \phi) \otimes^{-1} R(\theta) \qquad \text{(Eq. 8)}$$

The SD method is susceptible to noise, producing spurious negative lobes in the *FODs*. Thus, it is necessary to use a low-pass filter to attenuate or eliminate high angular frequency components from the *FOD*. This filter implementation is called filtered spherical deconvolution (filtered SD), however, instead of filtering there is the option of constraining these negative values in the *FOD*. The *FOD* is expected to be mostly over zero, defined by peaks corresponding to the fiber orientations, and the elimination of under zero values reduces the high frequency noise. This method of constraint the *FOD* is referred as constrained spherical deconvolution (CSD) (TOURNIER; CALAMANTE; CONNELLY, 2007), that has shown to be a robust way to model the diffusion within the voxel especially for high *b* values (TOURNIER et al., 2008).

There are many approaches to modeling diffusion data, to better resolve this limitations, as Q-ball imaging (TUCH, 2004), Diffusion Kurtosis Imaging (DKI) (JENSEN et al., 2005), Diffusion Spectrum Imaging (DSI) (WEDEEN et al., 2005), among many others. They all require a more refined acquisition protocol to the diffusion data with more diffusion directions and higher *b* values.

According to the acquisition protocol and the idea of what to understand and extract from your data, one can choose which model fits better to the research goals. After the decision of which is the best model for your analysis, one can explore the data, one type of analysis to understand the brain structure is to evaluate the brain pathways using tractography.

2.3.3. Tractography

From intravoxel diffusion characterization, tractography is a tool that allows a three-dimensional visualization of the reconstructed brain fiber tracts. It is a unique non-invasive technique to evaluate brain connections in living humans. There are different algorithms that can be used to reconstruct the streamlines that represent the fiber pathways of the brain. The tractography algorithms are model dependent, the fiber orientations in each voxel are used to reconstruct the pathways and connections of the brain. The simplest way, called deterministic or streamline tractography, is to start in many seed locations in the brain and follow the preferred directions of the streamlines until reach a stopping point.

When modelling the DW data to the DT, one of the most used and robust tractography method is called fiber assignment by continuous tracking (FACT) (MORI et al., 1999), which, continuously connects the voxels that have similar tensor orientations, considering angle and anisotropy thresholds to determine the end points of the streamlines.

As mentioned before, there are limitations in the DT model, as partial volume effects of different fiber bundles crossing within the voxels, many brain tracts pass through regions where many fiber populations are intersecting along their path, making tractography algorithms that rely on the DT model to sometimes reconstruct non-realistic tractograms.

Tractography reconstructions based on CSD seems to be a good option to get more realistic brain tracts (TOURNIER; CALAMANTE; CONNELLY, 2012). This deterministic method uses the FOD information in spherical harmonic basis, to connect the streamlines, step by step using local interpolations in tangent orientations to locate and connect the FODs peaks. The end points are similar to the prior, the level of anisotropy and angle threshold.

It is possible to reconstruct whole brain tractographies and, after that, to select specific tracts and connections of the brain from those. There are some well-known brain tracts that can be selected based on anatomical information (WAKANA et al., 2007). These tracts can go through structural alterations in some diseases and in the healthy aging process, as mentioned before on Chapter 1, there are some diffusion parameters that are used to quantify and evaluate the integrity of the brain tracts for these situations.

2.3.4. Metrics

From the diffusion imaging it is possible to evaluate a few characteristics in the living brain. There are some parameters that can be extracted from the DW data that can be interpreted as myelination level, fiber density and axonal diameter, among other information from the characteristics of the diffusion of water in the tissue. These parameters can be divided into intra and intervoxel, the first are related to biomarkers estimated within each voxel, the second uses the intravoxel information to quantify the fiber connections in the brain.

In the DT model, the eigenvalues ($\lambda_1, \lambda_2\ and\ \lambda_3$) and eigenvectors ($\overrightarrow{v_1}, \overrightarrow{v_2}\ and\ \overrightarrow{v_3}$) are calculated and used to extract information concerning the integrity of the white matter structure. Images are created using this information to reflect the diffusion properties of the brain tissues. The most common intravoxel parameters are the fractional anisotropy, mean, axial and radial diffusivities.

Fractional anisotropy (FA), describes the level of anisotropy of the water molecules within the voxel, how directional is the diffusion. This value varies between 0 and 1. In a region that has perfect isotropic diffusion, all the eigenvalues are the same, the diffusion tensor describes a sphere and FA=0. In regions where the diffusion has a preferential direction, FA values are above 0

until 1. For anisotropic diffusion, the more the eigenvalues differ the more the diffusion ellipsoid becomes elongated. The calculation of FA is shown in equation 9:

$$FA = \sqrt{\frac{3}{2}} \frac{\sqrt{(\lambda_1-\bar{\lambda})^2+(\lambda_2-\bar{\lambda})^2+(\lambda_3-\bar{\lambda})^2}}{\sqrt{\lambda_1^2+\lambda_2^2+\lambda_3^2}} \qquad \text{(Eq. 9)}$$

The mean diffusivity (MD), is calculated as the average of the eigenvalues, equation 10, the axial diffusivity (AD) is the main eigenvalue, equation 11, and the radial diffusivity (RD) is the average between the transverse eigenvalues, equation 12.

$$MD = \frac{\lambda_1+\lambda_2+\lambda_3}{3} = \bar{\lambda} \qquad \text{(Eq. 10)}$$

$$AD = \lambda_1 \qquad \text{(Eq. 11)}$$

$$RD = \frac{\lambda_2+\lambda_3}{2} \qquad \text{(Eq. 12)}$$

These parameters can be interpreted according to the brain structure, as axonal density, WM maturation, axonal degeneration and myelination. FA measures indirectly the microstructural orientation of the underlying axonal architecture of the WM, associated to myelin, axonal membranes and transports (CLARK et al., 2011; SCHOLZ; TOMASSINI; JOHANSEN-BERG, 2014; WINSTON, 2012). It is shown higher values of FA for the WM compared to the GM, it is highly sensitive to microstructural change but not specific to the type of change. MD is a measure of the amount of diffusion occurring and the membrane density, the value is very similar for gray and white matter, it is sensitive to cellularity, edema and necrosis of the tissues (CLARK et al., 2011; WINSTON, 2012). AD have not a direct interpretation about the tissue integrity, but it is related to axonal integrity, it has shown to change in WM alterations and pathologies, for example, decrease AD appear in axonal injuries (WHEELER-KINGSHOTT; CERCIGNANI, 2009). RD is related to degree of restriction due to myelination levels, axonal diameters and fiber density (WHEELER-KINGSHOTT; CERCIGNANI, 2009).

Using the CSD diffusion model it is possible to assess another intravoxel WM integrity parameter, AFD, that describes the density of fibers in the white matter, measured by the proportion of space occupied by the fibers aligned in each direction (RAFFELT et al., 2012, 2017). It is used to compare this parameter between groups, and it makes possible to evaluate the effects in each direction.

One intervoxel analysis of the diffusion data is to construct a connectome from the whole brain tractograms, evaluating the connections between particular brain regions. A connection matrix is built summarizing the fibers connecting every cortical region, from a previously anatomically parcellated brain. Network connection parameters can also be evaluated to comprehend the maps of neural links in the brain. Global and local brain connectivity aspects can be assessed using network parameters as global and local efficiency, betweenness centrality, among others, to evaluate the structural connectivities in the aging brain (RUBINOV; SPORNS, 2010; SPORNS; TONONI; KÖTTER, 2005). This parameters describe how the network connections are altering, the local efficiency of a node describes how efficiently its neighbors exchange information when this node is removed, global efficiency evaluate how efficient is the information exchange in the entire network, and betweenness centrality represent the degree on connection between nodes based on shortest path between them. The structural analysis of the brain is performed using the anatomical and diffusion images to extract information related to the integrity of white matter and its connections within the brain. There are different models to comprehend our data and many parameters that can evaluate the microstructural changes in brain tissues. The methodology used for this healthy aging study is described next.

3. Methods

The materials and methods used in our study are detailed in this chapter, including casuistry, acquisition protocols, image processing for cortical thickness and diffusion data, evaluation of tractography algorithms, tract selection, connectome studies and statistical estimates.

3.1. Subject Description

- Clinics Hospital of Ribeirão Preto

The study was approved by the local Research Ethics Committee of the College of Philosophy, Sciences and Literature of Ribeirão Preto, University of São Paulo, with the Clinics Hospital of Ribeirão Preto as a co-participant institution. The image data were collected retrospectively from the Center of Image Sciences and Medical Physics, in the Medical School of Ribeirão Preto, University of São Paulo (CCIFM/HC-FMRP), with the approval of the Radiology Department head, Prof. Dr. Antonio Carlos dos Santos. The data consists of DWI and T1-weighted images of 164 healthy individuals, aged between 18 and 83 years old, acquired in a 3T Philips Achieva MR scanner. The images were collected by fellow researchers, between 2009 and 2016, in the university hospital for their projects, with approved Research Ethics Committee, and they politely gave us access to their data.

The subject's data were included in our analysis based on three inclusion criteria: (1) no previous neurological diseases, (2) have both DWI and T1-weighted images, (3) sufficient image quality. From the initial 164 individuals, one was excluded by the criteria number one, four by number 2 and one by number 3 (reconstruction of the image was not done properly due to a different DWI sequence used in the scanner). The remaining 158 subjects were classified in three categories by their age: Group 1 – individuals aged between 18 and 40 years old, Group 2 – between 41 and 60 years old and Group 3 – over 61 years

old. Table 1 and Figure 13a show the information about the subjects from each group.

Table 1 Sample characteristics of the subject groups.

Group	Number of subjects	Ages (years)	Mean Age (years)
1	78 (43 Male)	18- 40	27.1
2	34 (19 Male)	41-60	49.8
3	46 (15 Male)	60-83	69.1
Total	158 (77 Male)	18-83	44.2

Figure 13 Demographic characteristics

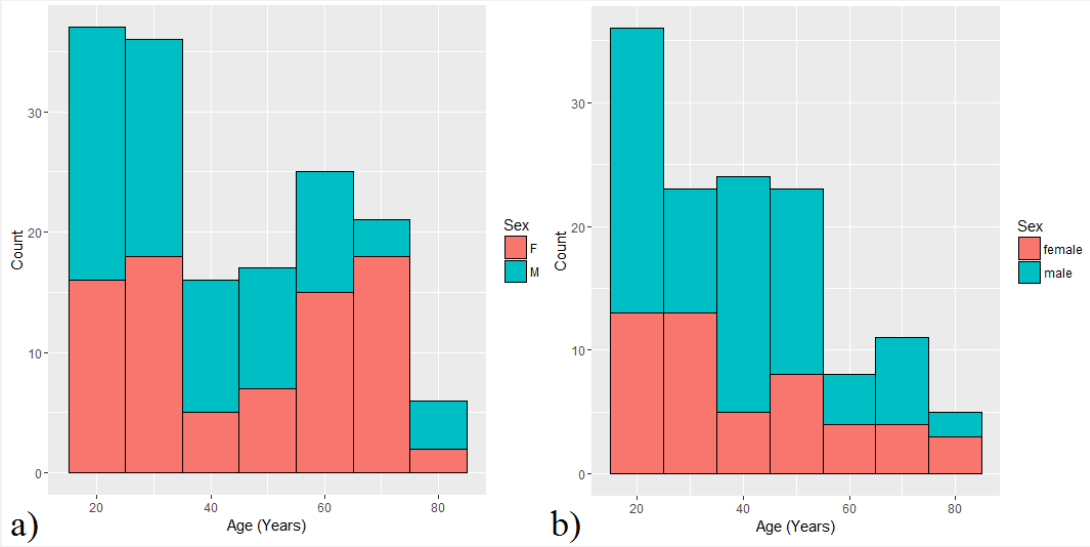

Ribeirão Preto (a) and the NKI/Rockland sample (b) data.

Source: Author

- NKI/Rockland sample

The NKI/Rockland sample (http://fcon_1000.projects.nitrc.org/indi/pro/nki.html) (NOONER et al., 2012) is an open neuroimaging sample, consisting of MRI data obtained from subjects aged between 4 and 85 years-old. All individuals underwent diagnostic psychiatric interviews, and a battery of psychiatric, cognitive and behavioral assessments, gathering the information of healthy individuals, with anatomical images.

The data was collected at NKI located in Orangeburg, New York, in a 3T SIEMENS MAGNETOM TrioTim MR scanner. The images from 130 (80 Male) right-handed subjects, aged between 18 and 81 years old (mean age: 40.4 years old), free of visible movement artifacts were used. Figure 13 b shows the information about the subjects used in this study.

3.2. Acquisition Protocol

- Clinics Hospital of Ribeirão Preto

The images were acquired using a 3T Achieva Philips MR scanner, installed in the Clinics Hospital of Ribeirão Preto, with a head coil of eight channels. The sequences used were the standard ones in the clinic for the anatomical (3D-T1) and diffusion (DWI) images. The sequence parameters were the following:
Anatomical images: High resolution 3D GE sequence T1 weighted, MPRAGE with the following parameters: TR/TE = 2500/3.2 ms, 7.0 ms time echo spacing, 900 ms inversion time, voxel size= 1x1x1 mm^3, flip angle = 8°, FOV = 240x240mm^2, 160 slices.
Diffusion images: SE sequence combined with EPI acquisition, with the following parameters: TR/TE = 9300/54 ms, pixel size = 2x2 mm^2, slice thickness = 2 mm, EPI factor = 67, FOV = 256x256 mm^2, acquisition matrix = 128x128 pixels, 60 slices, 33 diffusion gradients, being 32 with b=1000 s/mm^2 and one with b=0, overplus= no.
The REC/PAR images collected from the scanner were converted to NIfTI format using dcm2nii extension from MRIcroGL (http://www.mccauslandcenter.sc.edu/mricrogl/).

- NKI/Rockland sample

The images were acquired in a 3T SIEMENS MAGNETOM TrioTim scanner, installed at NKI. The sequences used were the anatomical (3D MPRAGE).

Anatomical images: MPRAGE, 3D GE sequence T1 weighted, with the following parameters: TR/TE = 2500/3.5 ms, 8.2 ms time echo spacing, 1200ms inversion time, voxel size= 1x1x1 mm^3, flip angle = 8°, FOV = 256x256mm^2, 192 slices.

3.3. Cortical Thickness Data Processing

Anatomical images (3D-T1w) were processed using the *recon-all* routine in Freesurfer v5.3.0 (FISCHL, 2012), resulting in the following anatomical information: cortical thickness, area and volume and white matter volume estimates based on Desikan-Killiany (DESIKAN et al., 2006) and Destrieux (FISCHL et al., 2004) atlases, Figure 14. Desikan-Killiany parcellation has 35, and Destrieux has 74 brain regions in each hemisphere. From the automatic cortical parcellation file created in the *recon-all* procedure, we created cortical parcellated volumes for the Destrieux parcellation.

Figure 14 Anatomical data preprocessing

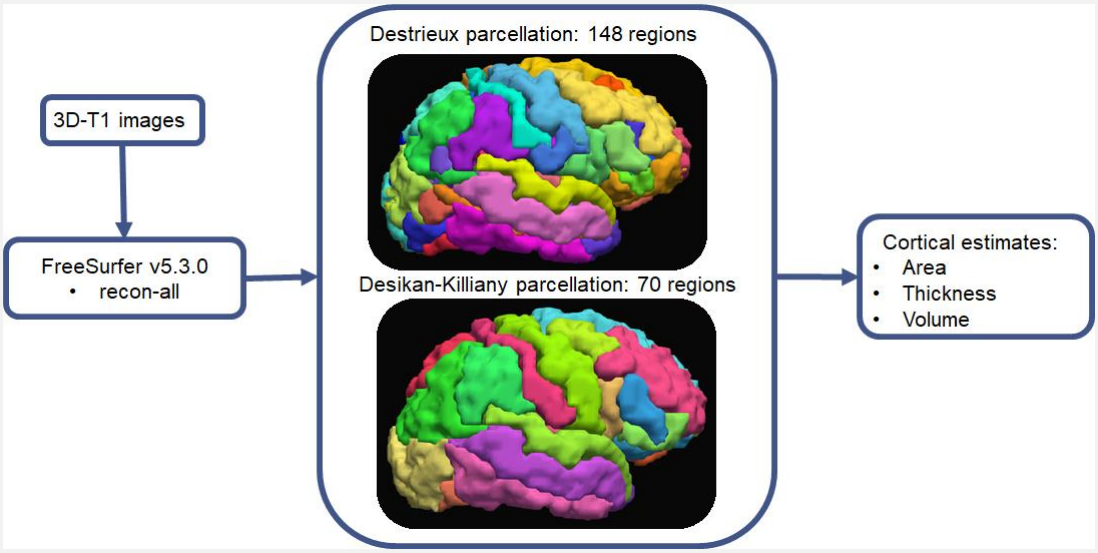

Source: Author

Anatomical and DWI images were corregistered, at FreeSurfer to create a registration file that describes a rigid-body transformation from the diffusion to the structural space. The anatomical volume was resampled into the diffusion space, applying the inverse transformation to our input volumes, so the parcellation

volumes are in accordance with the diffusion images orientation. The volume created contain the information of all parcellated regions, to separate each volume of the parcellation, the volume (or volume-encoded surface file) was binarized based on matching values from its color look-up-table (LUT). The parcellated volumes are used as ROIs for the selection of the tracts.

3.4. Diffusion Data Processing

Prior to data analysis, a basic and commonly used preprocessing pipeline was performed on the DWI data using two different softwares, Figure 15.

In FSL software (FMRIB, Oxford, England) (JENKINSON et al., 2012) the preprocessing pipeline includes eddy current distortions correction, brain extraction using BET, tensor model was fitted and FA and MD scalar maps were calculated using the FDT toolbox.

Diffusion imaging processing was also performed using the MRtrix package (J-D Tournier, Brain Research Institute, Melbourne, Australia, https://github.com/MRtrix3/mrtrix3) (Tournier et al. 2012) (TOURNIER; CALAMANTE; CONNELLY, 2012). For simplicity we converted the raw NIfTI, bvec and bvals files of each subject to MRtrix image format (.mif) that combines these three information into one, consisting of a text header, with data stored in binary format within the same file. Data was pre-processed, correcting for noise (VERAART et al., 2016; VERAART; FIEREMANS; NOVIKOV, 2016), image distortions (eddy current-induced distortion correction and motion correction, using FSL's tools) (ANDERSSON; SOTIROPOULOS, 2016; SMITH et al., 2004), bias correction (B1 field inhomogeneity correction using ANTS N4 (TUSTISON et al., 2010)), intensity normalization (reference image, b=0s/mm^2) and brain mask creation (RAFFELT; CONNELLY, 2016). Diffusion tensor estimation was performed using iteratively reweighted linear least squares estimator (VERAART et al., 2013), the maps of tensor-derived parameters (eigenvalues, eigenvectors, AD, FA, MD, RD) were generated. Constrained Spherical Deconvolution (CSD) (TOURNIER; CALAMANTE; CONNELLY, 2013) was also used for modeling the intravoxel diffusion, and AFD maps were created.

Figure 15 Diffusion data preprocessing

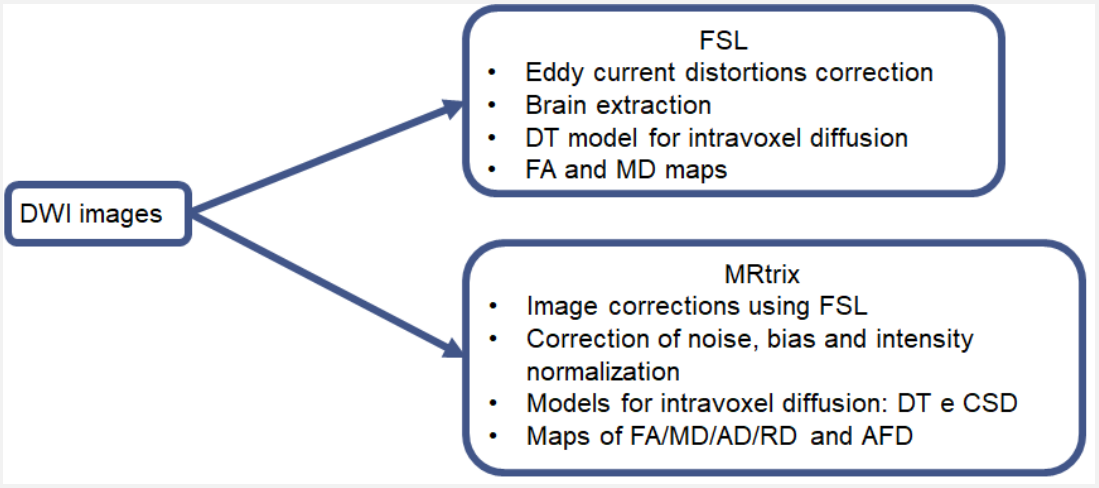

Source: Author

3.4.1. Tract Based Spatial Statistics - TBSS

From the FSL preprocessed diffusion data, voxelwise statistical analysis was carried out to study between-group differences, comparing the three groups of subjects of our dataset, two by two, using the FSL toolbox TBSS v1.2 (SMITH et al., 2004, 2006, 2007). Each subject's FA volume was registered to the group-average white matter skeleton (defined at an FA threshold of 0.2), and the resulting aligned images were utilized in the group analysis. The transformation matrices derived for the FA maps were applied to the diffusivity and T2-intensity (b=0) volumes for matched processing of all image volumes. The use of the TBSS skeleton allowed us to exclude regions of significant white-matter degeneration from the group analysis.

3.4.2. Manual Tract Selection

From the FSL pre-processed diffusion data, tract reconstruction was performed using Diffusion Toolkit software, part of TrackVis package (WANG et al., 2007). The processing occurs in two steps: 1) Reconstruction: diagonalization of diffusion data, in which the input data is the corrected 4D DWI image, bvec and

bval files; 2) Tracking: reconstruction of all fibers, considering angle threshold of 35°, FACT propagation algorithm, and inversion of the X diffusion gradient. Tract visualization and processing was performed with TrackVis software (https://www.trackvis.org/), in which track files, FA, FA color and MD maps are uploaded, for tract selection and analysis. FA can be color-coded, yielding a cartography of the tracts position and direction (red for left-right, blue for superior-inferior, and green for anterior-posterior).

Twenty two tracts were individually selected depeding on anatomical information during seed localization, namely: L/R Arcuate Fasciculus (AF), Corpus Callosum divided in Genu (GCC), Body (BCC) and Splenium (SCC), Corpus Callosum fibers selected by the interhemispheric connection between cortical regions of Destrieux atlas: Transverse frontopolar gyri and sulci (CC_frontopol), Superior frontal gyrus (CC_frontsup), Paracentral lobule and sulcus (CC_paracentral), Precuneus (CC_precuneus) and Superior occipital gyrus (CC_occipitalsup); L/R Cingulate part of the Cingulum (CGC); L/R Corticospinal Tract (CST); L/R Fornix (FX); L/R Inferior Longitudinal Fasciculus (ILF); L/R Inferior Occipitofrontal Fasciculus (IFOF) and L/R Uncinade Fasciculus (UF). The tract selection was done according to the criteria described at Table 2, whereas there is no default tract selection criteria in the literature.

Table 2 Inclusion and Exclusion criteria for tract selection

Tract	Inclusion Criteria	Exclusion Criteria
AF	In the color map, the coronal slice in which the green fibers are most intense, near the blue CST fibers. Select all green fibers in this region near the blue CST fibers. Identify the most inferior axial slice in which the fornix is visible, select the bundle of fibers projecting laterally to the sagittal stratum – Figure 39(WAKANA et al., 2007)	Any fibers crossing the hemispheres of the brain and fibers that are not part of the AF tract – Figure 40
GCC	ROIs drawn by anatomical information in the middle sagittal	
BCC		

Tract	Inclusion Criteria	Exclusion Criteria
SCC	slice –Figure 41(KOCHUNOV et al., 2011)	ROIs under and above the anatomical regions of the CC– Figure 43
CC_frontopol	Interhemispherical cortical connections from Destrieux parcellation atlas, Transverse frontopolar gyri and sulci (CC_frontopol), Superior frontal gyrus (CC_frontsup), Paracentral lobule and sulcus (CC_paracentral), Precuneus (CC_precuneus) and Superior occipital gyrus (CC_occipitalsup) – Figure 42	ROIs under and above the anatomical regions of the CC– Figure 43
CC_frontsup		
CC_paracentral		
CC_precuneus		
CC_occipitalsup		
CGC	In the most central coronal slice of the corpus callosum using the mid-sagittal slice, select fibers laterally above the corpus callosum. Coronal slice intersecting the middle of the splenium of the corpus callosum, select fibers laterally above the corpus callosum –Figure 44(WAKANA et al., 2007)	Any fibers crossing the hemispheres of the brain and fibers that are not part of the CGC tract – Figure 45
CST	Cerebral peduncle in the midbrain area, and primary motor cortex/precentral gyrus - Figure 46(TANG et al., 2010; VERSTRAETE et al., 2010)	Any fibers crossing the hemispheres of the brain and fibers near the cerebral peduncle that are not part of the CST tract – Figure 47
FX	Coronal slice in which the cerebral peduncles are most visible. In the color map, this slice is distinguished by the most intense bilateral color change of the corticospinal fibers from blue to	Any fibers crossing the hemispheres of the brain and fibers “between” the body and fimbria of the FX that are not part of the tract – Figure 49

Tract	Inclusion Criteria	Exclusion Criteria
	violet. Select fibers inferior to the corpus callosum, and in the axial slice select the region of the fimbria of hippocampus, placed at the level of the cerebral peduncles encompassing the hippocampal tail - Figure 48(CONCHA; BEAULIEU; GROSS, 2005)	
IFOF	In the coronal slice reaching the occipital regions, select both ROIs for each hemisphere. Coronal slice in which the tract bunches, select the ROI in the posterior edge of the genu of corpus callosum - Figure 50(WAKANA et al., 2007)	Fibers going to parietal regions, crossing the brain hemispheres and fibers that are not part of the tract– Figure 51
ILF	Most posterior coronal slice in which the frontal lobe is disconnected from the temporal lobe, select all fibers in the temporal lobe. Coronal slice that crosses the posterior edge of the cingulum, select all fibers included in the region of interest - Figure 52(WAKANA et al., 2007)	Fibers that are not part of the ILF tract, crossing the brain hemispheres and going to the frontal lobe (instead of temporal lobe) – Figure 53
UF	Most posterior coronal slice in which temporal and frontal lobes separate, typically located at the anterior portion of the fornix in the midsagittal view, for each hemisphere select ROIs in the temporal and frontal lobes - Figure 54(WAKANA et al., 2007)	Any fibers crossing the hemispheres of the brain and fibers in the temporal-frontal division that are not part of the UF tract – Figure 55

Obs 1. The images (Figures 34-50) are included in the appendix

Obs2. The tract selection example was done for a male subject of 31 years old.

Obs3. Other exclusion ROIs may be eventually necessary to remove all fibers that are not a part of the tract.

For each tract, FA and MD mean values were estimated based on the FA and MD maps created at FSL.

3.4.3. Automated Tract Selection

From the MRtrix preprocessed diffusion data, whole brain streamline tractography was performed in the same package using the DT and CSD for intravoxel diffusion model. Whole brain tractography was reconstructed using Fiber Assigned by Continuous Tracking (FACT) algorithm (MORI et al., 1999), for one million streamlines to be selected and 35 degrees as maximum angle between successive steps. To perform Constrained Spherical Deconvolution (CSD) tractography, the response function was estimated using Tournier algorithm (TOURNIER; CALAMANTE; CONNELLY, 2013), fiber orientation distributions (FODs) were calculated from diffusion data using Spherical Deconvolution (SD) (TOURNIER; CALAMANTE; CONNELLY, 2007), FODs were used for streamlines tractography for the whole brain based on SD (TOURNIER; CALAMANTE; CONNELLY, 2012), finally the tractogram was filtered using SIFT (SMITH et al., 2013).

The Automated Fiber Quantification (AFQ version 1.2) software package (YEATMAN et al., 2012) was used to identify 20 major white-matter fascicles (Left/Right Thalamic Radiation, Left/Right Corticospinal, Left/Right Cingulum Cingulate, Left/Right Cingulum Hippocampus, Callosum Forceps Major, Callosum Forceps Minor, Left/Right IFOF, Left/Right ILF, Left/Right SLF, Left/Right Uncinate, Left/Right Arcuate) from each healthy subject FACT and CSD tractograms. Tract profiles and diffusion parameters (FA/MD/AD/RD) were estimated along these fascicles for each subject. The tractograms for each subject were imported to Matlab environment, tract segmentation was done by two automated select ROIs selecting the fascicle that each fiber belongs to, from the whole brain tractography, defining the fiber trajectory and to a fiber tract probability map to remove streamlines that do not belong to the specific tract.

Finally, compute tract profiles for the diffusion properties along the trajectory of each fiber tract.

3.4.4. Apparent Fiber Density

From the whole brain tractographies reconstructed using DT and CSD models, in MRtrix package, it was performed fixel-analysis to estimate the Apparent Fiber Density (AFD). Fiber orientation distributions (FOD) were estimated using Constrained Spherical Deconvolution (CSD) modelling, fixel-based analysis was performed, AFD, cross-section (FC) metric and fibre density and cross-section (FDC) were estimated and whole-brain fiber tractography was performed on the template. Statistical two-tailed test was performed using connectivity-based fixel enhancement, comparing the groups two by two for FD, FC, and FDC.

3.4.5. Connectome

The anatomical images and cortical parcellations from both Destrieux and Desikan-Killiany atlases, obtained in FreeSurfer software, were transformed to diffusion MRI space, and the nodes for the connectome were created from the parcellated images. Streamlines from the whole brain tractographies reconstructed using DT and CSD models, in MRtrix package were mapped connecting the nodes to produce the connectome matrices. With the tractograms created using both algorithms (FACT and CSD) the connectomes were individually reconstructed, considering the number of fibers connecting regions as the connection weight, Figure 16. Brain Connectivity Toolbox (RUBINOV; SPORNS, 2010) was used for network analysis of degree, strength, density, clustering, global and local efficiency, betweenness and path length.

Figure 16 Connectome creation

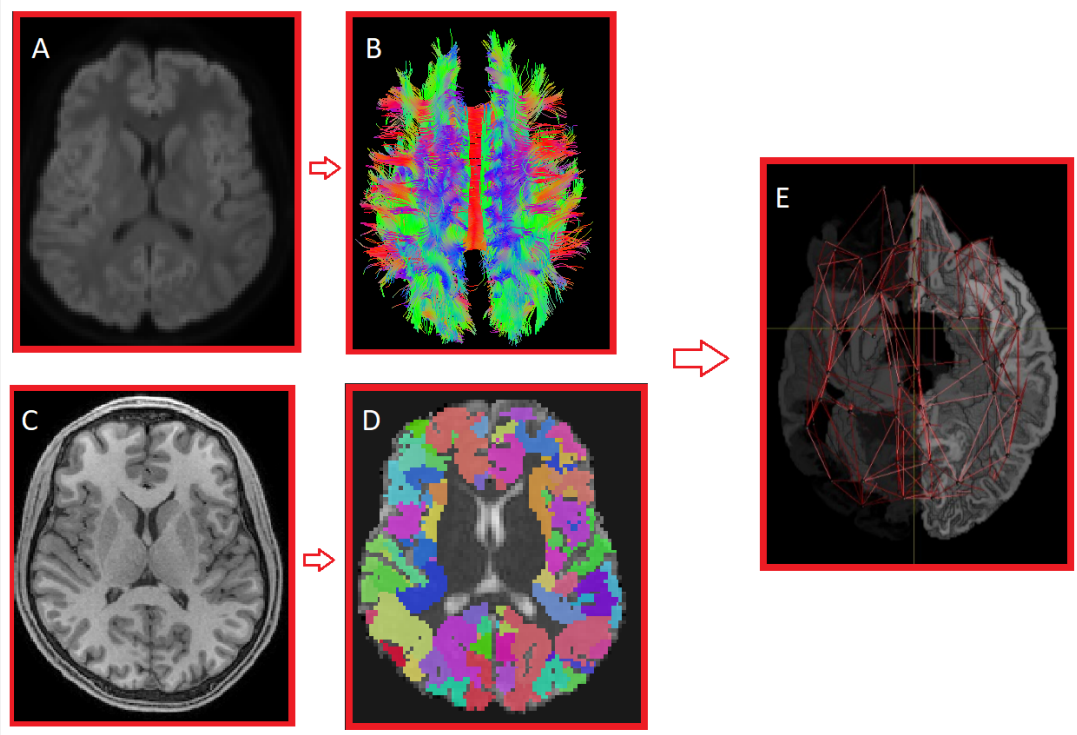

dMR individual images (A) were corrected, therefore the tractograms were created using DT and CSD models (B), anatomical T1-weigthed images (C) were parcellated for Desikan-Kiliany and Destrieux atlas (D) and transformed to dMRI space. Subject specific connectomes were created (E) and analyzed.

Source: Author

3.4.6. Connectome to Tract

Streamlines were extracted from the tractograms based on their assignment to parcellated nodes. The pairs of nodes chosen were the ones that we selected as connections endings of the twenty-two brain tracts, Table 3. Mean values of FA/MD/AD/RD were estimated for the streamlines in the tract.

Table 3 Cortical regions selected for each tract considering the area that most of the fibers of each tract were terminating, Destrieux atlas**.**

Tract	Cortical Region 1	Cortical Region 2
AF	R/L Middle temporal gyrus	R/L Precentral gyrus
CC-Genu	Right Superior Frontal gyrus	Left Superior Frontal gyrus
CC-Body	Right Superior Frontal gyrus	Left Superior Frontal gyrus
CC-Splenium	Right Precuneus	Left Precuneus
CC_frontopol	Right Transverse frontopolar gyri and sulci	Left Transverse frontopolar gyri and sulci
CC_frontsup	Right Superior Frontal gyrus	Left Superior Frontal gyrus
CC_paracentral	Right Paracentral lobule and sulcus	Left Paracentral lobule and sulcus
CC_precuneus	Right Precuneus	Left Precuneus
CC_occipitalsup	Right Superior occiputal gyrus	Left Superior occiputal gyrus
CGC	R/L Anterior part of the cingulate gyrus and sulcus	R/L Subparietal sulcus
CST	R/L Precentral gyrus	-
FX	R/L Subcallosal gyrus	R/L Temporal pole
IFOF	R/L Orbital gyrus	R/L Occipital pole
ILF	R/L Temporal pole	R/L Occipital pole
UF	R/L Temporal pole	R/L Fronto-marginal gyrus and sulcus

The analysis of the anatomical and diffusion data individually were performed using different softwares and techniques, a summary of the data processing pipeline is shown in Figure 17.

Figure 17 Pipeline of individual data processing

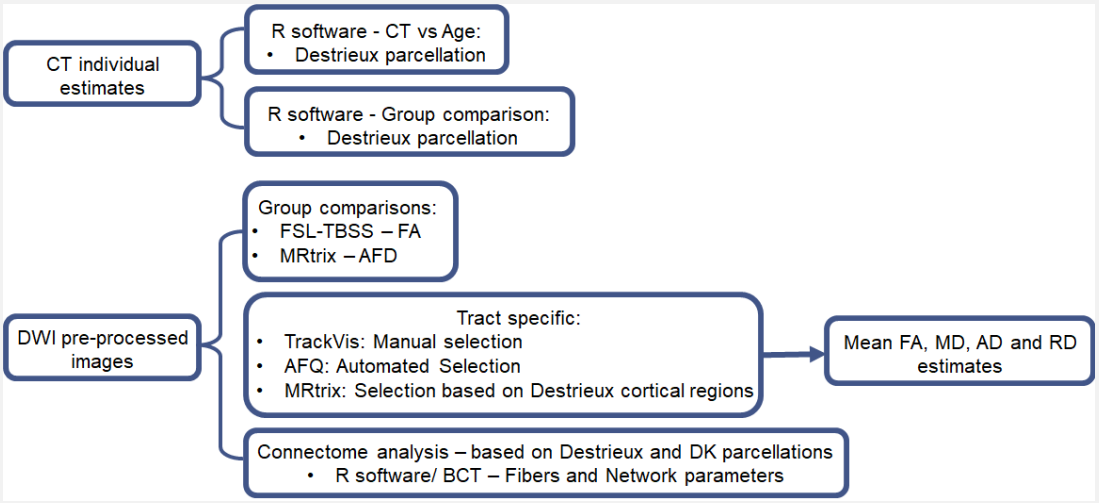

Source: Author

3.5. Diffusion + Cortical thickness

TrackVis software was used for manual selection of tracts, considering the DT model for tractography using preprocessed data from FSL software, and FreeSurfer for cortical parcellation and thickness estimation of the regions. For tract-cortical relationship, the cortical regions selected for each tract were chosen considering the area that most of the fibers of each tract were terminating, according to Table 3 and Figure 18.

Figure 18 Cortical regions selected for each tract considering the area that most of the fibers of each tract were terminating

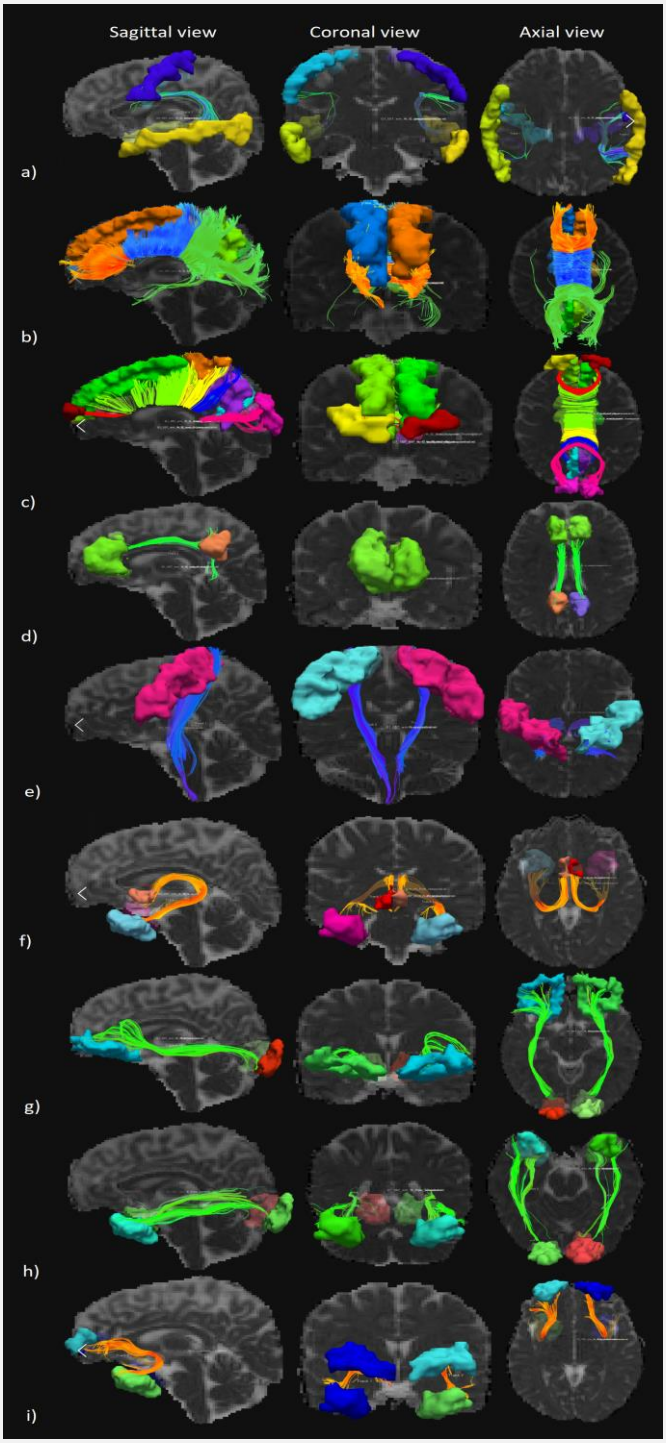

Sagittal, coronal and axial views for the tracts: a) Arcuate Fasciculus (AF); b) Corpus Callosum divided in Genu (GCC), Body (BCC) and Splenium (SCC); c) Corpus Callosum fibers selected by the interhemispheric cortical regions of Destrieux atlas: CC_frontopol, CC_frontsup, CC_paracentral, CC_precuneus and CC_occipitalsup; d) L/R Cingulate part of the Cingulum (CGC); e) L/R Corticospinal Tract (CST); f) L/R Fornix (FX); g) L/R Inferior Longitudinal Fasciculus (ILF); h) L/R Inferior Occipitofrontal Fasciculus (IFO) and i) L/R Uncinade Fasciculus (UF).

Source: Author

The tract-cortical associations were evaluated individually for each selected tract, considering the cortical thickness and diffusion metrics change rates and it's individual estimates, as demonstrated in Figure 19.

Figure 19 Pipeline of tract-cortical data processing

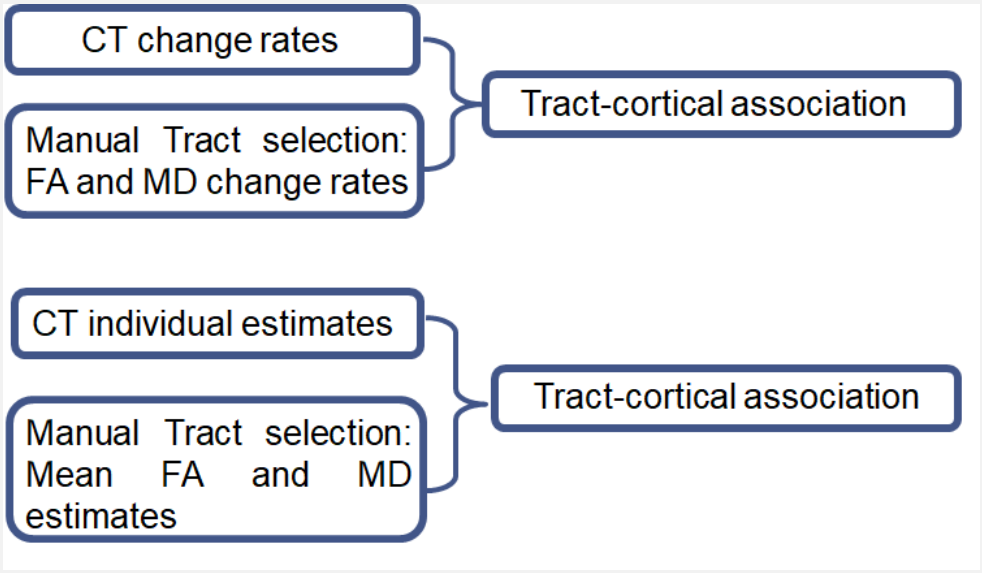

Source: Author

3.6. Statistical Analysis

Statistical analyses were performed in R statistical environment and language (https://www.r-project.org/). With the processed images for all subjects, we performed statistical analysis of the structural information (cortical thickness and diffusion parameters) in relation to age and comparations between tractography models and algorithms.

Cortical thickness of the 148 parcellated cortical regions were evaluated with respect to age. The linear fitting model was used for modelling the relationship of cortical thickness (CT) with aging, equation 13. Group analysis of cortical thickness information among the 3 healthy subject groups was performed to evaluate the patterns of cortical thinning between young, middle-age and elderly groups, two by two.

$$CT_i = \alpha_0 + \alpha_1 . Age_i + \epsilon_i \quad \text{(Eq. 13)}$$

TBSS was used to perform voxel-wise group statistics and a cluster-based inference, comparing groups the FA values G1, G2 and G3, two by two. MRtrix was used to perform the same voxel-wise group analysis for the AFD parameter ($p<0.05$).

Using R software, mean values of the diffusion were calculated for each brain tract, from manual and automated tract selection and from the connectomes, then the analysis with age were performed, equation 14. The linear fitting model was used for modelling the relationship of diffusion parameters with aging.

$$FA_i(or\ MD_i or\ AD_i or\ RD_i) = \alpha_0 + \alpha_1 . Age_i + \epsilon_i \quad \text{(Eq. 14)}$$

From the connectome the number of fibers connecting the nodes were evaluates, equation 15. The network parameters were extracted from the connectome analysis, the evaluation of the global and local parameters with age was performed, equation 15.

$$Fibers\ or\ Connectome\ Network\ Metric_i = \alpha_0 + \alpha_1 . Age_i + \epsilon_i \quad \text{(Eq. 15)}$$

The change rates, of the GM and WM integrity parameters for each cortical regions and brain tract, were calculated as the percentage of change from an initial value at 18 years, using the angular and linear coefficients of the linear regression. The modulus of the difference of the CT change rates were calculated of each brain tract connection and compared to the mean change rate difference of CT for each hemisphere. The FA/MD change rates for each tract were also evaluated in relation to the mean CT change rate in a linear fit for assessment of the association between them, equation 16.

$$FA\ rate_i = \alpha_0 + \alpha_1 . CT\ rate_i + \epsilon_i \quad \text{(Eq. 16)}$$

The association between cortical thickness of the regions in Table 3 and the mean values of FA and MD of the connecting tracts were studied using a linear

regression model, equations 17 and 18. This relation was also analyzed accounting for the age effect.

$$FA_i = \alpha_0 + \alpha_1 . Thickness_{1,i} + \alpha_2 . Thickness_{2,i} + \alpha_3 . Age_i + \epsilon_i \quad \text{(Eq. 17)}$$

$$MD_i = \alpha_0 + \alpha_1 . Thickness_{1,i} + \alpha_2 . Thickness_{2,i} + \alpha_3 . Age_i + \epsilon_i \quad \text{(Eq. 18)}$$

The p-values were adjusted considering multiple comparisons using the Benjamini-Hochberg False Discovery Rate (FDR) controlling procedure (BENJAMINI; HOCHBERG, 1995) in all statistical analysis.

4. Results

The main results of the brain structural changes during the lifespan here studied will be presented in this chapter. They are separated in cortical thickness assessment for two different samples, diffusion parameter analysis for whole-WM and specific brain tracts using different tractography algorithms and segmentation approaches, brain structural connectivities and its network parameters, and association between cortical thinning and WM integrity. Additionally, functional and structural connectivity results involving the corpus callosum are presented.

4.1. Cortical Thickness changes associated to brain aging

- Clinics Hospital of Ribeirão Preto

Analysis of cortical thickness information were carried out in relation to age for the 148 cortical regions based on Destrieux atlas, thus 131 regions show significant reduction in healthy aging ($p<0.05$ FDR corrected), Figure 20. These affected regions represent 88.5% of the cortical structures, 90.4% of the cortical surface area and 88.3% of the cortical volume. A high symmetry in the cortical thinning pattern is observed between hemispheres, except for the pericallosal sulcus with right predominance and postcentral sulcus with left predominance. The regions of most cortical thinning are Left Subcallosal gyrus (0.12mm/decade) and Right Transverse temporal sulcus (0.11mm/decade), Figure 21, with decline rates rather high compared to average previous findings (LEMAITRE et al., 2012a; SALAT et al., 2004). Other brain regions have reduced in the expected rate of 0.07mm/decade, as for example Right Anterior part of the cingulate gyrus and sulcus, Left Orbital part of the inferior frontal gyrus and Left Triangular part of the inferior frontal gyrus.

From the data, the linear model seems an adequate approach to characterize the relationship between cortical thickness and age in the interval used in this work, Figure 21.

Figure 20 Regions of cortical age-related thinning for the HCRP data based on Destrieux atlas

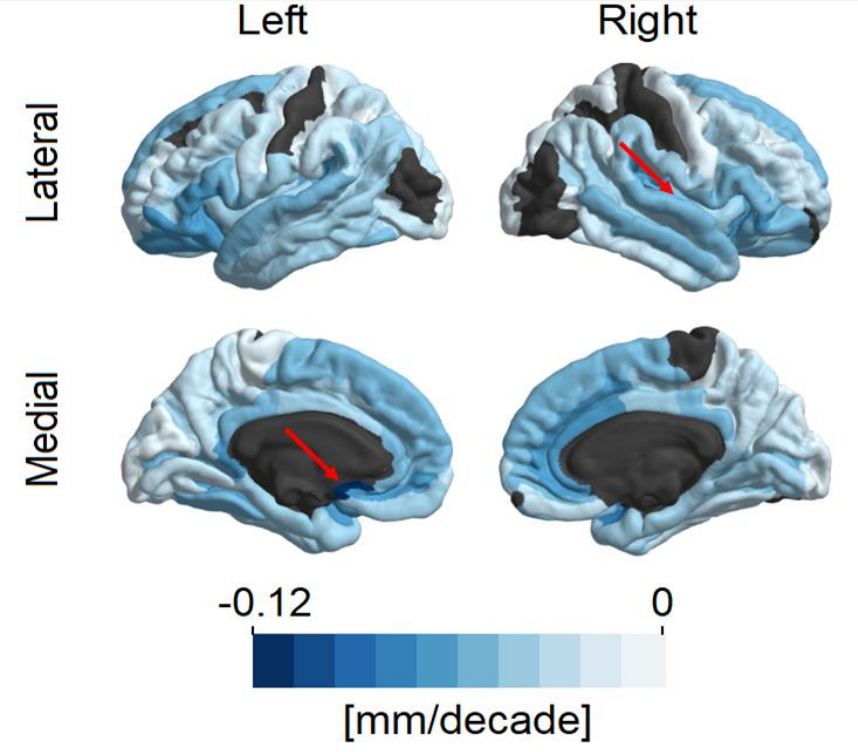

Left and right hemispheres of the brain ($p < 0.05$, BH correction), red arrows indicate the areas with most cortical thinning, Left Subcallosal gyrus (0.12mm/decade) and Right Transverse temporal sulcus (0.11mm/decade).

Source: Author

Figure 21 Age-associated cortical thinning, linear model for relationship between thickness and age, for the two regions that demonstrated most cortical thinning

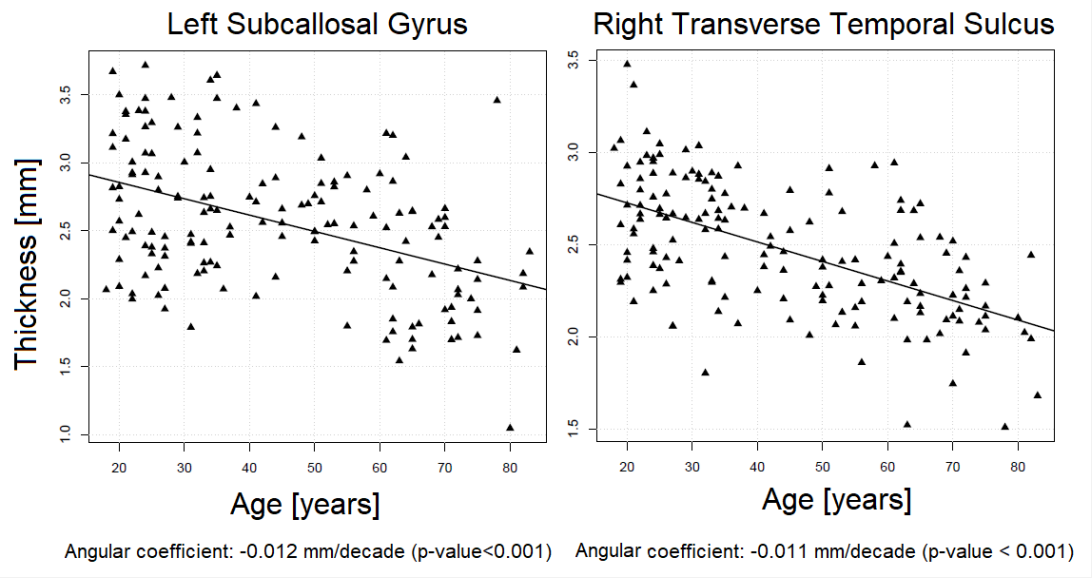

Source: Author

Pairwise group comparison between age groups, Table 1, of the cortical thinning patterns demonstrated that the number of cortical regions that differ significantly among the groups increase with age, according to Table 4. The comparison between groups 1 and 2 (young - middle groups) showed significant differences in 60 cortical regions, between groups 2 and 3 (middle - old groups) differences in 81 regions and between groups 1 and 3 (young and old groups) 131, demonstrating an explicit increase of brain regions and volume affected by the aging process.

Table 4 Results of the comparison between groups considering the cortical thickness of 148 cortical regions based on Destrieux atlas (p-corrected<0.05).

Groups	Number of regions	% of regions	% of surface area	% of volume	Volume (mm^3)
G1 – G2	60	40.5	42.6	44.1	228985
G2 – G3	81	54.7	58.6	61.1	325495
G1 – G3	131	89.1	87.1	90.1	471299

The regions mentioned on Table 4 are exhibited in Figure 22, showing the most affected regions in each of the group comparisons. Few regions are more affected only in early aging (red), some show cortical thinning throughout the life span (purple), especially in frontal and temporal areas, and several show extreme thinning in older ages (blue). Superior frontal and temporal regions were the most affected areas for cortical thinning, with considerably cortical thinning in frontal areas in early aging and in occipital and temporal regions in the elderly. A clear lack of symmetry is verified in the occipital ventral region, left side with early changes.

Figure 22 Group comparison of cortical thinning.

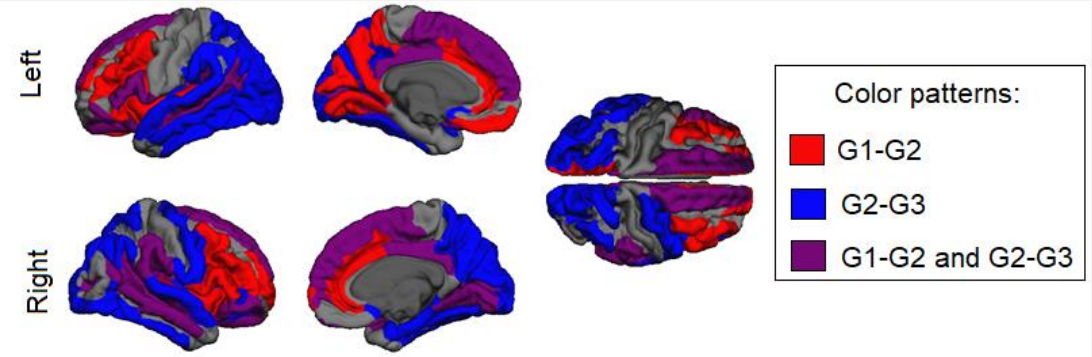

Group details are described in Table 1.

Source: Author

- NKI/Rockland sample

An identical analysis of cortical thickness were carried out using NKI/Rockland sample based on Destrieux atlas. A total of 118 regions showed significant reduction in healthy aging ($p<0.05$, FDR corrected), Figure 23. These affected regions represent 79.7% of the cortical structures, 82.9% of the cortical surface area and 82.1% of the cortical volume. The regions of largest cortical thinning (0.07mm/decade) are Left and Right Precentral gyrus and Anterior segment of the circular sulcus of the insula.

One of our results is the regional pattern of age-associated cortical thinning. By measuring changes in cortical thickness along the segmented cortical surface, areas of accelerated thinning and relative sparing were visualized. Figure 20 and Figure 23 present the results in terms of changes reaching a threshold level of statistical significance for two different subject groups, both healthy aging. However, it was shown that some regions do not demonstrate the same decline in cortical thickness for both datasets. The amplitude of the cortical thinning differs between the datasets, our sample demonstrated a higher thinning rate compared to the rate observed with NKI/Rockland sample.

The age-group comparison was not performed using these data, because our main goal of using this dataset was to compare our age-related cortical thinning results from HCRP data with one from another center.

Figure 23 Regions of cortical age-related thinning for NKI/Rockland sample data based on Destrieux atlas.

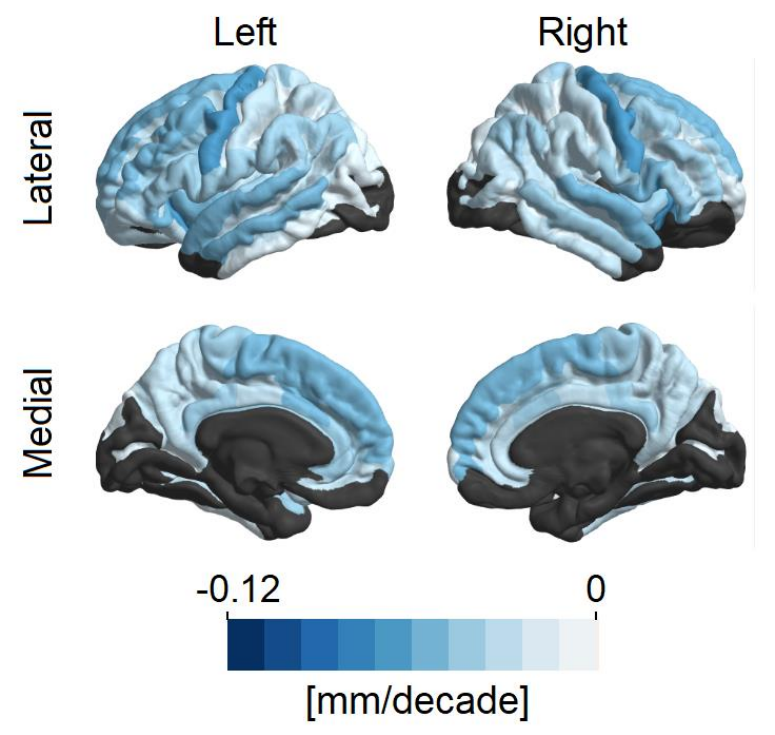

Left and right hemispheres of the brain. (p < 0.05, BH correction).

Source: Author

4.2. WM integrity during the aging process

4.2.1. Whole-WM Group Analysis

- FA-TBSS/FSL

The results in this section were obtained using the standard pipeline of TBSS tool on the young, middle-aged and old groups DWI data. The whole-WM TBSS analysis showed that older brains presented lower FA values. Figure 24 represents the regions with statistical difference between the groups defined in Table 1. In the statistical analysis we used the clusterization of the statistical significant voxels (p<0.05) for a broader view of the information contained in that analysis, see Table 5.

Figure 24 TBSS results showing patterns of FA differences in the group comparisons

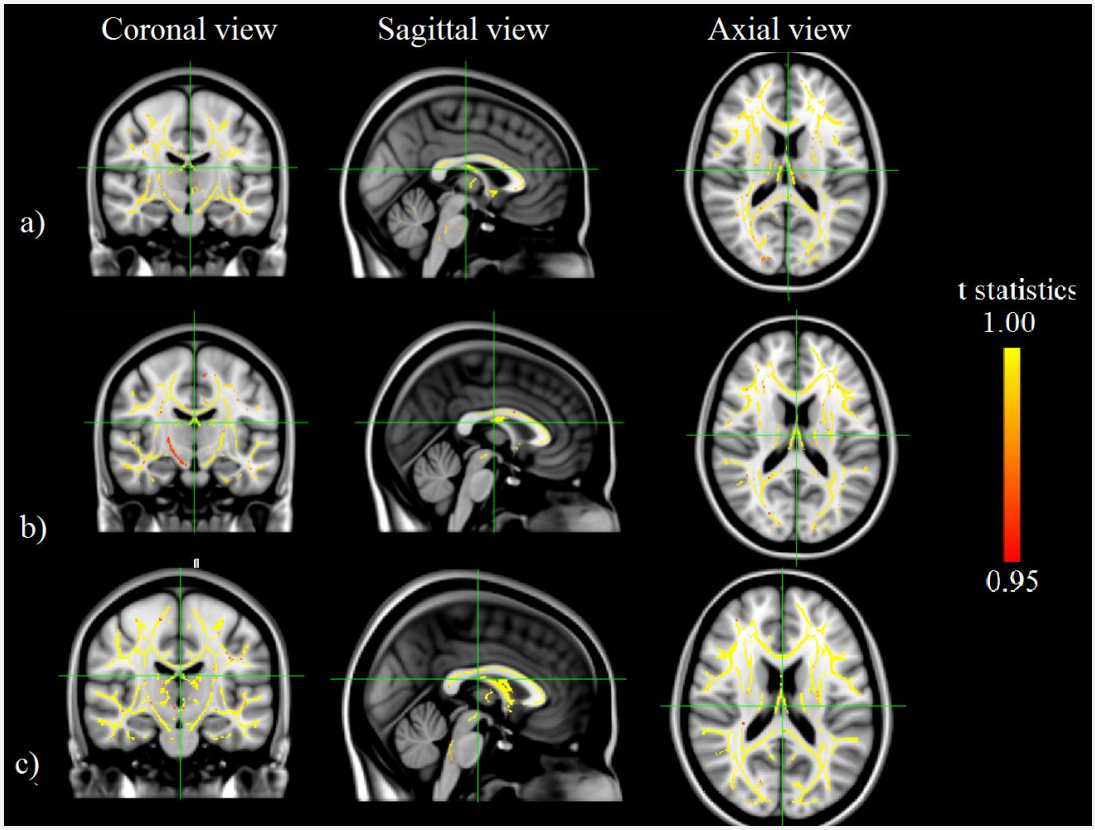

Between: young group and the middle group (G1 – G2) (a); middle group and the old group (G2 – G3) (b); young group and the old group (G1 – G3) (c) . Yellow–red color shows the significant FA. (FA: red: low significance, yellow: high significance). The position showed by the green cursor is the COG position, written in Table 5.

Source: Author

Table 5 Information about the TBSS group comparisons, with number of voxels with significant difference, maximum 1-p coordinates and tract position, the center of gravity (COG) coordinates and its anatomical position. Acccording to JHU DWI-based white-matter atlases.

Groups	Voxels	1-p MAX X/Y/Z (vox)	1-p MAX tract position	COG X/Y/Z (vox)	COG anatomical position
G1 – G2	57335	92/88/27	Right CST	91/110/88	Thalamus
G2 – G3	66844	49/117/35	Right ILF	89/112/89	Thalamus
G1 – G3	89285	49/116/33	Right ILF	90/108/89	Thalamus

The most important information comprehended in this table is the number of significant voxels from each group analysis, showing a clear increase in the number of clusterised voxels in older adults, following the same pattern as the

cortical thinning group comparison, Table 4. The more signifcant voxel have the same 1-p value (0.998) for all three analysis.

With the information contained in Table 5, the location of the Centre Of Gravity for the cluster (weighted average of the coordinates by the intensities within the cluster, equivalent to the concept of centre of mass for a object with distributed mass, where intensity substitutes for mass in this case) does not change for any of the group comparisons, its position in the brain is nearby the Fornix tract, demonstrated in Figure 24. Differently from the MAX coordinates (the location of the voxel with the maximum difference, given as X/Y/Z coordinate values in voxel coordinates) that are similar for the comparisons concerning the older group, indicating that this group has a higher weight in the analysis, since the bigger FA decreases occur in the elderly brain (over 60 years old), due to more advanced axonal degeneration.

- AFD-MRtrix

For the Apparent Fiber Density (AFD) analysis, the whole-WM group analysis demonstrated a significant ($p<0.05$ corrected) decrease in the AFD parameter with age. Figure 25 shows the regions in the white matter where this parameter is more affected.

It is possible to verify in Figure 25 that comparing between the younger groups there are very few regions with significant alterations of AFD, those being the following tracts: fornix, cerebellar peduncle and base of the cortico-spinal tract (CST). When comparing the elderly group there is a broader pattern of degeneration of the white matter tracts. The analysis between G2 and G3 demonstrated alterations in the corpus callosum, fornix, inferior lateral fasciculus, inferior fronto-occipital fasciculus and anterior thalamic radiation, and between G1 and G3 all of those were affected but also the CST and cerebellar peduncle.

Figure 25 Significant (p<0.05) differences in AFD parameter in the group comparisons.

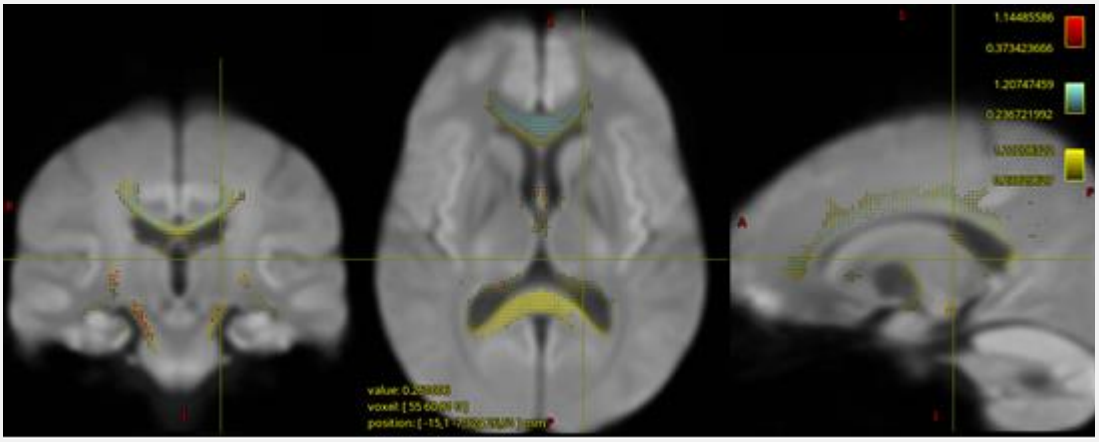

Coronal, axial and sagittal views of the brain. AFD differences: Red: G1 vs G2, Blue: G2 vs G3 and Yellow: G1 vs G3.

Source: Author

4.2.2. Tract-specific analysis

- Manual Tract Selection

From the structural images, it was possible to verify through the estimates for the Corpus Callosum (CC), an antero-posterior gradient of decrease in FA, Figure 27, as reported in the literature (SULLIVAN; PFEFFERBAUM, 2007; SULLIVAN et al., 2001). All selected tracts showed a significant (p<0.001) decrease of FA values and increased MD with age, in accordance with the literature (MICHIELSE et al., 2010), the rate of change (calculated as percentage of change from 18 years old, using the angular and linear coefficients of the linear regression) of this parameters are shown at Table 6.

It is important to notice that the MD alteration rate for the corpus callosum segmented by the structural cortical connections do not show the same antero-posterior gradient of alterations of FA in the aging process, Table 6. For FA parameter, and indication of the order of degeneration of the tracts, according to the percentage of change per decade, from the higher rate, is ordered in Figure 26, L/R fornix, frontal part of the corpus callosum, R/L cingulum, L arcuate fasciculus, central part of corpus callosum, L inferior longitudinal fasciculus, L

uncinate and inferior frontoccipital fasciculus, R arcuate and inferior longitudinal fasciculus, L/R cortico spinal tract, occipital part of corpus callosum and R arcuate and inferior longitudinal fasciculus.. For MD the order of degeneration considering the percentage of change per decade is L/R fornix, followed by the occipital part of the corpus callosum, genu, body, splenium of corpus callosum, frontal part of corpus callosum, L inferior frontoccipital, arcuate and uncinate fasciculus, L corticospinal tract a, R arcuate fasciculus, corticospinal tract and cingulum and L/R inferior longitudinal fasciculus. The corpus callosum tracts and the fornix are the ones with higher alteration rates of FA and MD among the selected ones for this study.

Figure 26 Tracts ordered by FA decrease in percentage per decade.

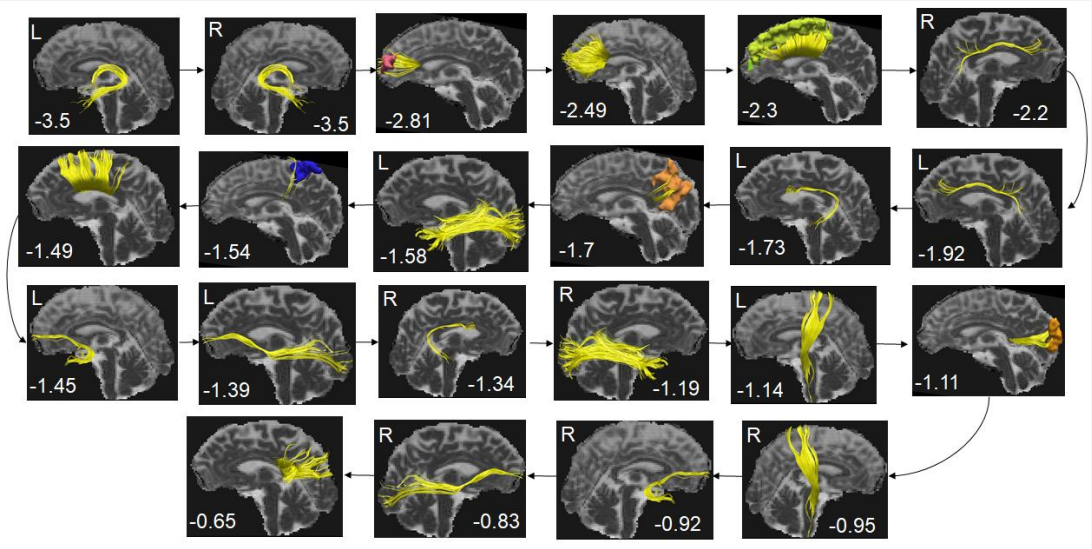

Brain tracts in yellow with the respective FA decrease rate [%/decade].

Source: Author

Figure 27 Linear fit of FA vs Age, for the different Corpus Callosum parts.

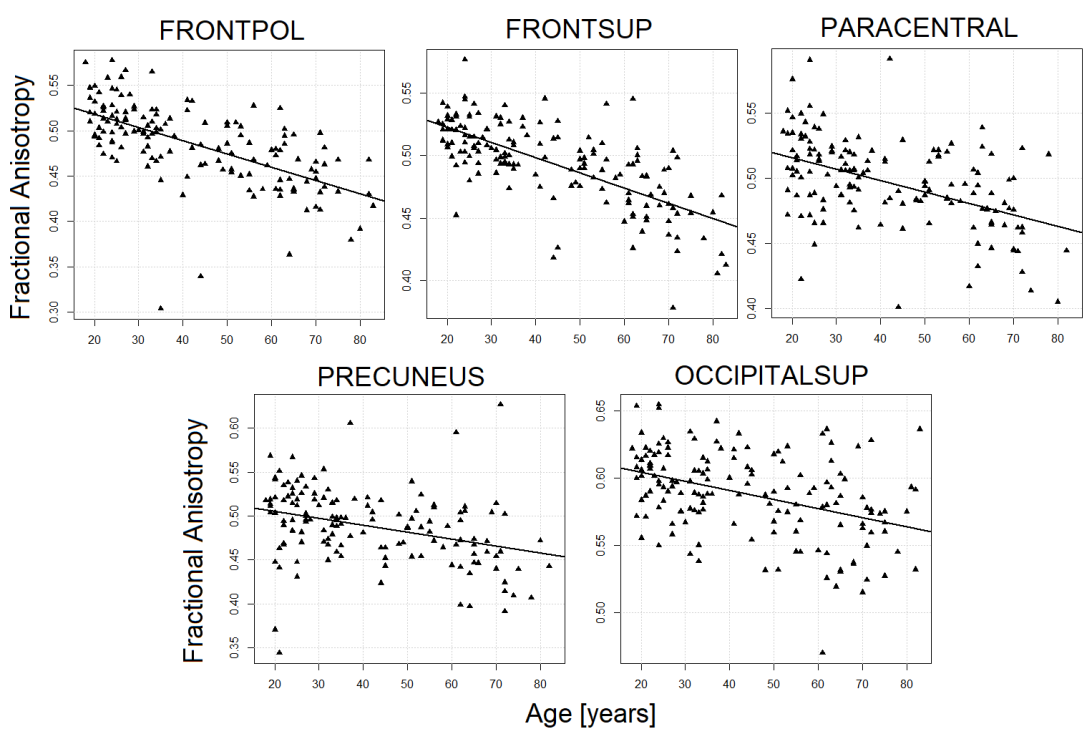

Source: Author

Table 6 Rate of the change of FA and MD per decade resulting of linear regression analysis vs. age for the manually selected tracts, all analysis presented p-value < 0.001 FDR corrected.

Tract	FA [/decade]	FA [%/decade]	MD [x10^{-6} mm^2/s/decade]	MD [%/decade]
AF_L	-0.0085	-1.73	9.0	1.28
AF_R	-0.0059	-1.34	8.5	1.18
GCC	-0.0131	-2.49	18.6	2.36
BCC	-0.0078	-1.49	16.1	2.05
SCC	-0.0037	-0.65	15.8	1.82
CC_frontopol	-0.0147	-2.81	12.7	1.62
CC_frontsup	-0.0121	-2.30	12.5	1.62
CC_paracentral	-0.0088	-1.70	8.2	1.05
CC_precuneus	-0.0078	-1.54	10.1	1.29
CC_occipital	-0.0067	-1.11	20.3	2.66
CGC_L	-0.0094	-1.92	8.2	1.17
CGC_R	-0.0104	-2.20	8.1	1.15

Tract	FA [/decade]	FA [%/decade]	MD [x10^{-6} mm^2/s/decade]	MD [%/decade]
CST_L	-0.0063	-1.14	9.4	1.31
CST_R	-0.0052	-0.95	8.7	1.17
FX_L	-0.0130	-3.50	45.9	4.38
FX_R	-0.0126	-3.50	44.5	3.97
IFOF_L	-0.0070	-1.39	11.1	1.43
IFOF_R	-0.0040	-0.83	8.0	1.02
ILF_L	-0.0076	-1.58	7.9	0.99
ILF_R	-0.0055	-1.19	5.3	0.66
UF_L	-0.0061	-1.45	9.6	1.24
UF_R	-0.0037	-0.92	9.0	1.15

Additionally, an asymmetry can be noticed, with exception to FA of CGC, for all the tracts the left hemisphere seems to be more damaged in the lifespan.

- Automated Tract Selection

The automated program, AFQ, uses anatomical information from the T1-weighted image to select ROIs and for the selection of 20 fiber bundles of the brain, and estimate the diffusion parameters (FA/MD/AD/RD) for each tract in 100 points along the tract. The mean values of the parameters were used to analyze the effect of these parameters, using the automated selection from both whole brain tractographies acquired using FACT and CSD modelling of the data. Figure

28 shows the selected streamlines for four fiber bundles using the FACT and CSD tractography for a healthy 25 years old male.

Figure 28 indicates that the tracts reconstructed from the CSD tractography algorithm are not adequate neither reliable, due to the poor reconstruction of the

Figure 28 Reconstructed tracts using AFQ package

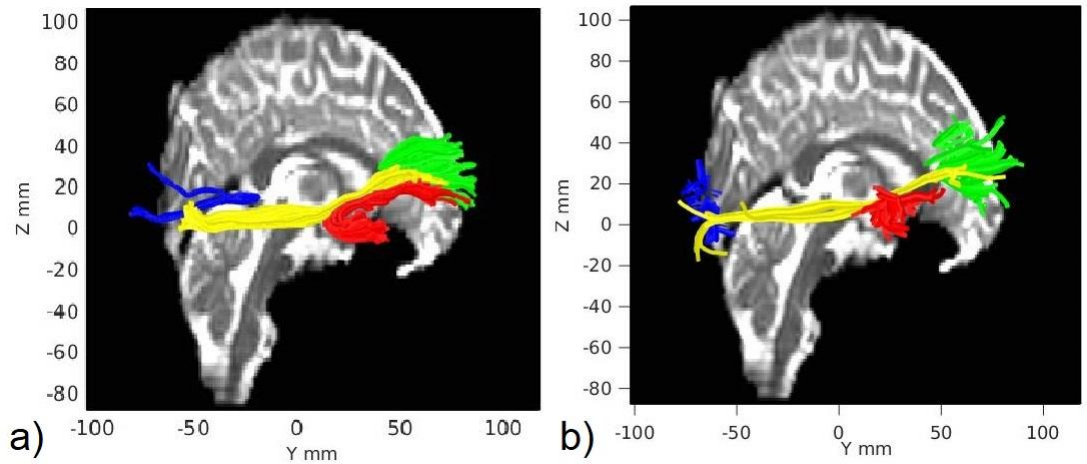

Tract selection from FACT (a) and CSD algorithms (b). Callosum Forceps Minor (green), Uncinate Fasciculus (red), Inferior Fronto-Occipital Fasciculus (yellow) and Callosum Forceps Major (blue).

Source: Author

brain fibers; thus, the parameter estimation from the tracts were evaluated only for the FACT reconstruction.

Table 7 demonstrates the change rate and effect of the diffusion parameters with age.

Table 7 Rate of the change of FA/MD/AD/RD per decade resulting of linear regression analysis vs. age for the automatically selected tracts using AFQ package, for FACT whole-brain tractography. Values in red represent p<0.05, FDR corrected.

Tract	FA [/decade]	MD [x10^{-6} mm^2/s/decade]	AD [x10^{-6} mm^2/s/decade]	RD [x10^{-6} mm^2/s/decade]
Left Thalamic Radiation	0.0003	0.98	2.10	0.42
Right Thalamic Radiation	-0.0004	0.07	-0.22	0.21
Left Corticospinal	-0.0040	-3.82	**-11.5**	0.02

Tract	FA [/decade]	MD [x10^{-6} mm^2/s/decade]	AD [x10^{-6} mm^2/s/decade]	RD [x10^{-6} mm^2/s/decade]
Right Corticospinal	**-0.0064**	**-5.86**	**-16.3**	-0.65
Left Cingulum Cingulate	**-0.0074**	**-5.54**	**-15.5**	-0.58
Right Cingulum Cingulate	-0.0061	-3.83	**-10.2**	-0.62
Left Cingulum Hippocampus	**-0.0066**	-4.46	-10.0	-1.68
Right Cingulum Hippocampus	**-0.0080**	-5.28	-11.7	-2.09
Callosum Forceps Major	-0.0102	-6.77	-19.1	-0.61
Callosum Forceps Minor	**-0.0143**	**-9.17**	**-24.0**	-1.74
Left IFOF	-0.0037	-1.07	-4.09	0.43
Right IFOF	-0.0041	-2.34	**-6.42**	-0.30
Left ILF	-0.0032	-2.00	-4.78	-0.62
Right ILF	**-0.0052**	**-3.28**	**-6.73**	-1.55
Left SLF	-0.0027	-0.62	-2.53	0.34
Right SLF	-0.0041	-2.11	-5.23	-0.55
Left Uncinate	**-0.0055**	**-3.18**	**7.44**	-1.05
Right Uncinate	**-0.0076**	**-3.99**	**-9.19**	-1.39
Left Arcuate	**-0.0063**	-2.97	**-7.74**	-0.59
Right Arcuate	**-0.0067**	-3.08	**-6.71**	-1.26

FA decreases with age in the majority of the fiber tracts, however there are just a few of them that are statistically significant, disagreeing with what was expected based on the manual tract selection results. The other parameters were expected to change in the aging process depending on the location of the tracts, in the

literature there are a few cases where the MD/AD/RD increases or decreases depending on the specific white matter regions.

- Tract Selection based on cortical areas

The connectomes generated from both FACT and CSD models, will be explained in the next topic, were used to reconstruct the fiber bundles from the tracts that we previously selected, except for GCC, BCC, SCC and CST, considering the cortico-cortical connection. Reconstructed tracts are showed in Figure 29.

Figure 29 Reconstructed tracts from the connectomes.

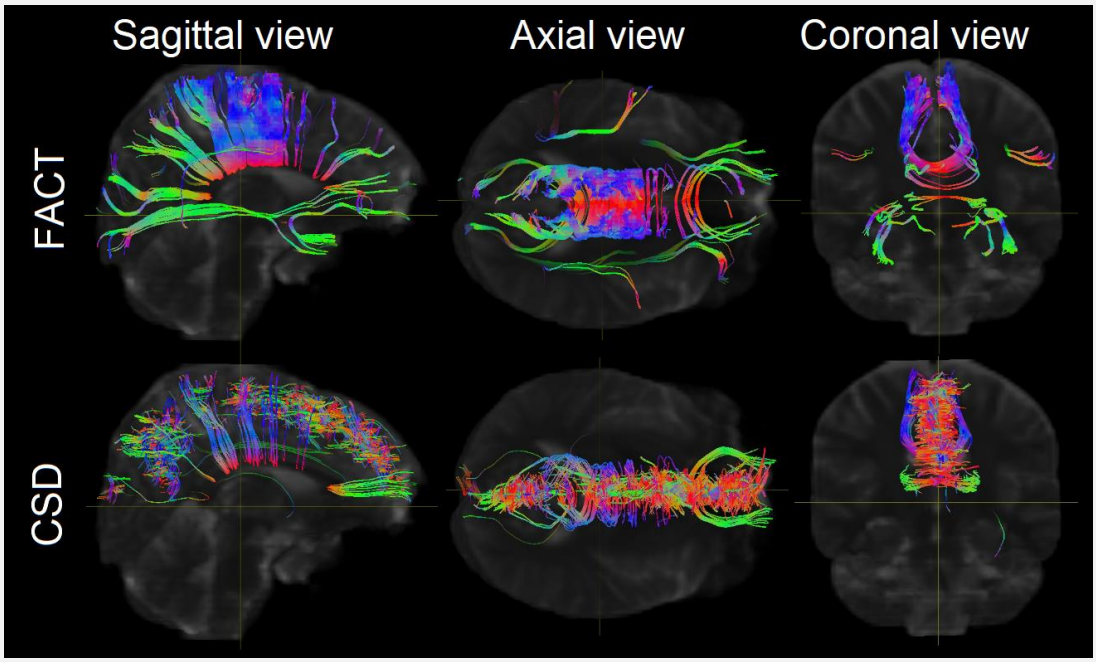

Using Destrieux atlas for selecting the cortical regions, for both diffusion tractography models: FACT and CSD.

Source: Author

Similar to the previous results, the CSD tract reconstruction were not reliable, so, we decided not to evaluate the diffusion parameters for those tracts. The rate of change of the diffusion parameters using FACT tractography for each of the group of streamlines are shown at Table 8.

Table 8 Rate of the change of FA/AD/MD/RD per decade resulting of linear regression analysis vs. age for the tracts selected from the connectome, for FACT whole-brain tractography. Values in red bold represent p<0.05, FDR corrected.

Tract	FA [/decade]	MD [x10^{-6} mm^2/s/decade]	AD [x10^{-6} mm^2/s/decade]	RD [x10^{-6} mm^2/s/decade]
AF_L	**-0.0083**	**3.79**	-2.66	**8.41**
AF_R	**-0.0066**	**8.28**	-2.07	**6.72**
CC_frontopol	**-0.0173**	**28.7**	**-10.6**	**17.7**
CC_frontsup	**-0.0236**	**12.5**	5.48	**40.3**
CC_paracentral	**-0.0132**	**30.7**	1.79	**20.7**
CC_precuneus	**-0.0324**	**5.17**	-2.91	**47.4**
CC_occipital	-0.0035	14.4	**14.5**	**11.4**
CGC_L	**-0.0106**	**4.64**	-5.69	**10.5**
CGC_R	**-0.0094**	2.48	-4.84	**9.38**
FX_L	**-0.0055**	**-21.4**	-6.51	6.98
FX_R	-0.0035	**4.65**	**-35.5**	**-14.4**
IFOF_L	**-0.0066**	**7.22**	-1.87	**7.91**
IFOF_R	**-0.0071**	4.88	1.29	**10.2**
ILF_L	**-0.0060**	0.68	-0.87	**7.75**
ILF_R	**-0.0065**	**8.94**	-7.94	4.99
UF_L	**-0.0067**	**6.70**	4.55	**11.1**
UF_R	**-0.0064**	8.65	1.58	**9.26**

Using the connectome to recreate the fiber tracts, the FACT tractography is shown to have better results for the tracts reconstruction, as demonstrated in Figure 32. The majority of fiber bundles were found for all subjects, only the fornix and the cingulum that for some subjects were not found. In the table above, it is possible to visualize the increase and decrease patterns of the diffusion parameters using the FACT algorithm for whole brain tractography. There are many significant age effects in the different diffusion parameters, 15/17 brain tracts demonstrated significant decreases in FA, 11/17 increased MD, 1/17 decreased MD, 1/17 increased AD, 2/17 decreased AD, 14/17 increased RD and 1/17 decreased RD. The right fornix was the one that decreased the MD/AD/RD

parameters. For the FA parameter the corpus callosum tracts demonstrated the higher significant rates of change, followed by the cingulum, arcuate fasciculus, inferior frontoccipital, inferior lateral and uncinate fasciculus.

In summary, the CSD tractography can be discarded due to insufficient data quality for this model. And for tract selection, looking at the FA and MD alteration rates for each tract selection method shown in Figure 30, combined with the qualitative information of tract selection, Figure 31, the manual selection demonstrates more accurate tract selections.

Figure 30 Bar graphs demonstrating the rate changes for FA and MD in the tracts selected using FACT whole brain tractography for manual, automated and based on cortical regions tract selection

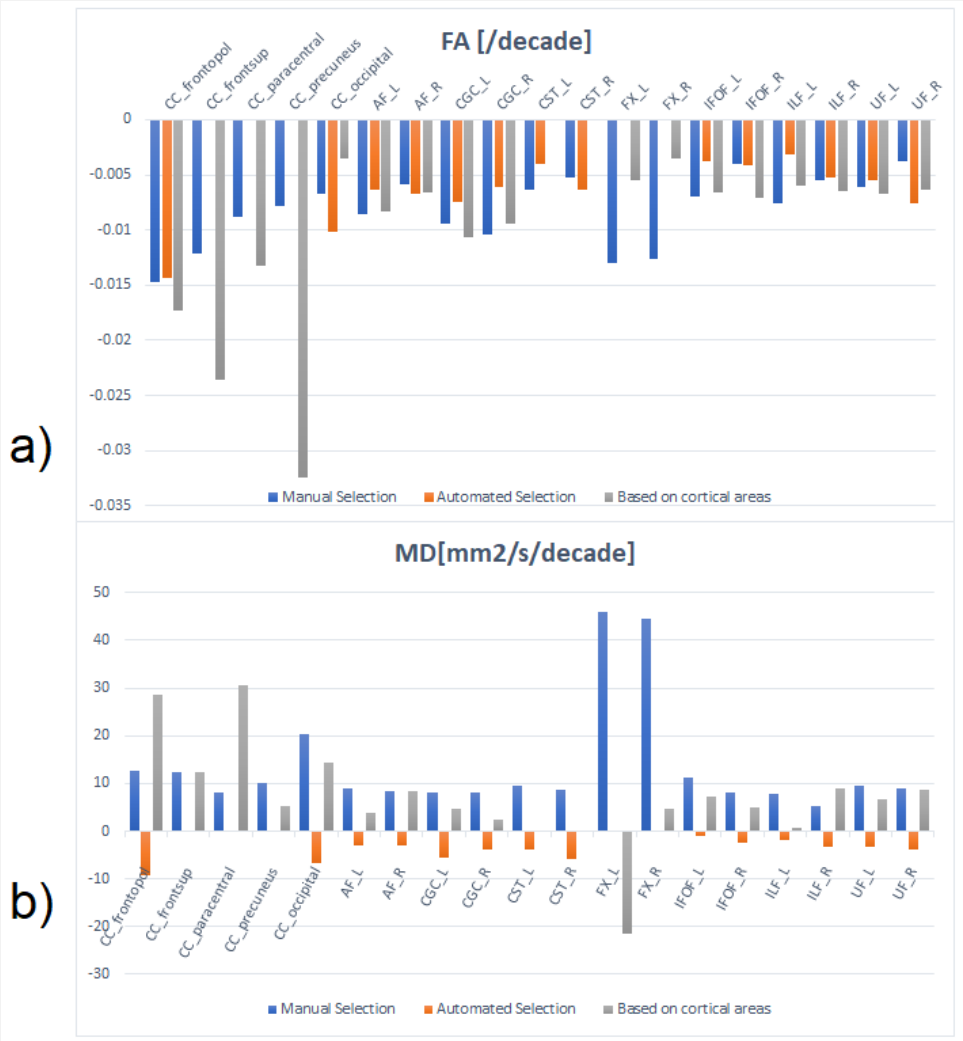

(a) FA [/decade] and (b) MD [x10^{-6} mm^2/s/decade]

Source: Author

Figure 31 Selection of four brain tracts with different methods (software) for a 25 year old woman.

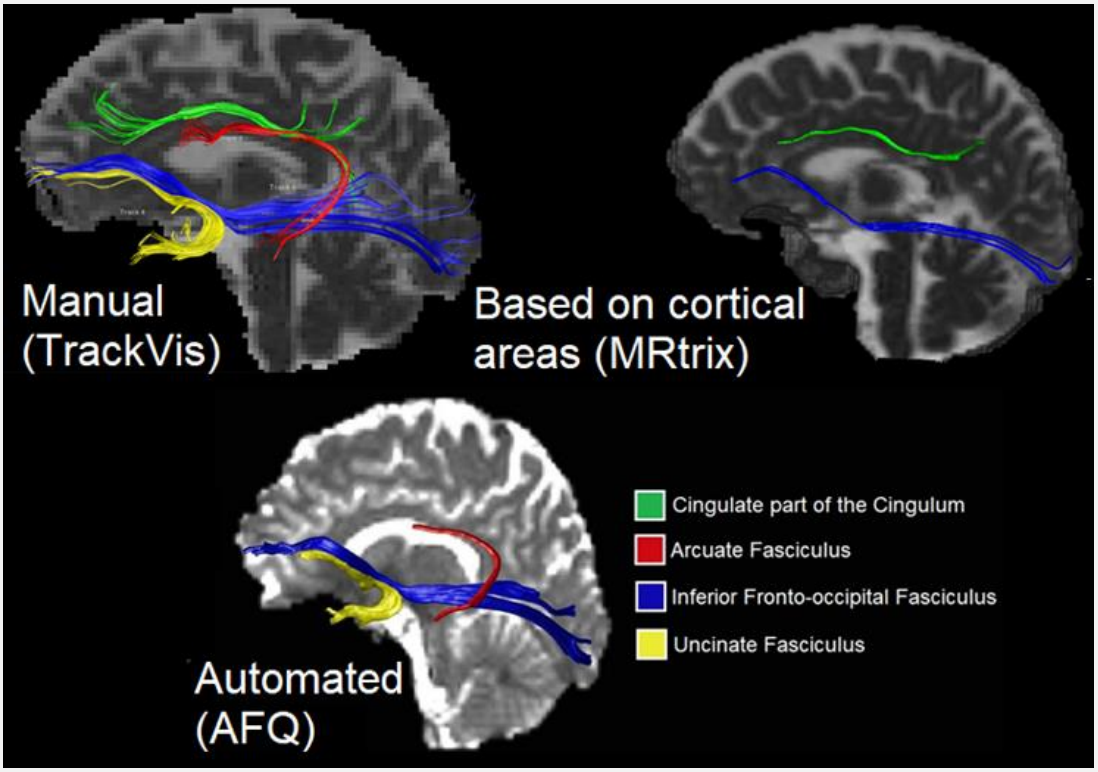

Source: Author

4.2.3. Structural connectivity and network analysis

In the first analysis a linear regression was performed between normalized number of fibers connecting each node of the parcellated cortex in function of age, the number of significant connections are shown in Table 9 and Figure 32.
Table 9 shows that the CSD modelling for the tractography results in more structural connections being significantly reduced in the aging process (considering that the weight used is number of fibers connecting cortical regions).
Figure 32 exhibit the structural connections described by the streamlines between the cortical regions considering Desikan-Killiany and Destrieux brain parcellations and DT and CSD diffusion models.
From the binarized connectome, the network parameters were evaluated, the results are shown in

Table 10 and Table 11. All local and global metrics are reducing in the structural networks evaluated. There is a significant decrease in the degree of the connectomes in the aging process, it is a decrease in the number of links connected to the node with age, for almost half of the nodes of each parcellations atlas, and it is not highly dependent on the tractography algorithm. For the other local network metrics, there is a greater percentage of the cortical regions (nodes) in the DK parcellation reducing the network metrics, as local efficiency, betweenness and clustering coefficient, when comparing to Destrieux parcellation. In the comparison between the whole-brain tractography algorithm using the same parcellation, the affected nodes are similar but not completely the same. For the global network metrics, these are decreasing with age with characteristic alteration rates, the density of the connectome, ie, ratio present/possible connections, global efficiency and path length show significant ($p<0.05$ FDR corrected) reductions in the aging process. The local efficiency of some nodes is more susceptible to the age effect than others, however the global efficiency is affected by this factor in a similar way independent of atlas nor tractography model, Figure 33.

Table 9 Number of significant connections being reduced with age and the percentage comparing all possible connections, p-value<0.05 FDR corrected

Parcellation Atlas	DT model	CSD model
Desikan-Killiany	22/2312 (0.95%)	36/2312 (1.55%)
Destrieux	7/10956 (0.06%)	57/10952 (0.52%)

Figure 32 Structural connectome considering different brain parcellations and diffusion models. Connections with significant normalized number of fibers decreasing with age (adjusted p-value < 0.05) are in red

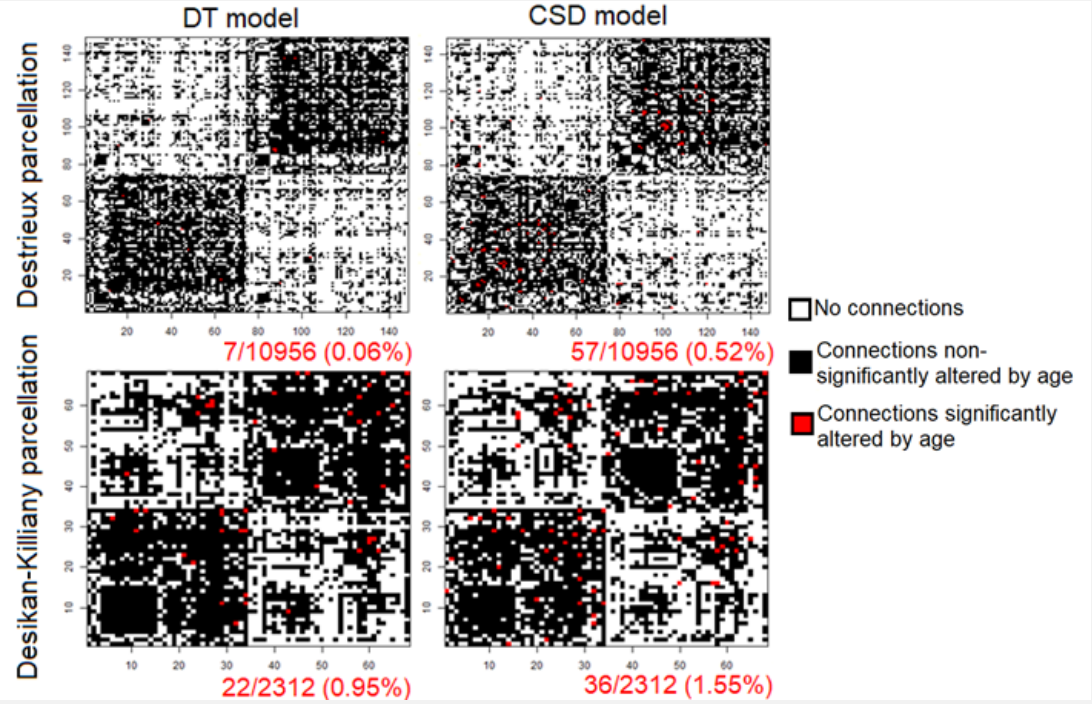

Source: Author

Table 10 Percentage of significant alterations for local network parameters with age considering different brain parcellations and diffusion models, p-value<0.05 FDR corrected

Local Metrics				
Network Metric	**DK – DT model**	**DK – CSD model**	**Dex – DT model**	**Dex – CSD model**
Degree	39.7%	38.2%	42.6%	39.9%
Strength	39.7%	38.2%	42.6%	39.9%
Clustering coefficient	26.5%	19.1%	20.3%	17.6%
Local Efficiency	30.9%	22.0%	22.3%	16.2%
Betweenness	29.4%	25.0%	18.9%	20.9%

Table 11 Global network parameters coefficients altering per decade, p-value<0.05 FDR corrected

Global Metrics				
Network Metric	**DK – DT model**	**DK – CSD model**	**Dex – DT model**	**Dex – CSD model**
Density	-0.0023	-0.0017	-0.0017	-0.0015
Global Efficiency	-0.0022	-0.0020	-0.0023	-0.0021
Path Length	-0.0094	-0.0090	-0.0135	-0.0119

Figure 33 Fitted Global Efficiency with age, for the connectomes created from DT and CSD models and using Desikan-Killiany (DK) and Destrieux (Dex).

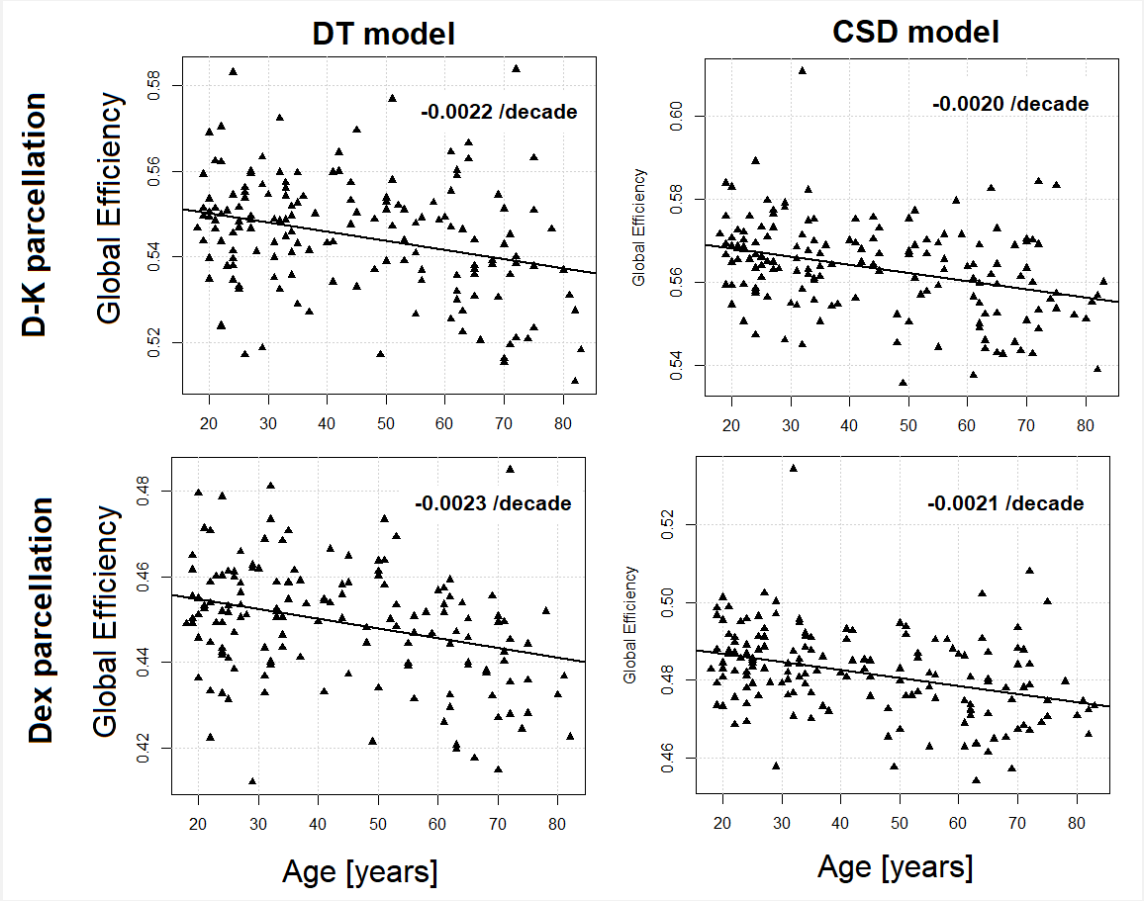

Source: Author

4.3. WM integrity and cortical thickness association in the lifespan

Considering as the gold standard the manual tract selection for whole-brain tractographies created using DT modeling. For this data, we correlated the cortical thickness information and WM integrity parameters for the specific fiber tracts that were selected and the information of the cortical regions that are the most significant endings of the fibers bundles, Table 3.

All analyzed tracts presented decrease of FA and increase of MD with age and many cortical regions demonstrated significant cortical thinning; bilateral tracts and regions show similar results, as shown previously.

Cortical thickness change rates were evaluated for the connecting regions of each tract. Figure 34 demonstrates that the absolute differences between the cortical thinning rates of the cortical regions connected by the tracts are usually under or near the mean of this difference considering all cortical regions of each hemisphere (dash line in Figure 34).

Figure 34 Modulus of cortical thinning rate differences between both cortical areas linked by each tract. Dashed lines demonstrate the mean of the thinning rate absolute differences between all the cortical regions of each hemisphere.

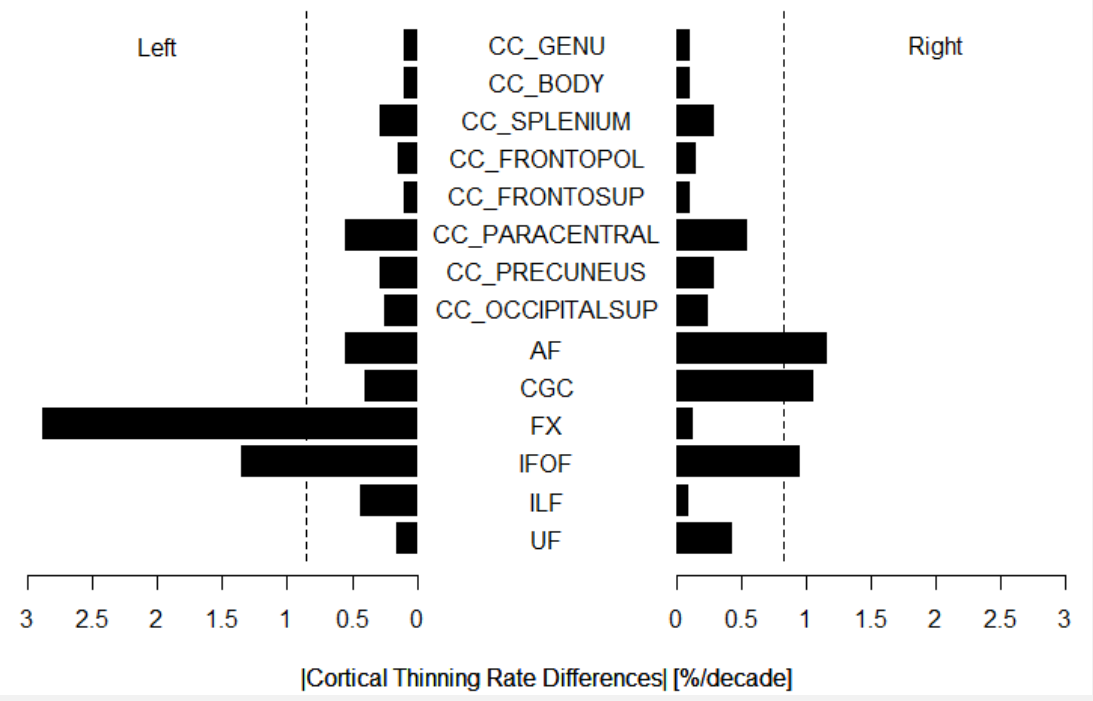

The averages of the cortical thickness change rates between the cortical regions linked by the tracts are significantly correlated to the alteration rates of the WM integrity parameters (FA and MD) of the corresponding tracts, Figure 35. This result motivates a direct evaluation whether the alterations of each cortical region connecting the tracts are correlated with the correspondent WM integrity parameters, removing the age effect.

Figure 35 Association between FA and MD change rates and mean cortical thickness change rates for the specific tracts. Each point in both graphs is associated to specific tracts.

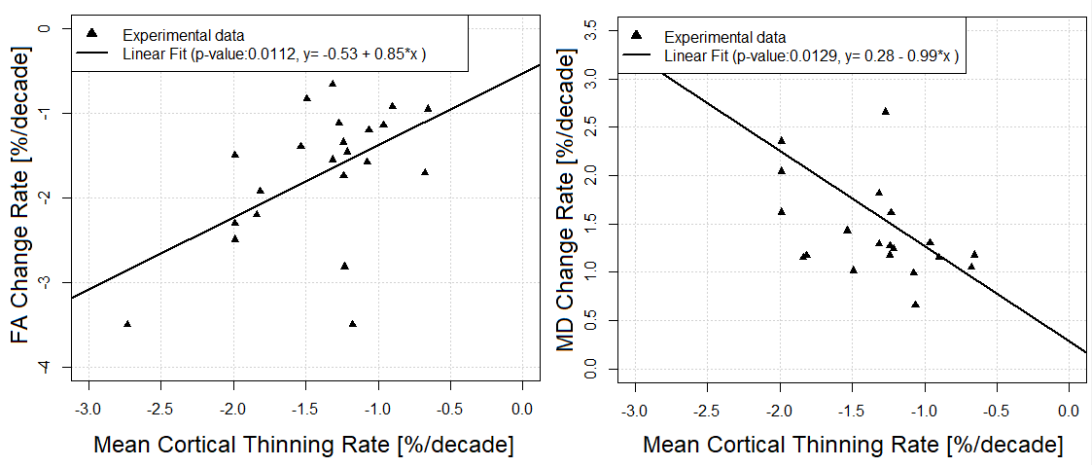

Source: Author

In order to analyze the associations between WM integrity parameters (FA/MD) and cortical thickness information, Equations 17 and 18 were used to fit the data from the cortical regions connecting ends of each brain tract in the aging process. We obtained that the age was the most significant parameter for all of the tracts, with a p-value<0.001 (FDR corrected). The cortical thickness was not significant in the regression for the majority of the tracts to explain FA and MD alterations. Except for the fornix, in which the Subcallosal gyrus cortical thickness was significantly (p<0.05 FDR corrected) correlated with the FA and MD alterations, in both hemispheres for MD and in the left hemisphere for FA, Figure 36. The left Subcallosal gyrus was the region of with greater cortical thinning.

Figure 36 FA and MD change rates [%/decade] in left/right fornix versus the mean cortical thickness change rate [%/decade] of the Subcallosal gyrus, accounting for the Age and Cortical Thickness of the Temporal Pole. Presented p-values are FDR corrected.

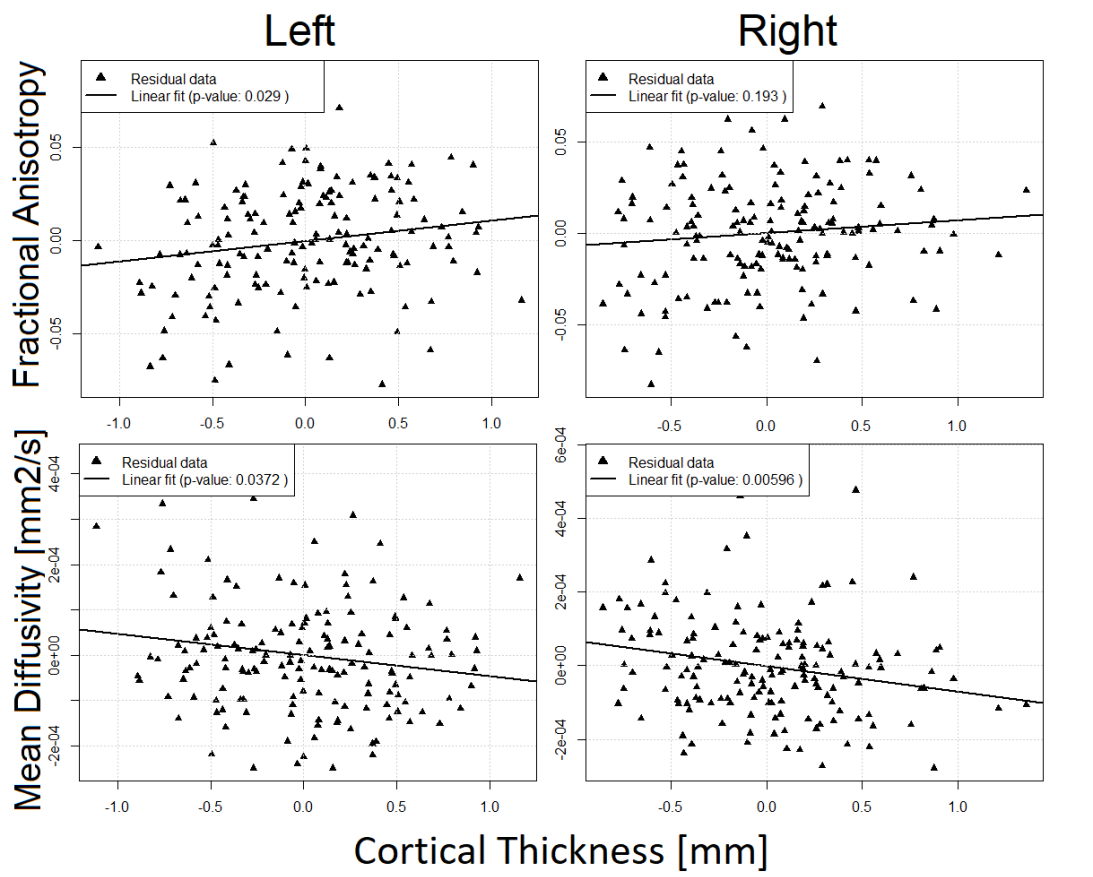

Source: Author

Several studies indicated whole-brain age-related cortical thinning, in pre-frontal cortex areas (SALAT et al., 2004), superior and inferior frontal gyrus and temporal lobe (FJELL et al., 2009; LEMAITRE et al., 2012b), precentral, paracentral, postcentral and orbitofrontal gyrus (LEMAITRE et al., 2012a; THAMBISETTY et al., 2010). In this study, frontal and temporal patterns of cortical thinning were demonstrated in both datasets, Figure 20 and Figure 23, in accordance with the literature (FREEMAN et al., 2008; LEMAITRE et al., 2012a; SALAT et al., 2004), yet HCRP data showed a broader pattern in significant cortical thinning ($p<0.05$ FDR level) in these regions.

There were some regional differences between the results from the datasets. NKI/Rockland results show a significant reduction in cortical thickness in the postcentral gyrus, agreeing with literature that there is a cortical thinning in primary somatosensory areas (LEMAITRE et al., 2012a; THAMBISETTY et al., 2010), while HCRP results did not show any significant reduction in left or right postcentral regions. The difference in the cortical thinning estimates between the two datasets could be caused by the difference in the demography of the data. Also, the data from NKI/Rockland sample is defaced, and it can affect how the FreeSurfer software does structural analysis compared to normal data (discussed at: https://www.mail-archive.com/freesurfer@nmr.mgh.harvard.edu/msg44605.html). Another factor that could influence why the cortical estimates differ in some brain regions could be the acquisition parameters used for the anatomical images, HCRP data used a TI of 900ms, while NKI/Rockland used 1200 ms, this parameter could be affect the contrast to noise ratio (CNR) of the image. In Figure 37, the first one, HCRP anatomical image, seem to have more contrast compared to the second, from NKI/Rockland sample.

Figure 37 Anatomical images of HCRP (a) and NKI/Rockland (b) datasets.

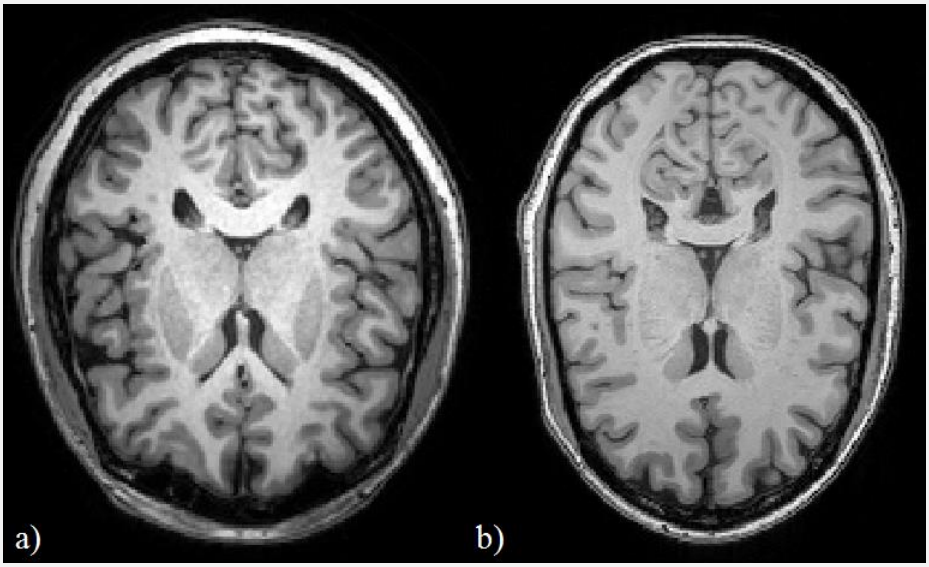

50 years old healthy women.

Source: Author

Previous results from our research group in a similar data were different. Most accentuated cortical thinning in young adults (0.13mm/decade in the left post central gyrus, 0.09mm/decade in the right anterior rostral cingulum), with a thinning rate 65% bigger than old adults (0.06mm/decade in the right inferior frontal gyrus and in the left superior temporal lobe), indicating a decline in cortical thinning with aging (CUNHA, 2014), contrasting with the majority of results in many studies, including this one, in which the post central gyrus does not present a significant thinning. Probably, the used fitting model can have generated these differences.

In the group comparison of cortical thinning patterns, it was expected that, due to known cortical alterations with aging (FREEMAN et al., 2008; SALAT et al., 2004), the older the age the bigger differences compared to the middle age group. The result shown in Table 4 and Figure 22, demonstrated that the aging process affects the brain structure. Specifically, the cortical thickness is most affected after the sixth decade of life. Post-mortem studies report age-related cortical thinning that is particularly accelerated during the sixth and seventh decades (KEMPER et al., 1994).

Cortical thinning with age does not necessarily correspond with neuronal loss, but alterations in neuronal architecture, reduced synapses and lower metabolic cell activity (ESIRI, 2007; FREEMAN et al., 2008; TERRY; DETERESA; HANSEN, 1987). Analysis of white matter integrity may provide additional information about the structural alterations occurring in the brain aging.

The whole-WM voxel-wise analysis was performed on the diffusion parameter FA in the TBSS pipeline for measurements of the group differences related to age. The results are demonstrated at Table 5 and Figure 24. COG position is the same in the three comparisons. On the other hand, the MAX tract position is in the CST for the comparison between the younger groups and in the left ILF for the comparisons concerning the older group. From the 6th decade of life it was seen that there is a more extensive area of significantly diminished FA compared to younger groups, due to more advanced axonal degeneration.

It is possible to see the difference between younger and older compared to middle aged adults in Figure 38. Overlaying the younger over the older adult brains shows clearly which are the WM regions that differ with aging, showing an evident enlargment of WM areas that are affected in the elderly. Location of the voxel with highest significant FA difference between groups changes to temporal lobe when the older group is considered, indicating more pronounced damage in that area.

Figure 38 TBSS results comparing patterns of FA differences.

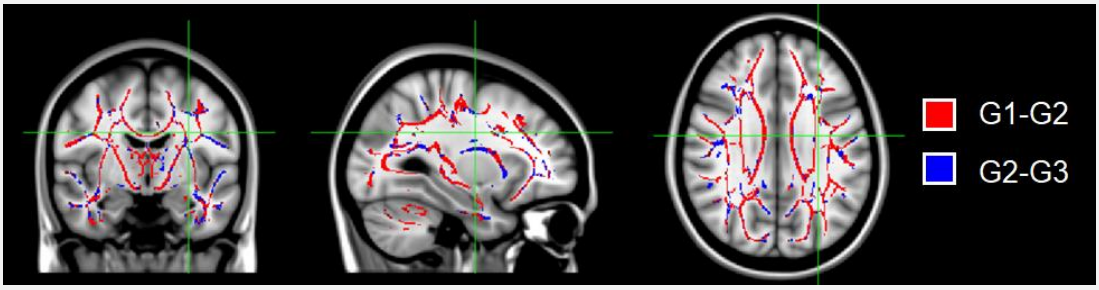

Between young and middle-age groups (G1 – G2): red; middle-age and old groups (G2 – G3): blue. Red patterns are superimposed over the blue.

Source: Author

FSLview offers an atlas tool that overlays the final significance map upon the mean FA skeleton image and the affected anatomical region can be inferred with

the guidance of JHU ICBMDTI-81 atlas (HUA et al., 2008; WAKANA et al., 2007), the tract identification was performed according to the regional names in this atlas. As shown in Figure 24 and Figure 38, the FA decreases in the groups in some WM regions, including: genu of corpus callosum (GCC), body of corpus callosum (BCC), anterior corona radiata (ACR), superior corona radiata (SCR), superior longitudinal fasciculus (SLF), and Fornix (FX). Uncinate fasciculus presents a non-linear pattern of alteration of FA with age, since this only showed a statistically significant decrease in comparisons with the older group. Although many of the regions were identified based on the atlas guidance, there were regions with no labels, which could not be identified. TBSS provides voxelwise statistics, but the analysis is limited to skeleton voxels with many neglected WM regions.

An additional group analysis with the diffusion data was performed, considering the AFD parameter of the CSD modeling. In Figure 25, the comparison between G1 and G2 show few regions with significant alterations of AFD, fornix, cerebellar peduncle and base of the CST, comparing between G2 and G3 demonstrated alterations in the CC, CGC, FX, ILF, IFOF and anterior thalamic radiation, and between G1 and G3 all of those were affected but also the CST and cerebellar peduncle. Demonstrating significant alterations in the streamline density in the aging process in different parts of the brain, as prefrontal, precentral, parahippocampal and cingulate gyrus, corpus callosum and temporal lobes, in accordance with the literature (STADLBAUER et al., 2012).Showing that from the 6th decade of age the brain integrity changes occurs more abruptly.

These results suggest that neuronal changes underlying FA decrease with healthy aging affect white matter microstructure throughout the brain, more significantly in the elderly (over 60 years) due to more advanced axonal degeneration (MARNER et al., 2003). Our results point to steeper axonal degradation from the sixth decade of life. When comparing the regions of the clusters for the TBSS, Figure 24, and AFD comparisons, Figure 25, there was an evident amplification of the WM regions that are affected in the older subjects, affecting several brain tracts, including the ones responsible for cognitive processes and memory, such as the uncinate fasciculus(METZLER-BADDELEY et al., 2011). With these results, it is understood that the white matter degeneration, considering FA and fiber density parameters, occurs in the tract

specific way, and some tracts are more affected in different age ranges, the fornix being one of the first tracts to be affected in this natural degeneration process. These results agree with the literature shown for FA (KOCHUNOV et al., 2007). In this way, AFD seems to show complementary information for understanding the white matter integrity (RAFFELT et al., 2017) alterations throughout the lifespan, that haven't been demonstrated yet in the aging process.

Combining the group analysis of the diffusion data, Figure 24 and Figure 25, with the one performed previously, concerning the cortical thinning pattern, the tests present an age-associate decline in the structural integrity parameters of the grey and white matter. Apparently a more marked degradation of the tissues is seen from the sixth decade of life onwards, seeming that these two parameters of tissue integrity may be correlated in the aging process. Cortical thinning in normal aging is known to be caused by structural neuronal changes, and it is conceivable that these changes in turn may affect connecting WM tracts.

For the tract specific analysis of the diffusion parameters there were different methods for tracts selection, as manual, automated and based on cortical regions, using DT and CSD diffusion models for some. In the aging process the water diffusion tends to become more isotropic, due to structural alterations on the WM fibers, tissue organization and extracellular water content, so we evaluated these alterations by the diffusion parameters.

In the manual tract selection, it was possible to verify FA reductions, Figure 27, and MD increases in the life span, Table 6 (STADLBAUER et al., 2012). The FA reduction was verified for all tracts, demonstrating, once more, that these are age-sensitive parameters that are useful for aging studies, agreeing with the literature (LEBEL et al., 2012; MICHIELSE et al., 2010; YASMIN et al., 2009). From these findings, we hypothesize that the aging process affects the brain structural connectivity in a tract specific way. Structural changes in the white matter architecture and degeneration of fiber integrity, such as demyelination and change in the microstructure that compose WM. The differences in the order of the rate of change of these parameters with age could be related to the different structural alteration in the WM connections of these specific fibers, producing different patterns of alteration of FA and MD.

The fornix presented a high rate of change in the aging process, in agreement with the literature, the limbic regions connected by this tract are also more

affected by normal aging (YASMIN et al., 2009). The corpus callosum exhibit an antero-posterior gradient of FA decrease, as previously reported in the literature (LEBEL; CAVERHILL-GODKEWITSCH; BEAULIEU, 2010; SALAT et al., 2005), and the use of cortical regions for CC streamlines selection is very useful for studying the interhemispheric connections (PARK et al., 2008). It is important to notice that the MD alteration rate for the corpus callosum segmented by the structural cortical connections do not show the same antero-posterior gradient of alterations of FA in the aging process. This result is concordant to previous results in which the antero-posterior degeneration pattern is not observed for the MD parameter in the aging process (LEBEL; CAVERHILL-GODKEWITSCH; BEAULIEU, 2010).

For automated selection of brain tracts using AFQ software, the FACT tractography algorithm, the reconstruction of tracts was correct for most of them, in the age effect analysis,

Table 7, 10/20 brain tract demonstrated significant decrease in FA, 14/20 decreased AD, 8/20 decreased MD and none changed significantly RD. Using the CSD tractography algorithm, the automated selection from the CSD tractograms showed a sub-optimal selection of many tracts, leading us to the idea that the results for the Forceps Major and Minor of the Corpus Callosum, IFOF and Uncinate Fasciculus would not be the most realistic representation of this tracts from this tractography algorithm, Figure 28. Mean FA values are higher in the automated selection of tracts comparing with the manual selection using the TrackVis software.

From the connectomes, we reconstructed some known fiber tracts based on cortical regions, the ones from DT tractography showed anatomical similarities for the fiber bundles, Figure 29, and the behavior of the diffusion parameters in the aging process are in accordance to what was expected, Table 8, the majority of FA decreases, and alterations in MD/AD/RD according to each tracts. Using CSD tractography generated some inconsistencies, for example, the corpus callosum fibers, were not well reconstructed, showing many spurious fibers in the interhemispheric region near the cortex, where there was not supposed to have any fibers crossing. This pattern was found for the majority of the subjects, due to that, even though there were significant effects of age in the diffusion parameters for the different parts of the corpus callosum, they should be

discarded. The cingulum was the only fiber tract that was fairly reconstructed from this CSD tractograms, for them the FA decreased with age and MD and RD increased. The others tracts were not found in many subjects, and also did not show significant alterations in the aging process.

CSD algorithm is better for resolving crossing fibers and because of that, in theory, the FA estimation is more accurate for the selected tracts. One factor is the selection of tracts, manual selection is more precise and accurate, but very time consuming, the automated selection is very fast, but works fine for some tracts better than others. Another factor that must be considered is the quality of our data, with only 32 gradient directions and one b value of 1000s/mm^2, for that, the FACT algorithm seems better for our data. From the previous results, of automated tract selection and based on cortical regions, for our dataset (1 non-dWI, 32 directions with b-value of 1000 mm/s^2) the DT model (FACT whole-brain tractography algorithm) seems more adequate for the analysis and gives more reliable results comparing to the reconstruction limitations from the CSD algorithm, that is not suitable for our data.

The general results of the tract specific analysis are demonstrated in Figure 30, the FA reduction is consistent for all the methods of selecting the brain tracts. However, the MD showed a majority of increases for the manual and based on cortical regions, while the automated selection resulted in decreases of these parameters for all the tracts we evaluated. The antero-posterior decrease gradient of FA in the corpus callosum is only observed when selecting manually the tracts. Taking the results of Figure 30 and Figure 31 into account, the manual selection of tracts from the FACT whole-brain tractography demonstrate more reliable data for further analysis. Considering the results from this tract selection procedure, our findings demonstrate higher rate changes of the diffusion parameters for projection (fornix) and commissural (frontal part of the corpus callosum) fibers, according to Figure 4 tract classification. FA and MD rate changes do not show the same pattern for all the tracts, for the fornix there is an agreement between the parameters that the integrity of the streamlines is altering with a much higher rate than others, and for the CC the antero-posterior gradient of deterioration is not seen for the MD parameter. Showing that the two parameters give complementary information about the tract integrity in the aging process.

For the connectome analysis, it was expected a linear decrease of the number of streamlines with age, as it has been reported previously (SZCZEPANKIEWICZ et al., 2013), so, our results agree with that in some specific connections of the healthy aging brain there are significant reductions, Figure 32, with a high dependency of the tractography algorithm used. The Desikan-Killiany parcellation presents more regions being significantly reduced, probably because the cortical regions are bigger and have more fibers crossing through them, so it is better for verifying these changes.

As expected the reduction of global efficiency with age, Figure 33, independent of parcellation atlas, nor tractography algorithm, (ZHU et al., 2012). Reduction of local efficiency was found in the healthy control participants, mainly located in the prefrontal, temporal, and parietal regions and their connections, regions that are known for significant alterations in white matter integrity in the aging process, supporting its relation with age-related functional alterations and its relationship with cognitive decline (GONG et al., 2010).

Therefore, for our dataset (1 non-dWI, 32 directions and b-value of 1000 mm/s^2, 3T) the DT model seems more adequate for the analysis and gives reliable results considering its limitations. In general, CSD is indeed a good model to describe the diffusion in the brain tissues, as the FOD does not loose information in a single voxel that has multiple fibers bundles crossing in different orientations (FARQUHARSON et al., 2013; TOURNIER; CALAMANTE; CONNELLY, 2012). However, it is necessary that the diffusion data is acquired in a high angular resolution imaging modality to have a robust result for the CSD modelling. In all, CSD model seems to give better connectomic results, however, it is necessary to be very careful when analyzing this kind of data, and knowing the limitations of your dataset, because this could give results and interpretations that does not correspond correctly to the white matter pathways since there is not enough information, due to the imaging modality used in the acquisition (SOTIROPOULOS; ZALESKY, 2017). Our results suggest that the DT model is the most appropriated algorithm to perform tractographies in our data.

Now, relating the cortical thickness information for each tract connections, Figure 34 represents the absolute difference of cortical thinning rates in the areas connected by the tracts. It was shown that for most of the tracts, the connected regions age with similar rates (modulus of differences under the mean thinning

rate differences of each hemisphere). For five tracts (left/right inferior fronto-occipital fasciculus, left fornix, right cingulate part of the cingulum and right arcuate fasciculus) show higher differences, demonstrating that for these connections one of the cortical areas is more affected than the other in the aging process, that can be due to the degree of WM degradation.

From Figure 35, a significant relationship between FA and MD change rates with mean cortical thinning rates of the regions connected by the tracts was found. This finding supports the nexus between axonal integrity and cortical organization. Additionally, FA and MD variations are significant even when the cortical thickness rate is null. Therefore, from the fitted linear relationship, even when our study is not longitudinal, we can suggest that white matter alterations as detected by MRI are more sensitive than cortical thickness variations. This evidence confirms previous studies indicating FA decrease and MD increase in WM as sensitive markers of aging (GIORGIO et al., 2010; HUGENSCHMIDT et al., 2008; MICHIELSE et al., 2010; TEIPEL et al., 2014; VOINESKOS et al., 2012).

Using equations 17 and 18, for all tract-cortical relationships, the main factor that explains the FA and MD variations between subjects is the age (p-value<0.001, FDR corrected). Most tracts did not show a significant association with cortical thickness in the multiple regression after use the age as a confounding factor. Only left and right fornix demonstrated a significant direct association between FA and MD with cortical thicknesses of one of its ending cortical areas, Figure 36. This fact leads us to understand that the aging process affects the brain structural connectivity in a tract specific way. This tract specific finding can be related to well-known reports of cognitive decline in the elderly (METZLER-BADDELEY et al., 2011), providing that diffusion integrity of this limbic tract is related to the GM structure and therefore, to cognitive functions (GRIEVE et al., 2011). Numerous alterations in the brain structure and function with age affect total brain volume and WM integrity and also predicts cognitive decline. Studies demonstrated that cognitive decline related to the aging process are expressed after a threshold of structural deterioration (RAZ, 2000).

Some limitations can be noted in our cross-sectional study. An additional longitudinal study would be of great value to assess the tract-cortico relations in the aging process to evaluate if the findings obtained here are valid for individual

subjects. Using a bigger cohort of healthy subjects, we could have a more robust study and also evaluate the sex effect in this relation. Another limitation is related to the data, a standard acquisition protocol of the diffusion images, with one b-value of 1000s/mm^2 and only one b0, limited the possible models to characterize the intravoxel diffusion. For further studies we aim to use more sophisticated acquisition protocols for multi-shell data to use other diffusion models and tractography algorithms, for removing some bias from the limitation of one direction of streamline per voxel. And also examine the tract-cortico relations involving more brain tracts. Additionally, more detailed cortical parcellations could help in a better definition of the tract endings.

6. Conclusion

Spatial patterns of degeneration of FA and AFD were heterogeneous, some white matter regions were affected before others in the aging process.

Tract specific change rate for the diffusion parameters was observed, describing a different WM integrity degeneration for each tract throughout lifespan, being the most affected the corpus callosum, mainly the anterior part, and the fornix.

In the connectome study, the structural network connections between brain regions demonstrated alterations during the normal aging process, independently of the parcellations atlases.

For our dataset, the diffusion tensor model seemed more adequate for the analysis and gave reliable results considering its limitations.

For the tract-cortical analysis, the cortical regions connected by tracts demonstrated similar thinning patterns for the majority of tracts; a significant relation between mean cortical thinning rate and FA/MD alteration rates were found; and in the tract specific analysis, the age was the main effect controlling the parameters alterations, except for the fornix, in which the cortical thickness of the Subcallosal gyrus is significantly related to the alterations of the diffusion parameters.

Accepted, Presented and Submitted Abstracts in National and International Conferences

Pinto, M. S., Santos, A. C., Salmon, C. E. G. “Assessment of the Decline in Fractional Anisotropy and Cortical Thinning with Age in Healthy Adults” – XV Semana da Física Médica, Ribeirao Preto-SP-Brazil 2016

Pinto, M. S., Vieira, B. H., Santos, A. C., Salmon, C. E. G. “Tract Integrity Alterations Throughout Life Span” - 4th BRAINN Congress, Campinas-SP-Brazil 2017

Pinto, M. S., Santos, A. C., Salmon, C. E. G. “Cross-Sectional Assessment of Diffusion Parameters in Specific Brain Tracts correlated with Cortical Thinning throughout Healthy Aging” - ISMRM 25th Annual Meeting, Honolulu-HI-United States 2017

Vieira, B. H., Pinto, M. S., Salmon, C. E. G. “Grey and White Matter Integrity Assessment Along Brain Tracts Throughout Normal Aging” - OHBM 2017 Annual Meeting, Vancouver-BC-Canada 2017

Pinto, M. S., Santos, A. C., Salmon, C. E. G. “Structural and Functional Connectivities in Corpus Callosum Tracts over Normal Aging” - OHBM 2017 Annual Meeting, Vancouver-BC-Canada 2017

Pinto, M. S., Santos, A. C., Salmon, C. E. G. “Comparação da integridade das fibras cerebrais no envelhecimento normal utilizando análise TBSS” – Congresso Brasileiro de Física Médica 2017, Ribeirao Preto-SP-Brazil 2017

Pinto, M. S., Salmon, C. E. G. “Assessment of Diffusion Parameters in Specific Brain Tracts During Aging Using Two Approaches” – XVI Semana da Física Médica 2017, Ribeirao Preto-SP-Brazil 2017

Pinto, M. S., Santos, A. C., Salmon, C. E. G. “Apparent Fiber Density Alterations in Healthy Aging” – 8º Simpósio de Instrumentação e Imagens Médicas, São Bernardo do Campo-SP-Brazil 2017

Pinto, M. S., Santos, A. C., Salmon, C. E. G. “Group Analysis of Healthy Aging Microstructural Integrity Parameters” - ISMRM 26th Annual Meeting, Paris – France 2018

7. References

ALEXANDER, D. C.; BARKER, G. J.; ARRIDGE, S. R. Detection and modeling of non-Gaussian apparent diffusion coefficient profiles in human brain data. **Magnetic Resonance in Medicine**, v. 48, n. 2, p. 331–340, 2002.

ANDERSSON, J. L. R.; SOTIROPOULOS, S. N. An integrated approach to correction for off-resonance effects and subject movement in diffusion MR imaging. **NeuroImage**, v. 125, p. 1063–1078, 2016.

ASSAF, Y. et al. New modeling and experimental framework to characterize hindered and restricted water diffusion in brain white matter. **Magnetic Resonance in Medicine**, v. 52, n. 5, p. 965–978, 2004.

BASSER, P. J.; MATTIELLO, J.; LEBIHAN, D. MR diffusion tensor spectroscopy and imaging. **Biophysical Journal**, v. 66, n. 1, p. 259–267, 1994.

BASSETT, D. S. et al. Conserved and variable architecture of human white matter connectivity. **NeuroImage**, v. 54, n. 2, p. 1262–1279, 2011.

BEHRENS, T. E. J. et al. Probabilistic diffusion tractography with multiple fibre orientations: What can we gain? **NeuroImage**, v. 34, n. 1, p. 144–155, 2007.

BENDER, A. R.; VOLKLE, M. C.; RAZ, N. Differential aging of cerebral white matter in middle-aged and older adults: A seven-year follow-up. **NeuroImage**, v. 125, p. 74–83, 2016.

BENJAMINI, Y.; HOCHBERG, Y. Controlling the False Discovery Rate: a Practical and Powerful Approach to Multiple Testing. **Journal of the Royal Statistical Society**, v. 57, n. 1, p. 289–300, 1995.

CLARK, K. A. et al. Mean diffusivity and fractional anisotropy as indicators of disease and genetic liability to schizophrenia. **Journal of Psychiatric Research**, v. 45, n. 7, p. 980–988, 2011.

CONCHA, L.; BEAULIEU, C.; GROSS, D. W. Bilateral limbic diffusion abnormalities in unilateral temporal lobe epilepsy. **Annals of Neurology**, v. 57, n. 2, p. 188–196, fev. 2005.

CUNHA, H. H. Desenvolvimento de um software para geração de redes complexas formadas a partir de estimativas de conectividade cerebral: Um estudo da espessura cortical no cérebro de indíviduos saudáveis e pacientes com epilepsia. p. 97, 2014.

DE STEFANO, N. et al. Evidence of early cortical atrophy in MS: Relevance to white matter changes and disability. **Neurology**, v. 60, n. 7, p. 1157–1162, 2003.

DEKABAN, A. S.; SADOWSKY, D. Changes in brain weight during the span of human life: relation of brain weight to body height and body weight. **Ann. Neurol.**, v. 4, p. 345, 1978.

DESIKAN, R. S. et al. An automated labeling system for subdividing the human cerebral cortex on MRI scans into gyral based regions of interest. **NeuroImage**, v. 31, n. 3, p. 968–980, 2006.

ESIRI, M. Ageing and the brain. **The Journal of Pathology**, v. 211, n. 2, p. 181–187, jan. 2007.

FARQUHARSON, S. et al. White matter fiber tractography: why we need to move beyond DTI. **J Neurosurg**, v. 118, n. June, p. 1367–1377, 2013.

FISCHL, B. et al. Automatically Parcellating the Human Cerebral Cortex. **Cerebral Cortex**, v. 14, n. 1, p. 11–22, 2004.

FISCHL, B. FreeSurfer. **Neuroimage2**, v. 62, n. 2, p. 774–781, 2012.

FISCHL, B.; DALE, A. M. Measuring the thickness of the human cerebral cortex from magnetic resonance images. v. 2000, n. Track II, 2000.

FJELL, A. M. et al. High consistency of regional cortical thinning in aging across multiple samples. **Cerebral Cortex**, v. 19, n. 9, p. 2001–2012, 2009.

FREEMAN, S. H. et al. Preservation of neuronal number despite age-related cortical brain atrophy in elderly subjects without Alzheimer disease. **J Neuropathol Exp Neurol**, v. 67, n. 12, p. 1205–1212, 2008.

GIORGIO, A. et al. Age-related changes in grey and white matter structure throughout adulthood. **NeuroImage**, v. 51, n. 3, p. 943–951, 2010.

GONG, G. et al. Age- and gender-related differences in the coritcal anatomical network. **Journal of Neuroscience**, v. 29, n. 50, p. 15684–15693, 2010.

GRIEVE, S. M. et al. Regional heterogeneity in limbic maturational changes: Evidence from integrating cortical thickness, volumetric and diffusion tensor imaging measures. **NeuroImage**, v. 55, n. 3, p. 868–879, 2011.

GUTTMANN, G. White matter changes with normal aging. **Neurology**, 1998.

HAGMANN, P. et al. Mapping the structural core of human cerebral cortex. **PLoS Biology**, v. 6, n. 7, p. 1479–1493, 2008.

HASAN, K. M. et al. Development and aging of the healthy human brain uncinate fasciculus across the lifespan using diffusion tensor tractography. **Brain**

Research, v. 1276, p. 67–76, 2009.

HUA, K. et al. Tract probability maps in stereotaxic spaces: Analyses of white matter anatomy and tract-specific quantification. **NeuroImage**, v. 39, n. 1, p. 336–347, 2008.

HUGENSCHMIDT, C. E. et al. Relating imaging indices of white matter integrity and volume in healthy older adults. **Cerebral Cortex**, v. 18, n. 2, p. 433–442, 2008.

JANG, S. H.; CHO, S.-H.; CHANG, M. C. Age-related degeneration of the fornix in the human brain: a diffusion tensor imaging study. **The International journal of neuroscience**, v. 121, n. 2, p. 94–100, 2011.

JANG, S. H.; SEO, J. P. Aging of corticospinal tract fibers according to the cerebral origin in the human brain: A diffusion tensor imaging study. **Neuroscience Letters**, v. 585, p. 77–81, 2015.

JENKINSON, M. et al. FSL. **NeuroImage**, v. 62, n. 2, p. 782–790, ago. 2012.

JENSEN, J. H. et al. Diffusional Kurtosis Imaging : The Quantification of Non-Gaussian Water Diffusion by Means of Magnetic Resonance Imaging. v. 1440, p. 1432–1440, 2005.

JERNIGAN, T. L.; PRESS, G. A.; HESSELINK, J. R. Methods for measuring brain morphologic features on magnetic resonance images. Validation and normal aging. **Arch Neurol**, v. 47, n. 1, p. 27–32, 1990.

KOCHUNOV, P. et al. Relationship between white matter fractional anisotropy and other indices of cerebral health in normal aging: Tract-based spatial statistics study of aging. **NeuroImage**, v. 35, n. 2, p. 478–487, 2007.

KOCHUNOV, P. et al. Fractional anisotropy of cerebral white matter and thickness of cortical gray matter across the lifespan. **NeuroImage**, v. 58, n. 1, p. 41–49, 2011.

LEBEL, C. et al. Diffusion tensor imaging of white matter tract evolution over the lifespan. **NeuroImage**, v. 60, n. 1, p. 340–352, 2012.

LEBEL, C.; CAVERHILL-GODKEWITSCH, S.; BEAULIEU, C. Age-related regional variations of the corpus callosum identified by diffusion tensor tractography. **NeuroImage**, v. 52, n. 1, p. 20–31, 2010.

LEMAITRE, H. et al. Normal age-related brain morphometric changes: Nonuniformity across cortical thickness, surface area and gray matter volume? **Neurobiology of Aging**, v. 33, n. 3, p. 617.e1-617.e9, 2012a.

LEMAITRE, H. et al. Normal age-related brain morphometric changes: Nonuniformity across cortical thickness, surface area and gray matter volume? **Neurobiology of Aging**, v. 33, n. 3, p. 617.e1-617.e9, 2012b.

MALYKHIN, N. et al. Diffusion tensor imaging tractography and reliability analysis for limbic and paralimbic white matter tracts. **Psychiatry Research - Neuroimaging**, v. 164, n. 2, p. 132–42, 2008.

MARNER, L. et al. Marked loss of myelinated nerve fibers in the human brain with age. **Journal of Comparative Neurology**, v. 462, n. 2, p. 144–152, 2003.

METZLER-BADDELEY, C. et al. Frontotemporal connections in episodic memory and aging: a diffusion MRI tractography study. **The Journal of neuroscience : the official journal of the Society for Neuroscience**, v. 31, n. 37, p. 13236–45, 2011.

MICHIELSE, S. et al. Selective effects of aging on brain white matter microstructure: A diffusion tensor imaging tractography study. **NeuroImage**, v. 52, n. 4, p. 1190–1201, 2010.

MONTEMBEAULT, M. et al. The impact of aging on gray matter structural covariance networks. **NeuroImage**, v. 63, n. 2, p. 754–759, 2012.

MORI, S. et al. Three-dimensional tracking of axonal projections in the brain by magnetic resonance imaging. **Annals of neurology**, v. 45, n. 2, p. 265–9, 1999.

MOSELEY, M. E. et al. Diffusion-weighted MR imaging of anisotropic water diffusion in cat central nervous system. **Radiology**, v. 176, n. 2, p. 439–445, 1990.

NOONER, K. B. et al. The NKI-Rockland sample: A model for accelerating the pace of discovery science in psychiatry. **Frontiers in Neuroscience**, v. 6, n. OCT, p. 1–11, 2012.

NUSBAUM, A. O. et al. Regional and global changes in cerebral diffusion with normal aging. **AJNR Am J Neuroradiol**, v. 22, n. 1, p. 136–142, 2001.

OWEN, J. P. et al. Test–Retest Reliability of Computational Network Measurements Derived from the Structural Connectome of the Human Brain. **Brain Connectivity**, v. 3, n. 2, p. 160–176, 2013.

PAKKENBERG, B.; GUNDERSEN, H. J. G. Neocortical Neuron Number in Humans : v. 320, n. January, p. 312–320, 1997.

PARK, H. J. et al. Corpus callosal connection mapping using cortical gray matter panellation and DT-MRI. **Human Brain Mapping**, v. 29, n. 5, p. 503–516, 2008.

PFEFFERBAUM, A. et al. Study Changes Morphology. **JAMA Neurology**, v. 51, n. 9, 1994.

RAFFELT, D. et al. Apparent Fibre Density: A novel measure for the analysis of diffusion-weighted magnetic resonance images. **NeuroImage**, v. 59, n. 4, p. 3976–3994, 2012.

RAFFELT, D. A. et al. Investigating white matter fibre density and morphology using fixel-based analysis. **NeuroImage**, v. 144, p. 58–73, 2017.

RAFFELT, D.; CONNELLY, A. Unsupervised 3-tissue response function estimation from single-shell or multi-shell diffusion MR data ... n. September, 2016.

RAZ, N. Aging of the brain and its impact on cognitive performance: integration of structural and functional findings BT - Handbook of Aging and Cognition. v. 2, n. June, p. 1–90, 2000.

RAZ, N. et al. Regional brain changes in aging healthy adults: General trends, individual differences and modifiers. **Cerebral Cortex**, v. 15, n. 11, p. 1676–1689, 2005.

RAZ, N. et al. Trajectories of brain aging in middle-aged and older adults: Regional and individual differences. **NeuroImage**, v. 51, n. 2, p. 501–511, 2010.

RAZ, N.; RODRIGUE, K. M. Differential aging of the brain: Patterns, cognitive correlates and modifiers. **Neuroscience and Biobehavioral Reviews**, v. 30, n. 6, p. 730–748, 2006.

ROBERTS, T. P. L. et al. Fiber density index correlates with reduced fractional anisotropy in white matter of patients with glioblastoma. **American Journal of Neuroradiology**, v. 26, n. 9, p. 2183–2186, 2005.

RUBINOV, M.; SPORNS, O. Complex network measures of brain connectivity : Uses and interpretations. **NeuroImage**, v. 52, n. 3, p. 1059–1069, 2010.

SALAT, D. H. et al. Thinning of the cerebral cortex in aging. **Cerebral Cortex**, v. 14, n. 7, p. 721–730, 2004.

SALAT, D. H. et al. Age-related alterations in white matter microstructure measured by diffusion tensor imaging. **Neurobiology of Aging**, v. 26, n. 8, p. 1215–1227, 2005.

SCAHILL, R. I. et al. A Longitudinal Study of Brain Volume Changes in Normal Aging Using Serial Registered Magnetic Resonance Imaging. **Archives of Neurology**, v. 60, n. 7, p. 989, 1 jul. 2003.

SCHOLZ, J.; TOMASSINI, V.; JOHANSEN-BERG, H. **Individual Differences in White Matter Microstructure in the Healthy Brain**. Second Edi ed. [s.l.] Elsevier, 2014.

SMITH, R. E. et al. SIFT: Spherical-deconvolution informed filtering of tractograms. **NeuroImage**, v. 67, p. 298–312, 2013.

SMITH, S. M. et al. Advances in functional and structural MR image analysis and implementation as FSL. **NeuroImage**, v. 23, n. SUPPL. 1, p. 208–219, 2004.

SMITH, S. M. et al. Tract-based spatial statistics: Voxelwise analysis of multi-subject diffusion data. **NeuroImage**, v. 31, n. 4, p. 1487–1505, 2006.

SMITH, S. M. et al. Acquisition and voxelwise analysis of multi-subject diffusion data with tract-based spatial statistics. **Nature protocols**, v. 2, n. 3, p. 499–503, 2007.

SOTIROPOULOS, S. N.; ZALESKY, A. Building connectomes using diffusion MRI : why , how and but. n. June 2016, p. 1–23, 2017.

SPORNS, O.; TONONI, G.; KÖTTER, R. The human connectome: A structural description of the human brain. **PLoS Computational Biology**, v. 1, n. 4, p. 0245–0251, 2005.

STADLBAUER, A. et al. Magnetic resonance fiber density mapping of age-related white matter changes. **European Journal of Radiology**, v. 81, n. 12, p. 4005–4012, 2012.

STEJSKAL, E. O.; TANNER, J. E. Spin Diffusion Measurements: Spin Echoes in the Presence of a Time-Dependent Field Gradient. **The Journal of Chemical Physics**, v. 42, n. 1, p. 288–292, 1965.

STORSVE, A. B. et al. Longitudinal changes in white matter tract integrity across the adult lifespan and its relation to cortical thinning. **PLoS ONE**, v. 11, n. 6, p. 1–21, 2016.

SULLIVAN, E. V.; ADALSTEINSSON, E.; PFEFFERBAUM, A. Selective age-related degradation of anterior callosal fiber bundles quantified In vivo with fiber tracking. **Cerebral Cortex**, v. 16, n. 7, p. 1030–1039, 2006.

SULLIVAN, E. V.; PFEFFERBAUM, A. Diffusion tensor imaging and aging. **Neuroscience and Biobehavioral Reviews**, v. 30, n. 6, p. 749–761, 2006.

SULLIVAN, E. V.; PFEFFERBAUM, A. Neuroradiological characterization of normal adult ageing. **British Journal of Radiology**, v. 80, n. SPEC. ISS. 2, p. 40–42, 2007.

SULLIVAN, E. V et al. Equivalent disruption of regional white matter microstructure in ageing healthy men and women. **Neuroreport**, v. 12, n. 1, p. 99–104, 2001.

SZCZEPANKIEWICZ, F. et al. Variability in diffusion kurtosis imaging: Impact on study design, statistical power and interpretation. **NeuroImage**, v. 76, p. 145–154, 2013.

TANG, P. F. et al. Tract-specific and region of interest analysis of corticospinal tract integrity in subcortical ischemic stroke: Reliability and correlation with motor function of affected lower extremity. **American Journal of Neuroradiology**, v. 31, n. 6, p. 1023–1030, 2010.

TANNER, J. E.; STEJSKAL, E. O. Restricted Self-Diffusion of Protons in Colloidal Systems by the Pulsed-Gradient, Spin-Echo Method. **The Journal of Chemical Physics**, v. 49, n. 4, p. 1768–1777, 1968.

TEIPEL, S. J. et al. Decline of fiber tract integrity over the adult age range: A diffusion spectrum imaging study. **Journal of Magnetic Resonance Imaging**, v. 40, n. 2, p. 348–359, 2014.

TERRY, R. D.; DETERESA, R.; HANSEN, L. A. Neocortical cell counts in normal human adult aging. **Annals of Neurology**, v. 21, n. 6, p. 530–539, 1987.

THAMBISETTY, M. et al. Longitudinal changes in cortical thickness associated with normal aging. **NeuroImage**, v. 52, n. 4, p. 1215–1223, 2010.

TOFTS, P. **Quantitative MRI of the Brain**. [s.l: s.n.].

TOFTS, P. **Quantitative MRI of the Brain**. [s.l: s.n.].

TOURNIER, J. et al. NeuroImage Resolving crossing fi bres using constrained spherical deconvolution : Validation using diffusion-weighted imaging phantom data. v. 42, p. 617–625, 2008.

TOURNIER, J.; CALAMANTE, F.; CONNELLY, A. Robust determination of the fibre orientation distribution in diffusion MRI : Non-negativity constrained super-resolved spherical deconvolution. v. 35, p. 1459–1472, 2007.

TOURNIER, J.; CALAMANTE, F.; CONNELLY, A. MRtrix : Diffusion Tractography in Crossing Fiber Regions. 2012.

TOURNIER, J. D. et al. Direct estimation of the fiber orientation density function from diffusion-weighted MRI data using spherical deconvolution. **NeuroImage**, v. 23, n. 3, p. 1176–1185, 2004.

TOURNIER, J. D.; CALAMANTE, F.; CONNELLY, A. Determination of the

appropriate b value and number of gradient directions for high-angular-resolution diffusion-weighted imaging. **NMR in Biomedicine**, v. 26, n. 12, p. 1775–1786, 2013.

TROLLOR, J. N.; VALENZUELA, M. J. Brain ageing in the new millennium. **Australian and New Zealand Journal of Psychiatry**, v. 35, n. 6, p. 788–805, 2001.

TUCH, D. S. Q-ball imaging. **Magnetic Resonance in Medicine**, v. 52, n. 6, p. 1358–1372, 2004.

TUSTISON, N. J. et al. N4ITK: Improved N3 Bias Correction. **IEEE Transactions on Medical Imaging**, v. 29, n. 6, p. 1310–1320, jun. 2010.

VERAART, J. et al. Weighted linear least squares estimation of diffusion MRI parameters: Strengths, limitations, and pitfalls. **NeuroImage**, v. 81, p. 335–346, 2013.

VERAART, J. et al. Denoising of diffusion MRI using random matrix theory. **NeuroImage**, v. 142, p. 394–406, 2016.

VERAART, J.; FIEREMANS, E.; NOVIKOV, D. S. Diffusion MRI noise mapping using random matrix theory. **Magnetic Resonance in Medicine**, v. 76, n. 5, p. 1582–1593, 2016.

VERSTRAETE, E. et al. Motor network degeneration in amyotrophic lateral sclerosis: A structural and functional connectivity study. **PLoS ONE**, v. 5, n. 10, p. 1–9, 2010.

VOINESKOS, A. N. et al. Age-related decline in white matter tract integrity and cognitive performance: A DTI tractography and structural equation modeling study. **Neurobiology of Aging**, v. 33, n. 1, p. 21–34, 2012.

WAKANA, S. et al. Fiber tract-based atlas of human white matter anatomy. **Radiology**, v. 230, n. 1, p. 77–87, 2004.

WAKANA, S. et al. Reproducibility of quantitative tractography methods applied to cerebral white matter. **NeuroImage**, v. 36, n. 3, p. 630–644, 2007.

WALLER, A. Experiments on the Section of the Glossopharyngeal and Hypoglossal Nerves of the Frog, and Observations of the Alterations Produced Thereby in the Structure of Their Primitive Fibres. **Philosophical Transactions of the Royal Society of London**, v. 140, n. 1850, p. 423–429, 1 jan. 1850.

WANG, D. et al. Tractography atlas-based spatial statistics: Statistical analysis of diffusion tensor image along fiber pathways. **NeuroImage**, v. 125, p. 301–310,

2016.

WANG, R. et al. Diffusion Toolkit : A Software Package for Diffusion Imaging Data Processing and Tractography. **Proc. Intl. Soc. Mag. Reson. Med.**, v. 15, p. 3720, 2007.

WEDEEN, V. J. et al. Mapping complex tissue architecture with diffusion spectrum magnetic resonance imaging. **Magnetic Resonance in Medicine**, v. 54, n. 6, p. 1377–1386, 2005.

WHEELER-KINGSHOTT, C. A. M.; CERCIGNANI, M. About “axial” and “radial” diffusivities. **Magnetic Resonance in Medicine**, v. 61, n. 5, p. 1255–1260, 2009.

WINSTON, G. P. The physical and biological basis of quantitative parameters derived from diffusion MRI. v. 2, n. 4, p. 254–265, 2012.

WU, K. et al. Age-related changes in topological organization of structural brain networks in healthy individuals. **Human Brain Mapping**, v. 33, n. 3, p. 552–568, 2012.

YASMIN, H. et al. Tract-specific analysis of white matter pathways in healthy subjects: A pilot study using diffusion tensor MRI. **Neuroradiology**, v. 51, n. 12, p. 831–840, 2009.

YEATMAN, J. D. et al. Tract Profiles of White Matter Properties : Automating Fiber-Tract Quantification. v. 7, n. 11, 2012.

ZHU, W. et al. Changing topological patterns in normal aging using large-scale structural networks. **Neurobiology of Aging**, v. 33, n. 5, p. 899–913, 2012.

8. APPENDIX

In this section there are some additional images showing the inclusion and exclusion ROIs for manual tract selection according to Table 2, in the most relevant visualization orientation.

Figure 39 Inclusion ROIs for the Arcuate Fasciculus (AF) tracts.

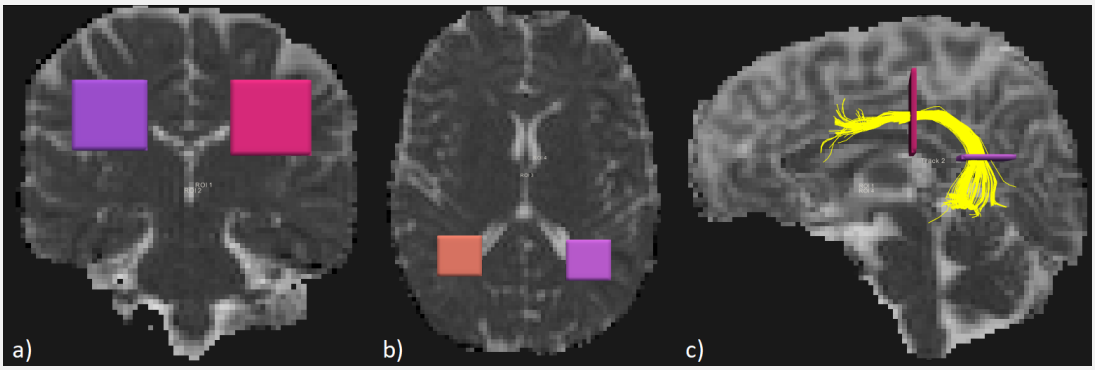

a) ROI selection near the CST fibers, in the coronal slice; b) ROI selection fibers projecting laterally to the sagittal stratum, in the axial slice; c) Reconstructed AF tract, sagittal view.

Source: Author

Figure 40 Exclusion ROIs for the Arcuate Fasciculus (AF) tracts.

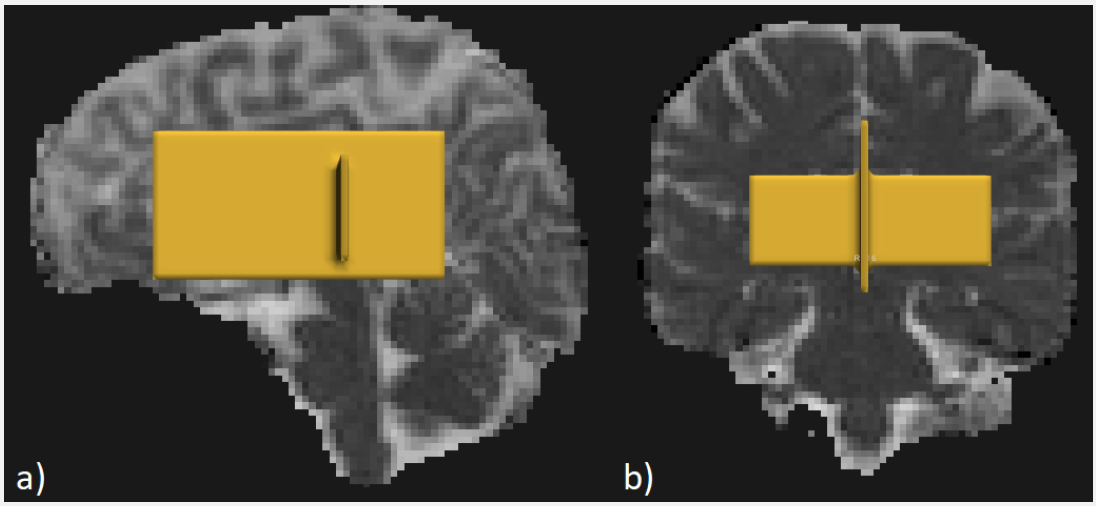

a) ROI selection blocking any fiber to cross the hemispheres, in the middle sagittal slice; b) ROI selection of fibers that are not part of the AF tract, in the coronal slice. Using the operator NOT for ROI filter for all the drawn ROIs.

Source: Author

Figure 41 Inclusion ROIs for the Corpus Callosum (CC) tracts.

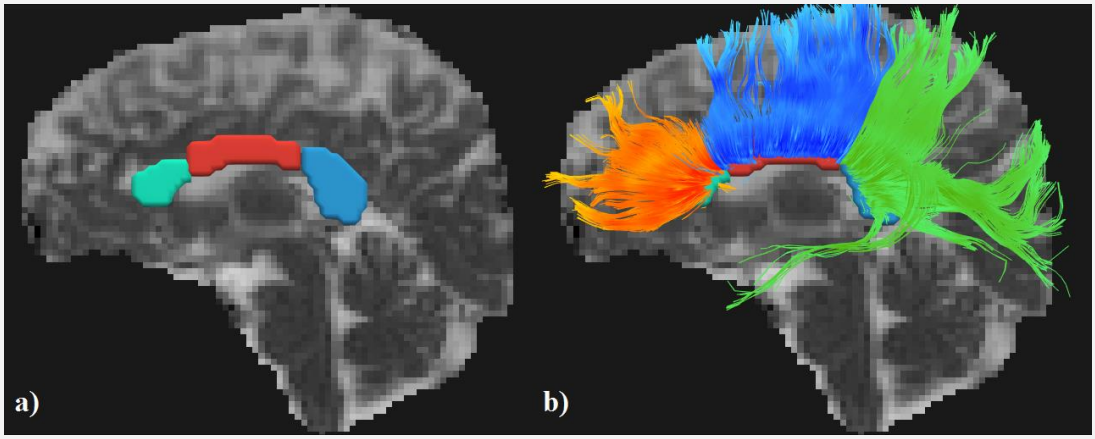

Inclusion ROIs for the CC tracts: a) ROI selection of Genu of CC (GCC - light green), Body of CC (BCC - red) and Splenium of CC (SCC - blue), all in the middle sagittal slice; b) Reconstructed tracts: GCC (orange), BCC (blue) and SCC (green), sagittal view.

Source: Author

Figure 42 Anatomical inclusion ROIs for the Corpus Callosum (CC) tracts considering its interhemispherical connections.

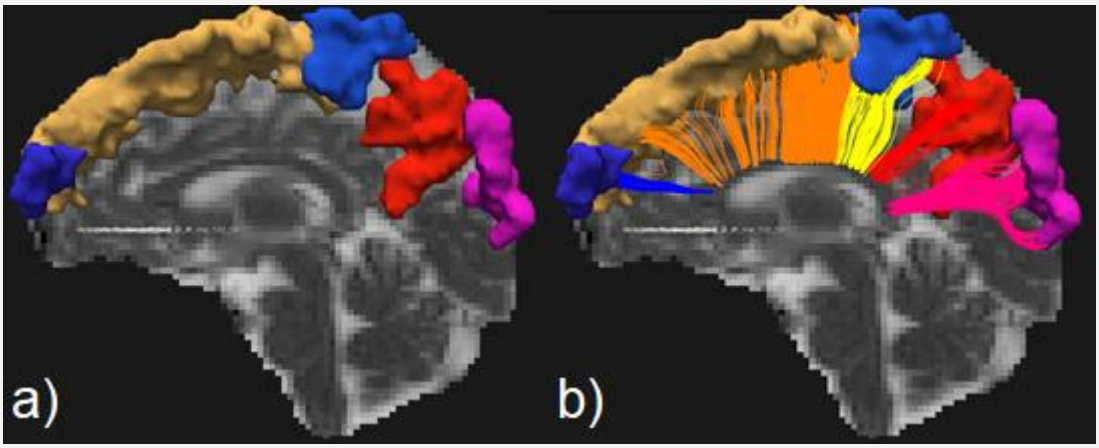

a) ROI selection from Destrieux parcellation atlas, CC_frontopol (dark blue), CC_frontsup (light orange), CC_paracentral (light blue), CC_precuneus (red) and CC_occipitalsup (pink), sagittal view; b) Reconstructed tracts: CC_frontopol (blue), CC_frontsup (orange), CC_paracentral (yellow), CC_precuneus (red) and CC_occipitalsup (pink), sagittal view.

Source: Author

Figure 43 Exclusion ROIs for the Corpus Callosum (CC) tracts.

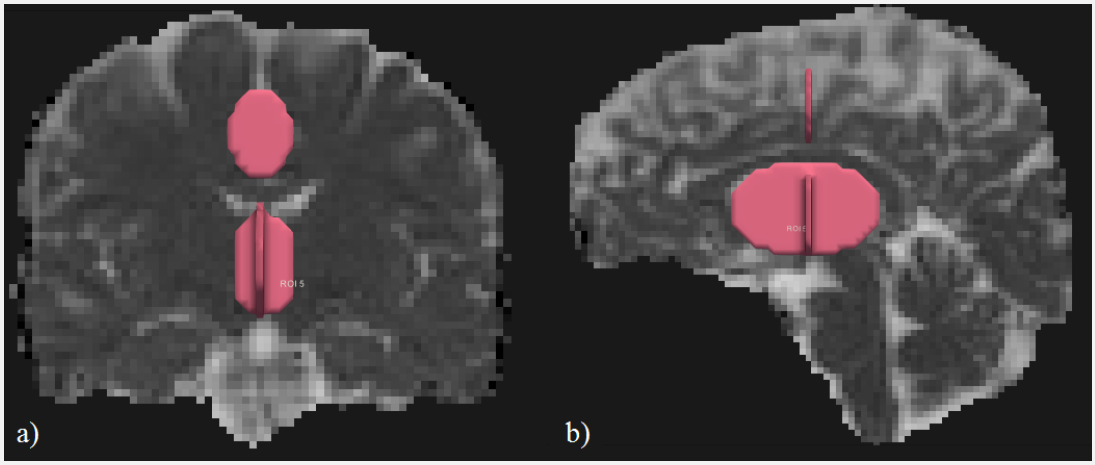

a) ROI selection over and under the anatomical region of the CC, in the coronal slice; b) ROI selection under the anatomical region of the CC, in the middle sagittal slice. Using the operator NOT for ROI filter for all the drawn ROIs.

Source: Author

Figure 44 Inclusion ROIs for the Cingulate part of the Cingulum (CGC) tracts.

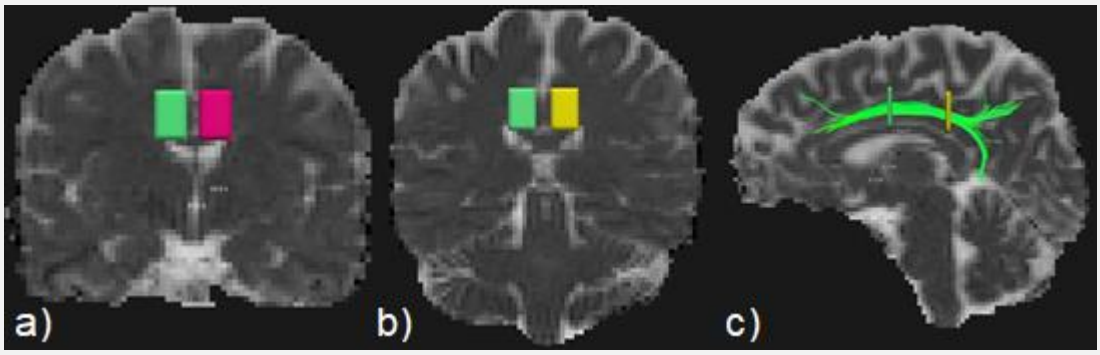

a) ROI selection in the middle of the corpus callosum, laterally located for each hemisphere, coronal slice; b) ROI selection near the splenium part of the corpus callosum, each located in each hemisphere; c) Reconstructed CGC tract, sagittal view.

Source: Author

Figure 45 Exclusion ROIs for the Cingulate part of the Cingulum (CGC) tracts.

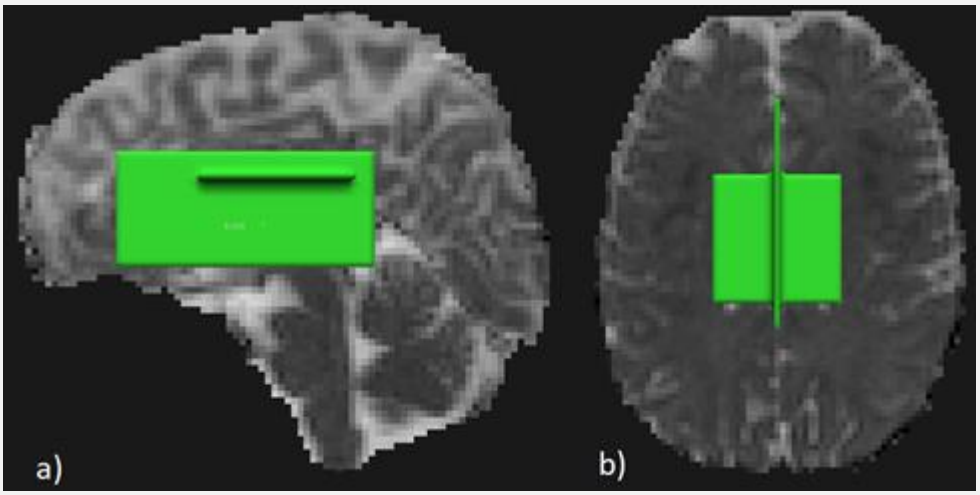

a) ROI selection blocking any fiber to cross the hemispheres, in the middle sagittal slice; b) ROI selection of fibers under the CGC tracts, in the axial slice. Using the operator NOT for ROI filter for all the drawn ROIs.

Source: Author

Figure 46 Inclusion ROIs for the Corticospinal Tract (CST) tracts.

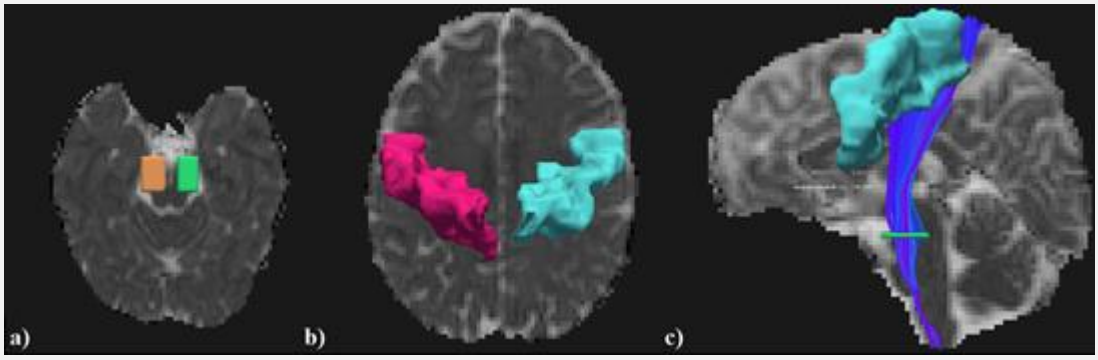

a) Cerebral penducle in the midbrain area, axial slice; b) Precentral gyrus/primary motor cortex, axial slice; c) Reconstructed CST tract, sagittal view.

Source: Author

Figure 47 Exclusion ROIs for the Corticospinal Tract (CST) tracts.

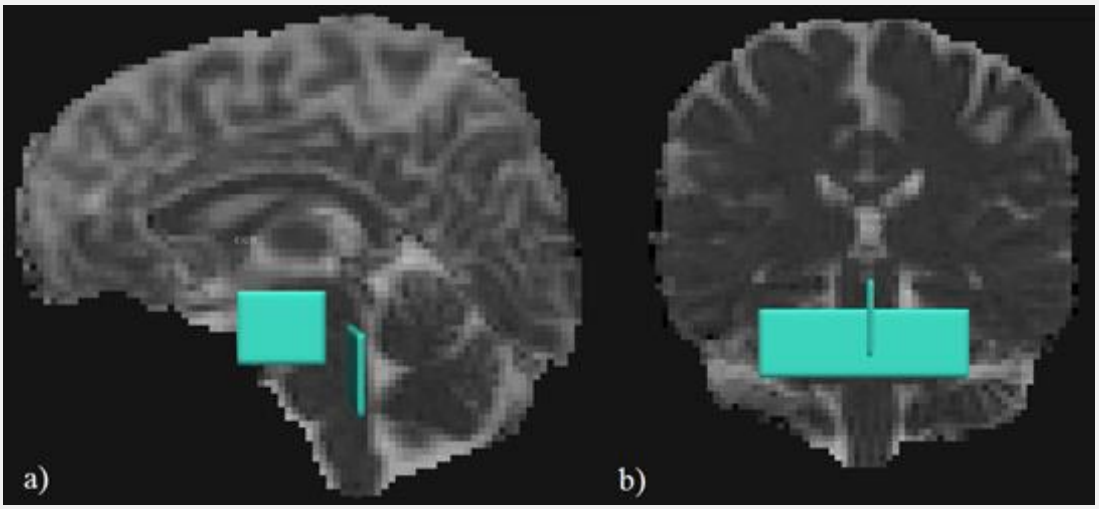

a) ROI selection blocking any fiber to cross the hemispheres, in the middle sagittal slice; b) ROI selection of fibers near the cerebral peduncle that are not part of the CST tract, in the coronal slice. Using the operator NOT for ROI filter for all the drawn ROIs.

Source: Author

Figure 48 Inclusion ROIs for the Fornix (FX) tracts.

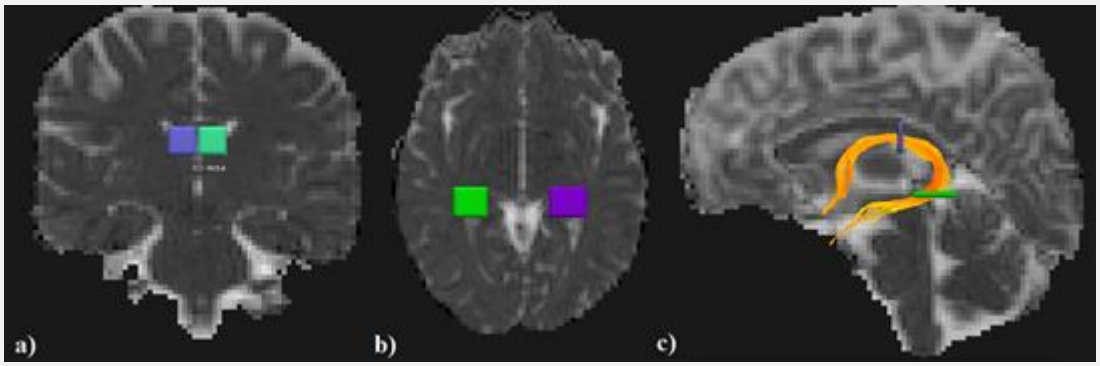

a) ROI selection inferior to the corpus callosum, in the coronal slice; b) ROI selection of the fimbria hippocampus, in the axial slice; c) Reconstructed FX tract, sagittal view.

Source: Author

Figure 49 Exclusion ROIs for the Fornix (FX) tracts.

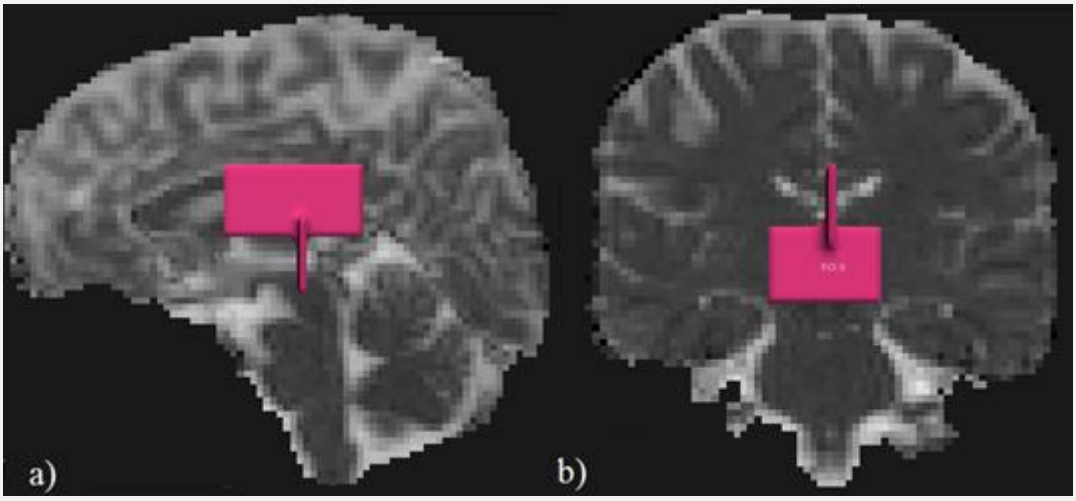

a) ROI selection excluding any fiber crossing the hemispheres, in the middle sagittal slice; b) ROI selection of fibers “between” the body and fimbria of the FX that are not part of the tract, in the coronal slice. Using the operator NOT for ROI filter for all the drawn ROIs.

Source: Author

Figure 50 Inclusion ROIs for the Inferior Frontoccipital Fasciculus (IFOF) tracts.

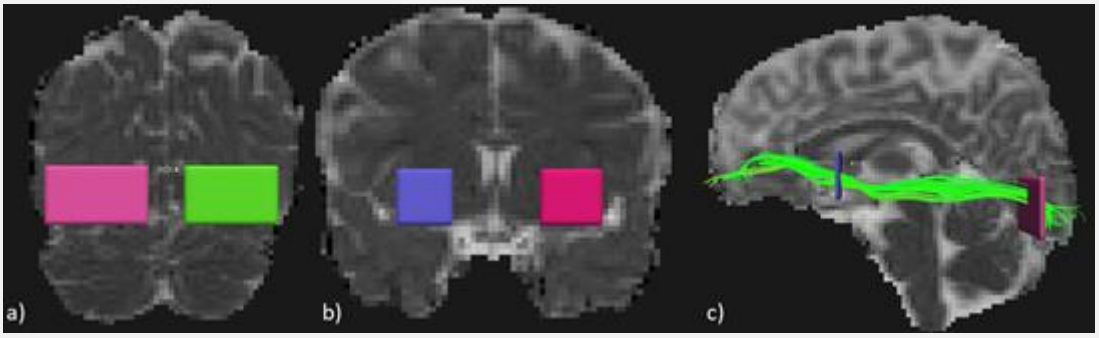

a) ROI selection of the occipital lobe, in the coronal slice; b) ROI selection of the bunched fibers, in the coronal slice; c) Reconstructed IFO tract, sagittal view.

Source: Author

Figure 51 Exclusion ROIs for the Inferior Frontoccipital Fasciculus (IFOF) tracts.

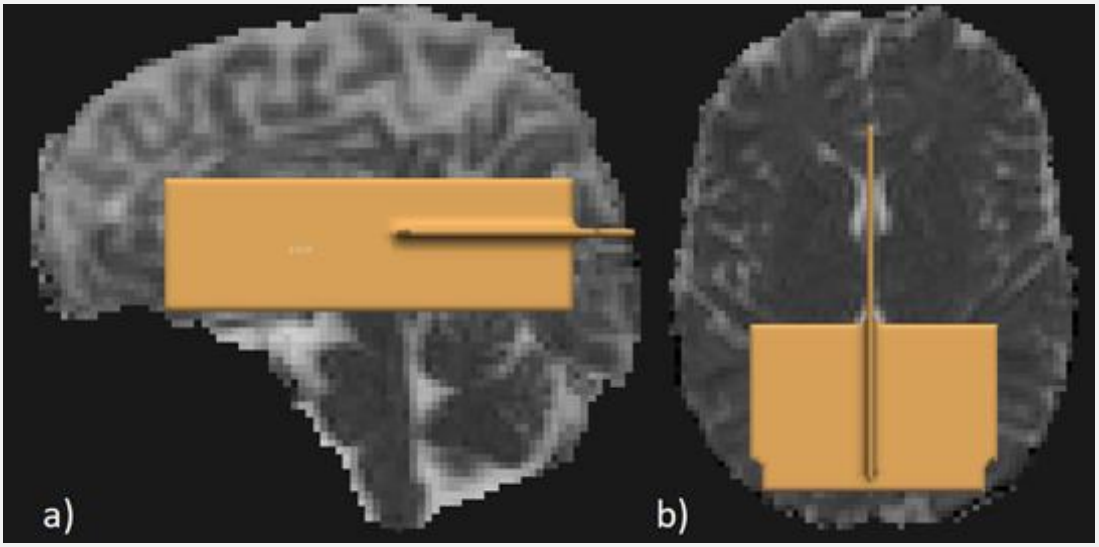

a) ROI selection blocking any fiber to cross the hemispheres, in the middle sagittal slice; b) ROI selection for fibers in the posterior part of the IFOF that are not part of the tract, in the axial slice. Using the operator NOT for ROI filter for all the drawn ROIs.

Source: Author

Figure 52 Inclusion ROIs for the Inferior Lateral Fasciculus (ILF) tracts.

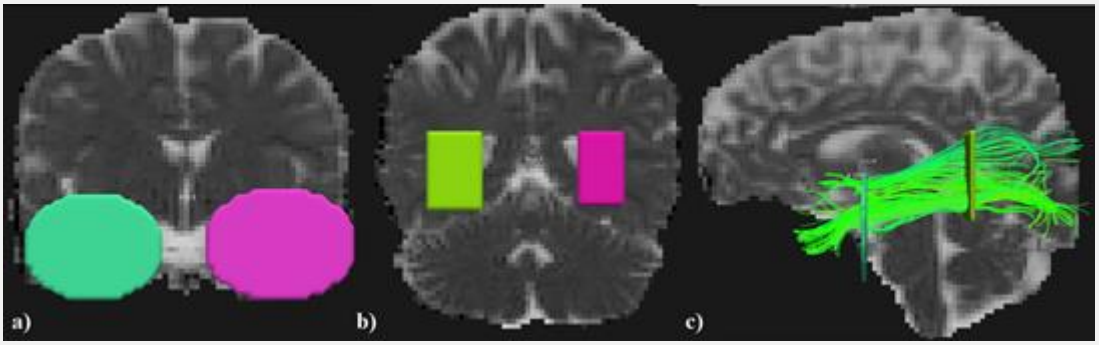

a) ROI selection of the temporal lobe, in the coronal slice; b) In the coronal slice containing the posterior edge of the cingulum, select ROIs in the regions of interest; c) Reconstructed ILF tract, sagittal view.

Source: Author

Figure 53 Exclusion ROIs for the Inferior Lateral Fasciculus (ILF) tracts.

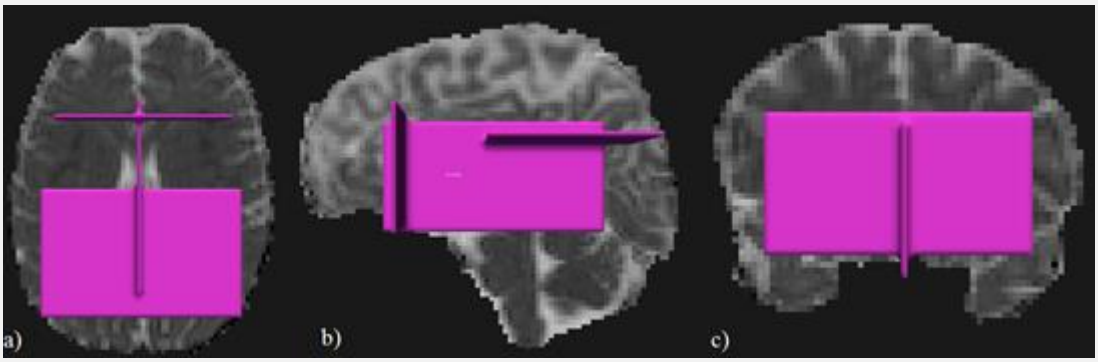

a) Excluding fibers that are not part of the tract, in the axial slice; b) ROI excluding fibers crossing the hemispheres, in the middle sagittal slice; c) Excluding fibers going to the frontal lobe (instead of temporal lobe), in the coronal slice. Using the operator NOT for ROI filter for all the drawn ROIs.

Source: Author

Figure 54 Inclusion ROIs for the Uncinate Fasciculus (UF) tracts.

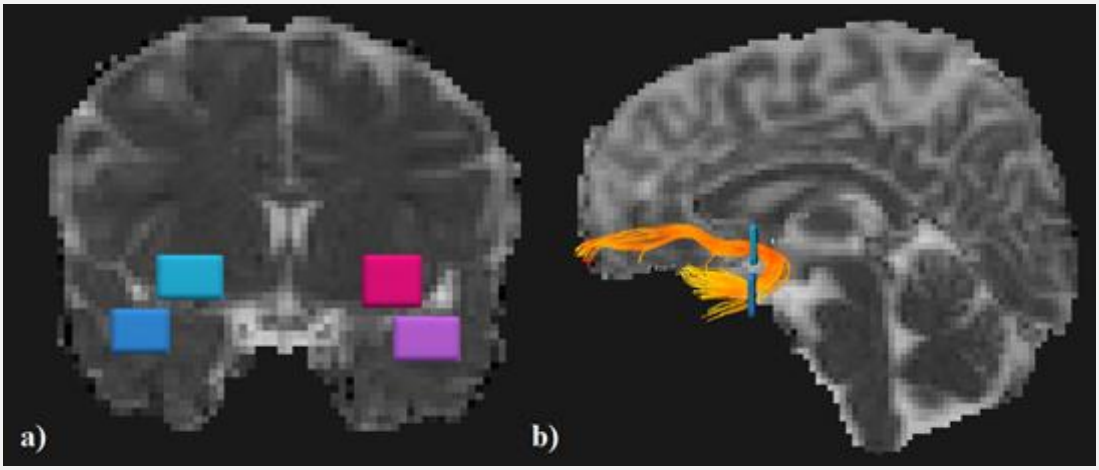

a) ROI selection for the fibers passing in the temporal (dark blue and purple) and in the frontal lobe (light blue and pink), in the coronal slice; b) Reconstructed UF tract, sagittal view.

Source: Author

Figure 55 Exclusion ROIs for the Uncinate Fasciculus (UF) tracts.

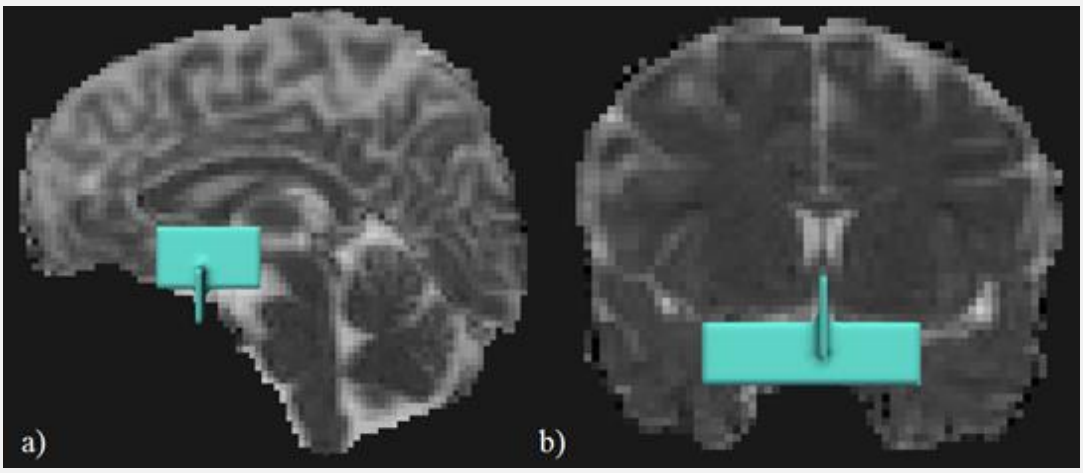

a) ROI selection blocking any fiber to cross the hemispheres, in the middle sagittal slice; b) ROI selection of fibers in the temporal-frontal division that are not part of the UF tract, in the coronal slice. Using the operator NOT for ROI filter for all the drawn ROIs.

Source: Author